Optimal Architectural Design of Parallel and Hybrid Manipulators

by

Kenneth H. Pittens
B.A.Sc., University of Waterloo, 1989

A Thesis Submitted in Partial Fulfillment of the
Requirements for the Degree of

MASTER OF APPLIED SCIENCE

in the Department of Mechanical Engineering

We accept this thesis as conforming
to the required standard.

[redacted]
Dr. R. P. Podhorodeski, Supervisor (Dept. of Mechanical Engineering)

[redacted]
Dr. Y. A. Stepanenko, Department Member (Dept. of Mechanical Engineering)

[redacted]
Dr. W. S. Lu, Outside Member (Dept. of Electrical and Computer Engineering)

[redacted]
Dr. S. Payandeh, External Examiner (School of Eng. Sci., Simon Fraser University)

University of Victoria

Supervisor: Dr. Ron P. Podhorodeski

Abstract

This thesis presents a study of the optimal design of a class of six degree-of-freedom (DOF) closed-chain manipulators. This class of manipulators, which are termed hybrid manipulators, consist of serial branches, each comprised of actuated and passive joints, acting in parallel on a common end effector. Dexterity measures based on instantaneous kinematic characteristics of the manipulator are used as the primary objective in isolating optimum designs.

The fully-parallel Stewart platform, which represents a limiting case of a hybrid manipulator where only one joint in each branch is actuated, is first examined. As an initial design step, manipulator configurations (manipulator architectures and end effector positions and orientations) optimizing local dexterity are determined. For a platform centred reference location and a given length for scaling purposes, a two-parameter family of optimal configurations is shown to exist. Through the use of a new performance measure based upon gradients of local dexterity measures, a unique optimum Stewart platform architecture is isolated from those possessing optimum local dexterity. The resulting optimum manipulator architecture is one in which the dimensions of the base are twice those of the platform and the linear actuator attachment points at the base and platform meet in alternating pairs.

Hybrid manipulators are then examined. Through consideration of preferred attributes relating to the performance of the manipulator, a specific hybrid chain structure is selected from possible six DOF structures for further investigation. A class of kinematically simple serial-chain branches suitable for the chosen hybrid structure is

defined and arguments based upon kinematic equivalency and mobility are used to show that only five unique branch structures with revolute joints belong to the kinematically simple class. A novel approach to manipulator configuration optimization for optimal local dexterity objectives is introduced. This new approach involves finding geometric characteristics of manipulator configurations which optimize dexterity and then finding actual manipulator configurations fitting these characteristics. The method is applied to find optimal configurations of hybrid manipulators utilizing the previously identified branch structures.

Examiners:

Dr. R. P. Podhorodeski, Supervisor (Dept. of Mechanical Engineering)

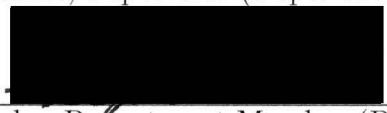

Dr. Y. A. Stepanenko, Department Member (Dept. of Mechanical Engineering)

Dr. W. S. Lu, Outside Member (Dept. of Electrical and Computer Engineering)

Dr. S. Payandeh, External Examiner (School of Eng. Sci., Simon Fraser University)

Contents

List of Figures

List of Tables

Acknowledgements

I wish to thank my supervisor, Dr. Ron Podhorodeski, for the many hours spent discussing kinematic theory and optimization methods which form a foundation of this work. His broad knowledge of robotics, mechanisms, and mathematics were a great asset in gaining the knowledge and understanding required to carry out the research. Furthermore, his fine attitude, positive criticism, and ever-present willingness to help aided me greatly in completing this thesis.

I also wish to express my gratitude to all members of the robotics and vision research groups at UVic for their thoughts and assistance. Special thanks to Glen Field for his technical aid and for the use of his NeXT computer which proved invaluable in creating many of the figures in this thesis.

I am also very grateful to my parents whose encouragement and confidence in me have lead me to complete this and many other endeavors.

Finally, I would like to acknowledge the financial support of the Natural Sciences and Engineering Council of Canada.

Chapter 1

Introduction

1.1 Serial, Parallel, and Hybrid Manipulators

The majority of manipulators in use today employ a serial open-chain arrangement of their links and associated actuators. This class of manipulators has been extensively studied in terms of their design, kinematic and dynamic modeling, and control (for example see [1, 3, 38, 53, 56, 61]). When properly designed, the serial-chain structure provides the benefit of possessing a large workspace volume in comparison to the physical size of the manipulator. However, the serial-chain structure has many drawbacks. These drawbacks include small payload capacity in comparison to manipulator weight, poor dynamic performance in terms of acceleration capabilities, and poor end effector stiffness and therefore poor accuracy.

A fully-parallel manipulator utilizes a closed-chain topology featuring a structure whereby all actuators act in parallel to effect a common payload. The number of kinematic branches connecting the base and end effector is equal to the number of actuators driving the manipulator. For example, the six degree-of-freedom (DOF) parallel manipulator commonly referred to as the Stewart Platform [51] is comprised

of six linear actuators acting in parallel on a common mobile platform. Parallel manipulators can provide the benefits of high payload capability, superior dynamic performance, and high stiffness and accuracy when compared to serial-chain manipulators. These benefits come at the expense of a reduced work volume for the manipulator.

Serial-chain and fully-parallel manipulators represent two extremes of a broader class of manipulator structures. This broader class consists of manipulator structures containing serial-chain branches, each comprised of actuated and passive joints, acting in parallel on a common end effector. Manipulators possessing these structures will be termed *hybrid* manipulators. A serial-chain can be considered to be a limiting case of a hybrid manipulator where there is a single branch having all joints actuated. Conversely, a fully-parallel manipulator is a limiting case where only one joint in each branch is actuated. An example of a hybrid manipulator with three branches is depicted in Figure 1.1. Through proper design, hybrid manipulators exploiting the advantages of both fully-parallel and serial chain devices can be developed for specific applications.

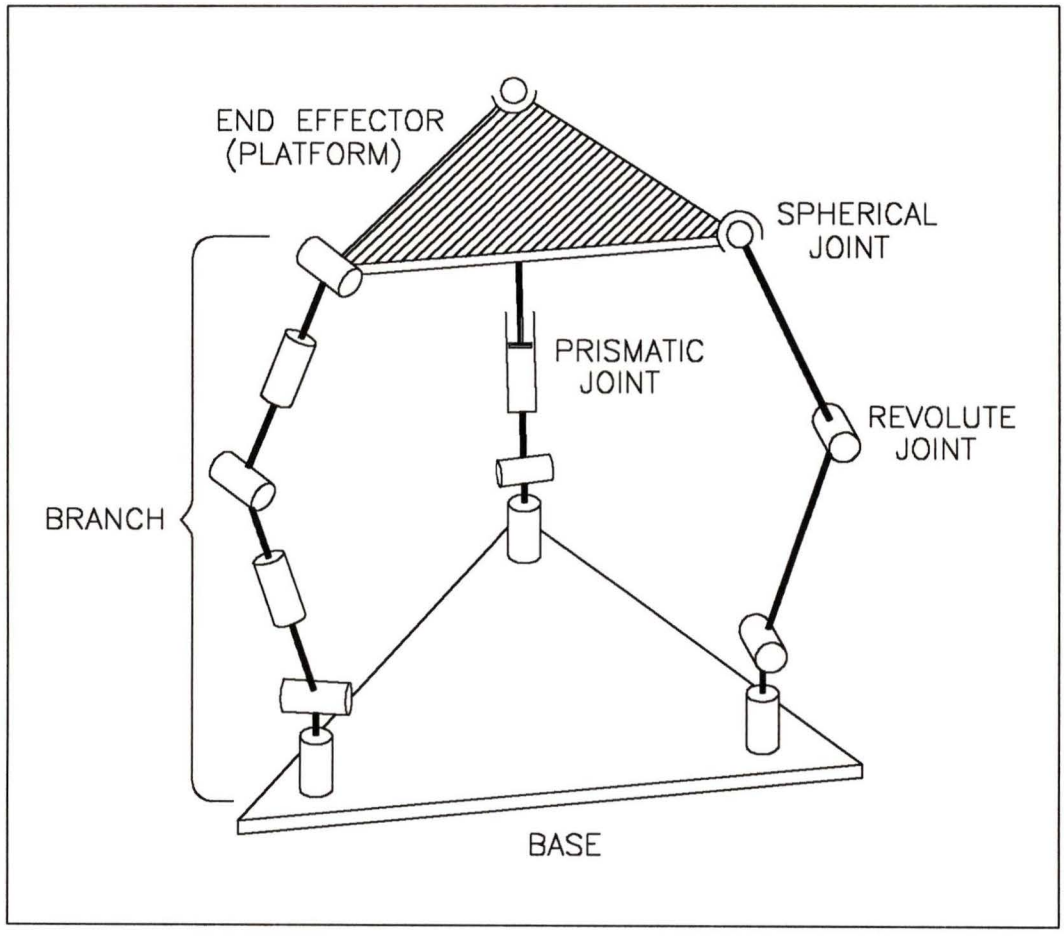

Figure 1.1: An Example Hybrid Manipulator Structure

1.2 Previous Work Relating to the Design of Closed-Chain Manipulators

In comparison to open-chain manipulators, closed-chain manipulators have received little attention with regards to their design and analysis. Most work on closed-chain manipulations has been centred on fully-parallel devices having structures similar to that of the so-called "Stewart platform" briefly described in Section 1.1. This structure was first introduced by Gough [18] in 1962 as a mechanism for an automobile tire testing machine. Later work by Stewart [51] (1965) introduced a slightly altered version of Gough's mechanism for use as a six DOF aircraft motion simulator. The elementary design and kinematics of manipulators possessing this structure were investigated by McCallion and Truong [31] (1979) as well as Yang and Lee [58] (1984). A six DOF parallel manipulator having pantograph leg mechanisms in place of linear actuators pairs was designed and analysed by Inoue et al. [23] (1985). A more recent work by Fichter [10] (1986) covers the position, rate and force kinematics of the Stewart platform manipulator in an in-depth manner. Fichter's work also includes practical design considerations related to the design of the manipulator's associated linear actuators and passive joints.

A systematic study of possible fully-parallel manipulator structures was carried out by Hunt [21] (1983) and many novel manipulator geometries were introduced. Two of the three DOF manipulator geometries proposed by Hunt were later analyzed by Gosselin and Angeles [13, 14] (1988,1989) with regards to the optimum architectural (manipulator joint and link layout and dimensions) design of the manipulators. These works were among the first to investigate the optimum design of closed-chain manipulators through consideration of symmetry, workspace and dexterity of the re-

sulting device. Dexterity considerations were also used by Ma and Angeles [30] (1990) to optimize the design of a six DOF Stewart platform manipulator. To the author's knowledge, the last three references represent the only work performed to date relating to the optimum design of closed-chain manipulators for desired performance objectives. Many recent works introducing and kinematically analyzing novel closed-chain designs can be found in the literature [8, 34, 42, 49], but the works do not include application of optimum design techniques. Work related to the optimum design of closed-chain manipulators includes the design of articulated hands [48], the design of parallel actuated linkages for open-chain manipulators [26], and the design of parallel drive mechanisms for direct drive robots [5].

1.3 Content and Organization of this Work

The optimal design of closed-chain parallel and hybrid manipulators possessing full six degree-of-freedom motion and force capability is examined in this thesis. The examination is limited to manipulator structures not possessing joint or actuation redundancy.

Dexterity measures related to the instantaneous kinematics of the manipulator are used as the primary objective in isolating the optimum design(s) of the structures considered. The optimizations are carried out in two basic steps. The first step being the isolation of manipulator configurations (manipulator architectures and end effector positions and orientations) optimizing local dexterity. Local dexterity being defined as the dexterity at a single point in the manipulator's workspace. This first step generally follows that utilized in some of the previous design optimization works mentioned above [13, 14, 30, 48]. The second step of the design optimization proce-

dure is the isolation of a unique manipulator architecture from those with optimum local dexterity through the consideration of performance objectives with global implications. In this manner, a manipulator with optimum local characteristics and best overall performance can be found. This method is particularly well suited to parallel closed-chain manipulators which are generally employed in applications requiring the use of only a portion of the manipulator's workspace.

The displacement and instantaneous kinematics (velocity and force) of parallel and hybrid manipulators must be investigated and understood before any design optimization can take place. In Chapter 2, solutions to the inverse displacement, inverse velocity, and forward static force problems are formulated for a hybrid manipulator of general structure. These solutions are applicable to both fully-parallel and hybrid manipulators of general structure. The forward displacement, forward velocity, and inverse static force problems are discussed with regards to direct, iterative, and numerical methods of obtaining their solutions.

The concepts of dexterity, manipulability and singular configurations are introduced and discussed in Chapter 3. Dexterity measures related to both the positional range of motion of the manipulator (geometric dexterity measures), and to those quantifying the instantaneous kinematic characteristics of the manipulator (kinematic dexterity measures) are examined for their applicability to the design of closed-chain devices. Kinematic dexterity measures are further examined from mathematical and geometrical viewpoints through the use of a singular value decomposition of the instantaneous transformation matrix of the manipulator under consideration. The frame and unit variability of kinematic dexterity measures are discussed with regards to the physical meaning of the measures and the consequences of a change in the frame of reference or in a change in the unit of length measure.

The treatment of required background material ends with a discussion of singular configurations of closed-chain manipulators. The singular configurations are classified according to their two basic types and are examined for their causes and the resulting behavior of a manipulator in or near singular configurations of both types.

The optimization of manipulator configurations and architectures begins in Chapter 4 with an investigation of the fully-parallel Stewart platform. The general structure of the manipulator is described and parameters characterizing its architecture and end effector spatial displacement are developed for optimization purposes as design variables. Utilizing the instantaneous kinematic equations developed in Chapter 2, configurations optimizing local dexterity of the Stewart platform (quantified by the condition number of the instantaneous force transformation matrix) are found for a platform centred frame of reference and a given characteristic length for scaling purposes. Relations defining the resulting family of optimum solutions are developed, and properties of the configurations are analyzed and discussed. The use of other kinematic dexterity measures and reference locations are examined and are shown to result in the definition of similar families of optimal Stewart platform configurations.

Having defined a family of optimum configurations, global performance measures are reviewed from a historical perspective for their applicability as objectives for the final optimization step of the Stewart platform architectural design. Due to the computational expense and difficulties involved with interpreting the results of these global measures, a new performance measure with global implications is introduced. This new measure utilizes spatial gradients of kinematic dexterity measures to form a first-order approximation to the characteristics of a manipulator at points displaced from a local optimum. This new measure is then employed to compare members of the family of local optimum configurations in order to isolate a unique optimum

Stewart platform architecture.

The optimum design of hybrid manipulator structures begins in Chapter 6 with an enumeration of potential six degree-of-freedom structures. Preferred attributes of hybrid manipulators and their associated branches are used to narrow the class of manipulator structures considered to a single type. A class of kinematically simple branches suitable for use in the chosen manipulator structure are defined and arguments based upon kinematic equivalency and mobility of the branches are used to identify all basic branch structures belonging to the class.

As a result of the large number of possible manipulator architectures utilizing the kinematically simple branch structures, a different approach than that used in Chapter 4 for the Stewart platform is developed to optimize the configuration of hybrid manipulators. This new method involves finding geometric characteristics of manipulator configurations which optimize kinematic dexterity, and then finding actual manipulator configurations fitting these characteristics. The new method is applied using several dexterity measures and a set of optimal geometric characteristics of hybrid manipulator configurations is found. Mathematical properties of the instantaneous kinematic transforms associated with manipulators possessing the optimal geometric characteristics are determined after further examination of the geometric characteristics. Finally, the optimal geometric characteristics are used to determine optimal configurations of hybrid manipulators which utilize the previously identified kinematically simple branch structures.

The thesis closes with conclusions of the presented work and a short discussion of recommended future research to continue the work started in this thesis.

1.4 Contribution of this Work

The work contained in this thesis is original work performed by the author. The following contributions are considered to be relevant:

1. The frame and unit variability of kinematic dexterity measures is demonstrated and taken into consideration during design optimizations. This fact is often overlooked, giving optimization results with little physical meaning.

2. For a platform centred reference frame location and a given length for scaling purposes, a two parameter family of optimal Stewart platform configurations is shown to exist. The results are extended for a reference frame location vertically displaced from the centre of the platform.

3. A new global dexterity measure based upon spatial gradients of kinematic dexterity is introduced to quantify the performance of a manipulator at points displaced from a local optimum configuration. This new measure has reduced computational requirements when compared to previously proposed global dexterity measures.

4. A class of kinematically simple serial-chain branches suitable for hybrid manipulators is defined and it is demonstrated that five unique branch structures with revolute joints belong to the class.

5. A novel approach to manipulator configuration optimization is introduced. This approach is based on determining the geometric characteristics of manipulator configurations which optimize dexterity, and then finding actual manipulator configurations fitting these characteristics. This approach allows any number of manipulators having similar structures to be optimized from the results of only one optimization.

6. For a platform centred reference frame location and a given length for scaling purposes, a one parameter family of optimal geometric characteristics is shown to exist for hybrid manipulators based on three kinematically simple branches. A unique set of geometric characteristics is shown to be potentially advantageous after consideration of changes in kinematic dexterity as the manipulator is moved away from the optimal configuration.

Chapter 2

Kinematics of Hybrid Manipulators

The displacement and instantaneous kinematic analysis of parallel and hybrid manipulators differ substantially from that for serial-chain devices. These differences are as a result of their inherently different architectures. However, many of the analysis techniques used for serial-chain manipulators form an integral part of the kinematics of parallel and hybrid manipulators. This is due to the serial branch components of the closed-chain devices.

As previously mentioned, a parallel manipulator represents a limiting case of a hybrid manipulator where only one joint in each serial branch is actuated. The kinematic analysis techniques developed in this chapter will be for a hybrid manipulator possessing a general architecture. Therefore, the analysis will cover all cases of both parallel and hybrid structures in a single unified manner.

2.1 Displacement Kinematics

Displacement kinematics are concerned with the relationships between actuated joint displacements and the position and orientation of the manipulator's output link. The forward displacement problem is defined as the determination of the position and orientation of the output link given a set of actuated joint displacements. This is sometimes referred to as the direct kinematic problem. Conversely, the inverse displacement problem is defined as the determination of the actuated joint displacements given the required position and orientation of the output link. This problem is also known as the inverse kinematic problem.

2.1.1 Inverse Displacement Analysis

The inverse displacement problem for hybrid manipulators requires resolving displacements of the actuated branch joints given the position and orientation of the platform (output link) relative to the base. To begin the analysis, right handed base (O) and end effector (E) coordinate frames are defined at convenient locations in the manipulator's base and platform respectively. Coordinate frames are also defined at both ends of each of the branches as shown in Figure 2.1. Frame B_i locates and orients the base of the branch whereas P_i locates and orients the end of the branch. The position of the branch base is described by the position vector ${}^{o}\mathbf{b}_i$ and the orientation is described by the rotation matrix ${}^{o}[\mathbf{R}]_{b_i}$. The branch base and its associated frame are fixed with respect to the manipulator's base and therefore ${}^{o}\mathbf{b}_i$ and ${}^{o}[\mathbf{R}]_{b_i}$ are constants for a given manipulator architecture. The position of the branch end is described by the position vector ${}^{e}\mathbf{p}_i$ and the orientation is described by the rotation matrix ${}^{e}[\mathbf{R}]_{p_i}$ with respect to the end effector frame. Since the branch end is fixed to the platform, these quantities are constants for a given manipulator architecture.

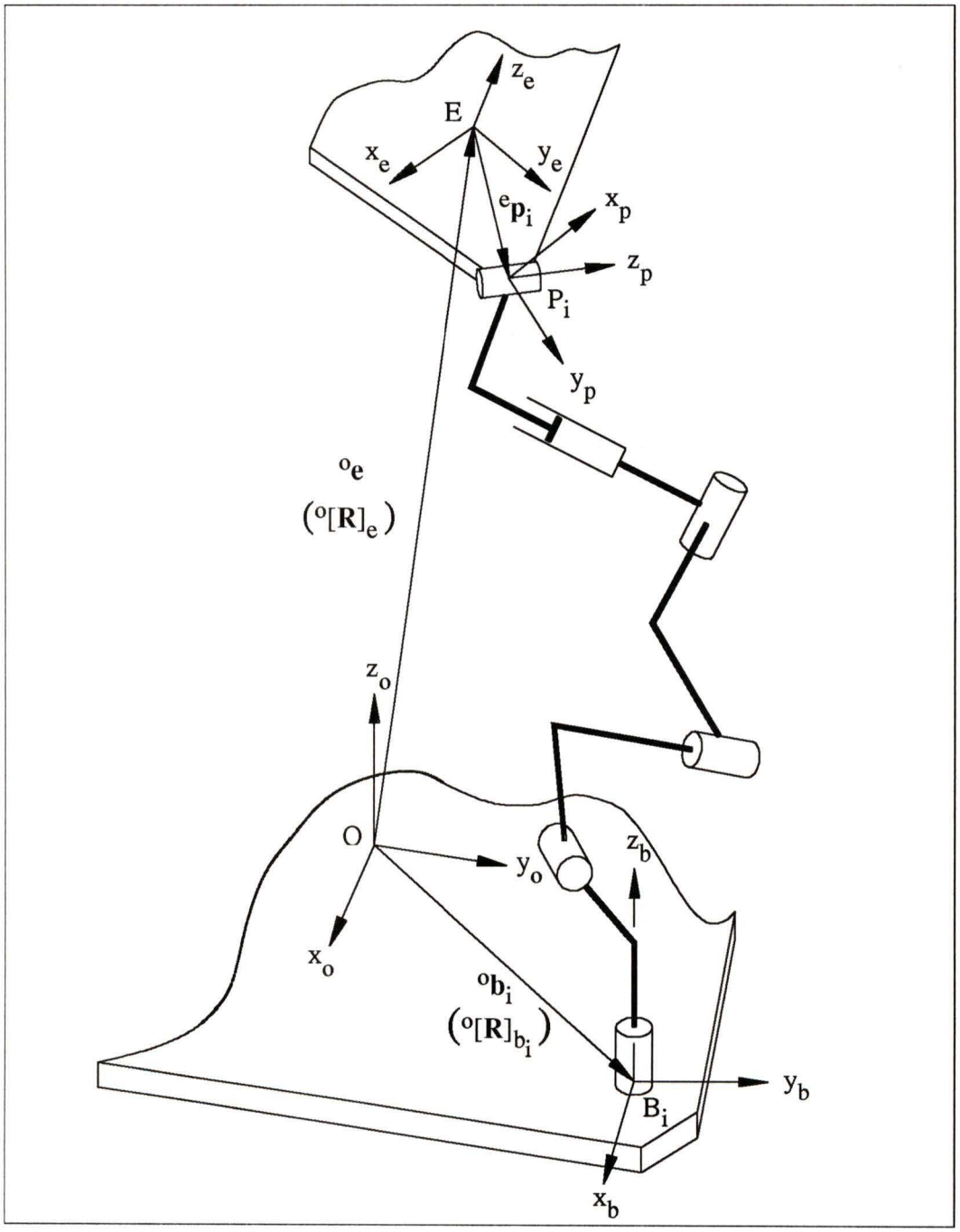

Figure 2.1: Coordinate frames and branch-end position vectors for a generalized hybrid manipulator

Let the position of the platform with respect to the base be described by the vector ${}^{o}\mathbf{e}$ from the origin of the base coordinate frame to the origin of the platform coordinate frame. Let the orientation of the platform with respect to the base be described by the rotation matrix ${}^{o}[\mathbf{R}]_{e}$. The position of the end of each branch with respect to the manipulator's base coordinate frame can be expressed as

$$ {}^{o}\mathbf{p}_i = {}^{o}\mathbf{e} + {}^{o}[\mathbf{R}]_{e}\,{}^{e}\mathbf{p}_i \tag{2.1} $$

In order to resolve the branch joint displacements the position of the end of each branch must be rewritten with respect to the branch base coordinate frame as follows:

$$ {}^{b_i}\mathbf{p}_i = {}^{o}[\mathbf{R}]_{b_i}^{T}\,({}^{o}\mathbf{p}_i - {}^{o}\mathbf{b}_i) \tag{2.2} $$

or

$$ {}^{b_i}\mathbf{p}_i = {}^{o}[\mathbf{R}]_{b_i}^{T}\,({}^{o}\mathbf{e} - {}^{o}\mathbf{b}_i + {}^{o}[\mathbf{R}]_{e}\,{}^{e}\mathbf{p}_i) \tag{2.3} $$

The transpose operator can be used in place of an inversion operation for ${}^{o}[\mathbf{R}]_{b_i}$ since rotation matrices are orthogonal.

The orientation of the end of the branch must also be known in order to determine the branch joint displacements. The orientation of the branch end with respect to the branch base can be expressed by the following rotation matrix:

$$ {}^{b_i}[\mathbf{R}]_{p_i} = {}^{o}[\mathbf{R}]_{b_i}^{T}\,{}^{o}[\mathbf{R}]_{e}\,{}^{e}[\mathbf{R}]_{p_i} \tag{2.4} $$

With the position and orientation of each branch end with respect to their bases being given by equations (2.3) and (2.4) respectively, the inverse displacement problem for the branches must be solved to give the required actuated joint displacements. The inverse displacement problem requires the solution of nonlinear simultaneous

equations which are difficult to solve and often result in multiple solutions. For general branch structures these solutions are not expressible in a closed form. A direct solution in the form of roots of a 16th order polynomial of a single variable can be formulated for general serial branches with six revolute joints as demonstrated by Raghavan and Roth [47]. The method will not be presented here since it is beyond the scope of this work.

Pieper [41] demonstrated that the inverse displacement solution for serial-chain branches with six or less joints and three consecutive intersecting joint axes can be expressed in closed form. Comparison and manipulation of homogeneous transforms from the forward kinematic solution are used to find closed form solutions for the required joint angles. Several examples using similar techniques of sequentially isolating each joint variable and solving for the joint displacement are given by Craig [9] and Paul [39]. Solutions based on spatial and planar geometry can also be applied for some simple branch structures as outlined in Craig [9].

The parallel and hybrid manipulator architectures examined in later chapters of this work possess branches belonging to the class considered by Pieper. However, the three consecutive intersecting joints are all passive and are located at the end of the branches to form spherical joint groups. These passive spherical joints decouple the branch displacements given by equation (2.3) from the branch end orientations given by equation (2.4). If only the actuated joint displacements are of interest in the manipulator's inverse displacement solution, as is often the case, only the positions of the branch ends need to be considered (equation 2.3). This greatly simplifies the branch inverse displacement solutions due to the reduction in the dimension of the problem from six to three.

2.1.2 Forward Displacement Analysis

The forward displacement solution requires resolving the end effector position and orientation knowing the actuated joint displacements. The solution to this kinematic problem is not required for the analyses performed in later chapters of this work, but an overview of existing solution techniques is given for completeness.

A direct formulation for resolving the forward displacement problem for hybrid manipulators of general structure is unknown. The forward displacement solution of a special form of the Stewart platform has been presented as a direct formulation in recent literature [19, 22, 33, 36]. This form of the Stewart platform is characterized by having coincident passive spherical joints centres for adjacent pairs of branches where the branches connect to the mobile platform. In these formulations the solution is expressed as a 16th order polynomial in a single variable, each root representing a possible assembly mode of the manipulator. In recent work by Innocenti and Parenti-Castelli [22] similar results are demonstrated to be applicable to a class of structures having three branches or sub-chains connected to the end effector by way of spherical joints, each sub-chain tip retaining only a single degree of freedom when disconnected from the end effector and all actuated joints are locked. In effect, this can be imagined as each sub-chain tip tracing a circle generated by its remaining passive degree of freedom. Forward displacement solution assembly modes correspond to end effector positions and orientations where the end effector's spherical connecting joints lie on their respective sub-chain tip traced circles. The parallel and hybrid manipulators studied in this work belong to the class considered in [22].

Iterative techniques based upon instantaneous kinematic transformations have been proposed and implemented by Podhorodeski [46] to resolve forward displacement

solutions for hybrid manipulators. These techniques are applicable to hybrid manipulators of arbitrary structure, but will yield only one forward displacement solution even through multiple solutions may exist. The single solution may be an incorrect solution corresponding to an assembly mode or solution branch differing from actual manipulator's assembly mode or solution branch. This would mainly occur when the manipulator nears a singular configuration and the instantaneous kinematic transformation becomes essentially non-invertible. However, with appropriate limiting of manipulator joint angles or by the inclusion of additional algorithms to deal with the problem, these iterative solution techniques become useful in applications where only a single forward displacement solution is required. For real-time manipulator control these iterative techniques become the preferred forward displacement solution method due to their superior speed performance and the need for only a single displacement solution corresponding to the actual displacement of the device.

2.2 Instantaneous Kinematics

Instantaneous kinematics are concerned with the relationships between sets of instantaneous actuated joint rates and the associated instantaneous velocity of the manipulator's output link. The forward velocity problem is defined as the determination of the the output link's linear and angular velocity given a set of actuated joint rates. The inverse velocity problem is defined as the determination of actuated joint rates given the linear and angular velocity of the manipulator's output link. The relationships between infinitesimal changes in actuated joint displacements and infinitesimal changes in the position and orientation of the output link can also be described by the same solutions.

In a serial open-chain manipulator, instantaneous motions produced by each of the joints sum in a serial manner to produce a resulting instantaneous motion at the end effector. Conversely, in a closed-chain parallel or hybrid manipulator, forces and moments produced by each of the manipulator's branches act in parallel to produce a resulting force and moment externally resisted at the end effector. This *series-parallel duality* as referred to by Waldron and Hunt [55] is a result of the duality, or *reciprocity* [20], between force and velocity systems. As a consequence of this series-parallel duality, solutions to the forward and inverse kinematic problems for hybrid manipulators reverse roles in terms of difficulty when compared to serial manipulators, while also requiring altered solution techniques.

The instantaneous kinematics of general parallel and hybrid manipulators have been studied by authors in recent literature. Mohamed and Duffy [35] applied screw theory and the orthogonal product of screws to solve the forward and inverse velocity problems. Later work by Sugimoto [52] used motor algebra and elimination of passive joint variables to define a "Jacobian" matrix for parallel and hybrid manipulators. This matrix was defined as the mapping from actuated joint rates to the velocity of the manipulator's output link; the same as that for serial-chain manipulators. A more recent work by Kumar [28] uses screw theory and the reciprocal product of screws to resolve inverse velocity solutions for manipulators with general closed-chain structures. This method is preferable to that presented in [35] since the reciprocal product of screws is frame invariant unlike the orthogonal product of screws.

The development of instantaneous kinematic solutions presented in the following sections follows the method outlined in [28]. A *reciprocal screw matrix* and a *reciprocal product matrix* will be defined which allow the instantaneous kinematic solutions to be written in a concise matrix form.

2.2.1 Instantaneous Motion Analysis

Let the instantaneous motion of the end effector (platform) of a generalized hybrid manipulator be described by a twist of amplitude ω about an instantaneous screw axis[1] $\$$. Using screw coordinates this quantity can also be written as

$$\omega \$ = \omega \begin{Bmatrix} \$ \\ \$_o \end{Bmatrix} = \begin{Bmatrix} \boldsymbol{\omega} \\ \mathbf{v} \end{Bmatrix} = \mathbf{V} \tag{2.5}$$

where $\boldsymbol{\omega}$ and $\mathbf{v}$ are the angular and linear velocities associated with the end effector, respectively. Since the end of the branches are attached to the common platform containing the end effector, the branch ends must also undergo the same instantaneous screw motion $\mathbf{V}$.

Considering a single branch of the manipulator, the instantaneous twist of the branch end can be expressed as the linear combination of its active and passive joint twists:

$$\sum \dot{q}_i \, \mathbf{S}_i = \mathbf{V} \tag{2.6}$$

where $\mathbf{S}_i$ are the unit screws coordinates of joint axis i and $\dot{q}_i$ are their respective joint rates.

Only the active joint rates are of interest since the passive joint motions are determined by the combined effort of all actuated joints in all branches. To isolate a desired active joint and solve for its joint rate, a screw $\mathbf{W}_j$ reciprocal to all joint screws in the branch except that associated with the active joint of interest $\mathbf{S}_j$ is used. Taking the reciprocal product of both sides of equation (2.6) with the reciprocal screw gives

$$\dot{q}_j \, (\mathbf{W}_j \, \chi \, \mathbf{S}_j) = \mathbf{W}_j \, \chi \, \mathbf{V} \tag{2.7}$$

[1] A short overview of screws, screw quantities and screw algebra are given in Appendix A.

since $\mathbf{W}_j \chi \mathbf{S}_i = 0$ when $i \neq j$. Solving for $\dot{q}_j$ yields the following joint rate solution:

$$\dot{q}_j = \frac{\mathbf{W}_j \chi \mathbf{V}}{\mathbf{W}_j \chi \mathbf{S}_j} \tag{2.8}$$

The above procedure of taking reciprocal products of both sides of equation (2.6) and solving for the joint rate can be repeated for all active joints of the hybrid manipulator. Solving for all the active joint rates in this manner constitutes the inverse velocity solution.

It is often helpful to express the inverse velocity solution in matrix form. This can be accomplished by defining a complement operator $(\cdot)^*$ which exchanges the two elements of a screw quantity when expressed in screw coordinate form (see Appendix A for further details). This operator allows the reciprocal product of screws to be expressed in standard algebraic notation permitting equation (2.8) to be rewritten as

$$\dot{q}_j = \frac{\mathbf{W}_j^{*T}}{\mathbf{W}_j^{*T} \mathbf{S}_j} \mathbf{V} \tag{2.9}$$

Assembling the joint rate solutions for all n active joints into a single matrix equation, the inverse velocity solution for a general hybrid manipulator is

$$\dot{\mathbf{q}} = \begin{bmatrix} \frac{1}{\mathbf{W}_1^{*T} \mathbf{S}_1} & & \mathbf{0} \\ & \ddots & \\ \mathbf{0} & & \frac{1}{\mathbf{W}_n^{*T} \mathbf{S}_n} \end{bmatrix} \begin{bmatrix} \mathbf{W}_1^{*T} \\ \vdots \\ \mathbf{W}_n^{*T} \end{bmatrix} \mathbf{V} = [\mathbf{B}] [\mathbf{W}^*]^T \mathbf{V} \tag{2.10}$$

or

$$\dot{\mathbf{q}} = \begin{bmatrix} \frac{\mathbf{W}_1^{*T}}{\mathbf{W}_1^{*T} \mathbf{S}_1} \\ \vdots \\ \frac{\mathbf{W}_n^{*T}}{\mathbf{W}_n^{*T} \mathbf{S}_n} \end{bmatrix} \mathbf{V} = [\mathbf{K}^*]^T \mathbf{V} \tag{2.11}$$

The matrix $[\mathbf{B}]$ is an $n \times n$ diagonal matrix of inverses of the reciprocal products associated with each of the active joints in the manipulator. This matrix will be termed the *reciprocal product matrix*. The matrix $[\mathbf{W}^*]^T$ is the complement and

transpose of the matrix [**W**] whose columns are the reciprocal screws $\mathbf{W}_j$ associated with each of the active joints. This $6 \times n$ matrix [**W**] will be termed the *reciprocal screw matrix*. The matrix [**K**] is defined as the product of [**W**] and [**B**] for convenience. The matrix $[\mathbf{K}^*]^T$ is commonly referred to as the "Jacobian" matrix for parallel and hybrid manipulators even though its mapping is in the opposite direction to that for serial-chain manipulators.

The forward velocity solution which gives the velocity of the end effector for a given set of active joint rates can be resolved by solving the system of linear equations represented by equation (2.11). This solution can be symbolically expressed as

$$\mathbf{V} = [\mathbf{K}^*]^{-T}\,\dot{\mathbf{q}} = [\mathbf{W}^*]^{-T}[\mathbf{B}]^{-1}\,\dot{\mathbf{q}} = [\mathbf{W}^*]^{-T} \begin{bmatrix} \mathbf{W}_1^{*T}\,\mathbf{S}_1 & & \mathbf{0} \\ & \ddots & \\ \mathbf{0} & & \mathbf{W}_n^{*T}\,\mathbf{S}_n \end{bmatrix} \dot{\mathbf{q}} \qquad (2.12)$$

The matrix inversion in the above equation would not normally be carried out either symbolically or numerically since methods of solving simultaneous linear equations are computationally far more efficient than actual matrix inversion.

2.2.2 Static Force Analysis

The relationships between actuated joint torques (forces, or wrench[2] intensities in general) and the static force and moment (wrench) acting at the manipulator's output link will now be analyzed. Similar to the velocity problems, the forward static force problem is defined as the determination of the wrench produced at the output link given a set of wrench intensities produced by the manipulator's actuators. Conversely, the inverse static force problem is defined as the determination of the wrench intensities required from the actuators to resist a given wrench acting on the output

[2] A wrench is a screw representation of a generalized force/moment combination. See Appendix A for further details on wrenches and wrench intensities.

link of the manipulator. The law of conservation of energy will be used in conjunction with the instantaneous motion results of the previous section in order to arrive at the required solutions.

To begin the analysis, consider a mechanical energy balance between the rate of work produced at the output of a manipulator and the outputs of the actuators. This energy balance can be written as

$$\boldsymbol{\tau} \cdot \dot{\mathbf{q}} = \mathbf{f} \cdot \mathbf{v} + \mathbf{m} \cdot \boldsymbol{\omega} + E_{friction} \tag{2.13}$$

where $\boldsymbol{\tau}$ is a vector of actuator wrench intensities, and $\mathbf{f}$ and $\mathbf{m}$ are the force and moment at the output link of the manipulator, respectively. The friction at the manipulator's active and passive joints will be assumed to be small in comparison to the actuator and end effector loading, therefore the energy loss due to friction $E_{friction}$ will be neglected in the remainder of the analysis. Dropping the friction term, the energy balance can be rewritten as

$$\boldsymbol{\tau}^T \dot{\mathbf{q}} = \mathbf{F}^{*T} \mathbf{V} \tag{2.14}$$

where $\mathbf{F} = \{ \mathbf{f} ; \mathbf{m} \}^T$ is the wrench produced at the output of the manipulator.

Substituting the hybrid manipulator inverse velocity solution of equation (2.11) into the above equation gives

$$\boldsymbol{\tau}^T [\mathbf{K}^*]^T \mathbf{V} = \mathbf{F}^{*T} \mathbf{V} \tag{2.15}$$

cancelling $\mathbf{V}$, then complementing and transposing both sides results in the following solution to the forward static force problem for generalized hybrid manipulators:

$$\mathbf{F} = [\mathbf{K}] \boldsymbol{\tau} = \left[\frac{\mathbf{W}_1}{\mathbf{W}_1^{*T} \mathbf{S}_1} \quad \cdots \quad \frac{\mathbf{W}_n}{\mathbf{W}_n^{*T} \mathbf{S}_n} \right] \boldsymbol{\tau} \tag{2.16}$$

Expanding the matrix [**K**] into the product of the reciprocal screw and the reciprocal product matrices yields

$$\mathbf{F} = \begin{bmatrix} \mathbf{W}_1 & \cdots & \mathbf{W}_n \end{bmatrix} \begin{bmatrix} \frac{1}{\mathbf{W}_1^{*T}\mathbf{S}_1} & & \mathbf{0} \\ & \ddots & \\ \mathbf{0} & & \frac{1}{\mathbf{W}_n^{*T}\mathbf{S}_n} \end{bmatrix} \boldsymbol{\tau} = [\mathbf{W}][\mathbf{B}]\boldsymbol{\tau} \qquad (2.17)$$

Examining equations (2.16) and (2.17) reveals that the wrench produced at the output of the manipulator is the scaled sum of the reciprocal screws $\mathbf{W}_j$ associated with each actuated joint,

$$\mathbf{F} = \sum_{j=1}^{n} \frac{\mathbf{W}_j}{\mathbf{W}_j^{*T}\mathbf{S}_j}\tau_j = \sum_{j=1}^{n} w_j \mathbf{W}_j \quad ; \quad w_j = \frac{\tau_j}{\mathbf{W}_j^{*T}\mathbf{S}_j} \qquad (2.18)$$

It follows from the above expression that the reciprocal screws $\mathbf{W}_j$ are the wrenches created by each of the active joints in the hybrid manipulator, their intensities being w_j. Furthermore, the reciprocal products in the denominator are the effective "moment arms" of these wrenches about the screw axis of the corresponding actuator. Therefore, as expected from the series-parallel duality discussed earlier, the wrenches produced by the actuators in the parallel acting branches sum to produce a resulting wrench at the end effector of the manipulator.

The inverse static force solution which gives the required joint wrench intensities to resist a given load at the manipulator's output link can be resolved by solving the system of linear equations represented by equation (2.16). This solution can be symbolically expressed as

$$\boldsymbol{\tau} = [\mathbf{K}]^{-1}\mathbf{F} = [\mathbf{B}]^{-1}[\mathbf{W}]^{-1}\mathbf{F} = \begin{bmatrix} \mathbf{W}_1^{*T}\mathbf{S}_1 & & \mathbf{0} \\ & \ddots & \\ \mathbf{0} & & \mathbf{W}_n^{*T}\mathbf{S}_n \end{bmatrix} [\mathbf{W}]^{-1}\mathbf{F} \qquad (2.19)$$

Once again, the matrix inversion in the above equation would not normally be carried out since methods of solving simultaneous linear equations are computationally far more efficient than actual matrix inversion.

Chapter 3

Dexterity and Singular Configurations

3.1 Dexterity and Manipulability

Several measures of *dexterity* or *manipulability* quantifying the kinematic performance of manipulators have been proposed to assess the optimality of both manipulator designs and their postures. Two distinct classes of dexterity measures exist. The first class of dexterity measures is concerned with the positional range of motion of a manipulator and its various joints. These *geometric dexterity measures* are based on the ability of the robot to arbitrarily orient its end effector about a point or by the joint ranges of motion available before encountering a joint limit. The second class of dexterity measures is concerned with quantifying the instantaneous kinematic characteristics of the manipulator and hence are termed *kinematic dexterity measures.* Both classes of dexterity measures contain indices which apply to a given posture of a manipulator or to any spatial segment of the manipulator's workspace. Dexterity measures which are used to assess the quality of a manipulator posture are termed *local dexterity measures* and those which quantify dexterity throughout the whole or a

portion of the workspace are termed *global dexterity measures.* In general, kinematic dexterity measures are defined in order to quantify local dexterity whereas geometric dexterity measures can be either local or global in nature. However, through integration over the workspace, any local dexterity measure can be used to quantify the global dexterity of a manipulator.

3.1.1 Geometric Dexterity Measures

As a first attempt to assess the geometric performance capabilities of manipulators Vinogradov, et al. [54] introduced the concept of the *service angle.* The service angle, as defined in later work by Yang and Lai [59], is the total range of the approach angle of a manipulator's end effector around a reachable point in space. Yang and Lai examine this concept in order to characterize the dexterity of wrist-partitioned serial-chain manipulators at a point in its workspace. This local dexterity measure is of significant value when designing and analyzing manipulators requiring large orientational freedoms of motion. Unfortunately, the determination of a manipulator's service angle is not a simple matter due to joint displacement limits and the multi-dimensional nature of end effector orientation. This is especially true when extending the concept to include closed-chain parallel and hybrid manipulators.

Similar in concept to the service angle is the concept of a *dexterous workspace* introduced by Kumar and Waldron [27]. The dexterous workspace is the portion of the workspace in which the end effector may assume any orientation. Therefore, the ratio of dexterous workspace volume to the reachable workspace volume is a measure of the global dexterity of a manipulator. Limits on joint displacements usually precludes the existence of a dexterous workspace for actual manipulator structures. However, the concept remains useful in the theoretical design and analysis of manipulator structures

such as the geometric optimization of six degree-of-freedom, revolute jointed, serial-chain manipulators performed by Vijaykumar et al. [53]. Closed-chain manipulators in general cannot possess full rotatability of their end effectors and therefore do not have a dexterous workspace due to branch interference as well as joint displacement limits. Nevertheless, a theoretical optimization ignoring mechanical limitations can be carried out to maximize the fraction of a closed-chain manipulator's workspace which is dexterous. It is doubtful whether such an optimization would produce meaningful results when applied to the design of an actual manipulator since mechanical limits affect the workspace size and shape of closed-chain devices to a much larger degree than that of open-chain devices.

A final geometric dexterity measure is *joint range availability.* This local dexterity measure was first introduced by Liégeois [29] to automatically reconfigure the distribution of joints angles for a task redundant robot so that the possibility of encountering a joint limit is minimized. The joint range availability is defined as the Euclidean, or 2 norm of the vector of joint displacements from their centres of travel. The joint displacements are usually scaled to reflect differing ranges of travel available from each joint. This dexterity measure was later used by Klein and Huang [24] for examining the properties of modified and non-modified pseudoinverse control of planar redundant manipulators. The work also investigated the use of other p-norms of the joint displacement vector, such as the ∞ norm, and the effects of these norms on the stability of the joint rate solutions. As demonstrated in these works, the joint range availability is a useful tool in the control and planning of redundant manipulation tasks. However, the measure is unfit for use as a primary design criteria since optimizing the joint displacement distribution for a desired posture simply requires the resetting of the joint centres of travel.

3.1.2 Velocity and Force Ellipsoids

As previously mentioned, kinematic dexterity measures are local dexterity measures quantifying the instantaneous kinematic characteristics of a manipulator. As such, the measures are based upon the mappings between joint rates and end effector rates, and the mappings between joint wrench intensities and end effector wrench intensities. Examination of equations (2.11) and (2.16) show that the matrix [**K**] and its complemented transpose describe these mappings for a generalized hybrid manipulator. For serial, open-chain manipulators, these instantaneous transforms can be simplified, resulting in the standard Jacobian matrix formulations. The Jacobian matrix [**J**] and its complemented transpose describe the instantaneous mappings as outlined below:

Forward Velocity Solution

$$\mathbf{V} = \left\{ \begin{array}{c} \omega \\ \mathrm{v} \end{array} \right\} = [\mathbf{J}]\,\dot{\mathbf{q}} \tag{3.1}$$

Inverse Static Force Solution

$$\boldsymbol{\tau} = [\mathbf{J}]^T \left\{ \begin{array}{c} \mathrm{m} \\ \mathrm{f} \end{array} \right\} = [\mathbf{J}]^T \mathbf{F}^* = [\mathbf{J}^*]^T \mathbf{F} \tag{3.2}$$

Therefore, kinematic dexterity measures are based upon characteristics of the matrices [**J**] and [**K**] for serial and hybrid manipulators respectively. Note that the columns of the Jacobian matrix for serial, open-chain manipulators [**J**] are the screw coordinates of the corresponding joints.

To best understand the physical meaning of the kinematic dexterity measures, it is helpful to view the manipulator as a multi-input, multi-output mechanical transformer. The inputs are the joint rates and actuator wrench intensities, and the outputs are the task space velocity and end effector wrench. The force and velocity transmission characteristics can be represented as ellipsoids defined by the singular values and

associated basis vectors from the singular value decomposition[1] of the corresponding instantaneous transformation matrix.

The Velocity Ellipsoid

The transformation from joint rates to end effector output velocity can be characterized in terms of a *velocity transmission ratio* for a desired motion direction. The velocity transmission ratio is defined as the ratio of the magnitude of the output velocity in m-dimensional space to the magnitude of the n input velocities or joint rates,

$$T_V = \frac{\| \mathbf{V} \|}{\| \dot{\mathbf{q}} \|} \tag{3.3}$$

These input and output quantities are related by the $m \times n$ $(n \geq m)$ instantaneous transformation matrix $[\mathbf{M}]$.

$$\mathbf{V}_{m\times 1} = [\mathbf{M}]_{m\times n} \dot{\mathbf{q}}_{n\times 1} \tag{3.4}$$

In the case where the manipulator has a serial-chain architecture, this transformation matrix is equivalent to the manipulator's Jacobian matrix. If the manipulator has a parallel or hybrid structure, the transformation takes on the form $[\mathbf{K}^*]^{-T}$, the inverse of matrix $[\mathbf{K}^*]^T$ defined in equation (2.11). Performing a singular value decomposition of $[\mathbf{M}]$ results in the following:

$$[\mathbf{M}] = [\mathbf{U}]\,[\mathbf{\Sigma}]\,[\mathbf{V}]^T = \begin{bmatrix} \mathbf{u}_1 & \cdots & \mathbf{u}_m \end{bmatrix} \begin{bmatrix} \sigma_1 & & \mathbf{0} \\ & \ddots & \\ \mathbf{0} & & \sigma_m \end{bmatrix} \begin{bmatrix} \mathbf{v}_1 & \cdots & \mathbf{v}_n \end{bmatrix}^T \tag{3.5}$$

The singular values σ_i give the lengths, and the basis vectors $\mathbf{u}_i$ the directions, of the semi-axes of an ellipsoid $\mathcal{E}_V$ defined by

$$\mathcal{E}_V = \{\mathbf{V} \mid \mathbf{V} = [\mathbf{M}]\,\dot{\mathbf{q}},\ \|\dot{\mathbf{q}}\| = 1\} \tag{3.6}$$

[1] See Appendix B for a short introduction to the singular value decomposition and its properties.

This ellipsoid is termed the *velocity ellipsoid.* For a manipulator capable of full six degree-of-freedom motion ($m = 6$) this ellipsoid will be a hyperellipsoid in six dimensional space. Figure 3.1 depicts an ellipsoid for the case when $m = 3$ as is the case for general translational or spherical motion. Since the surface of the velocity ellipsoid is defined by the points where $\| \dot{\mathbf{q}} \| = 1$, the distance from the centre of the ellipsoid to the surface of the ellipsoid in any direction represents the velocity transmission ratio in the same direction in task space. Therefore, the major axis of the ellipsoid represents the direction in which the velocity transmission ratio is at a maximum, the value of the transmission ratio being given by the maximum singular value $\sigma_{max} = \sigma_1$. Conversely, the minor axis of the ellipsoid corresponds to the direction with the minimum velocity transmission ratio, the numerical value of the transmission ratio being equal to the minimum singular value $\sigma_{min} = \sigma_m$.

A large velocity transmission ratio allows the generation of large task space velocities from relatively small joint rates. Unfortunately, this generally desirable amplification must be accompanied by an identical amplification in the joint displacement errors since differential displacements are related by the same instantaneous transformation as those for the velocities.

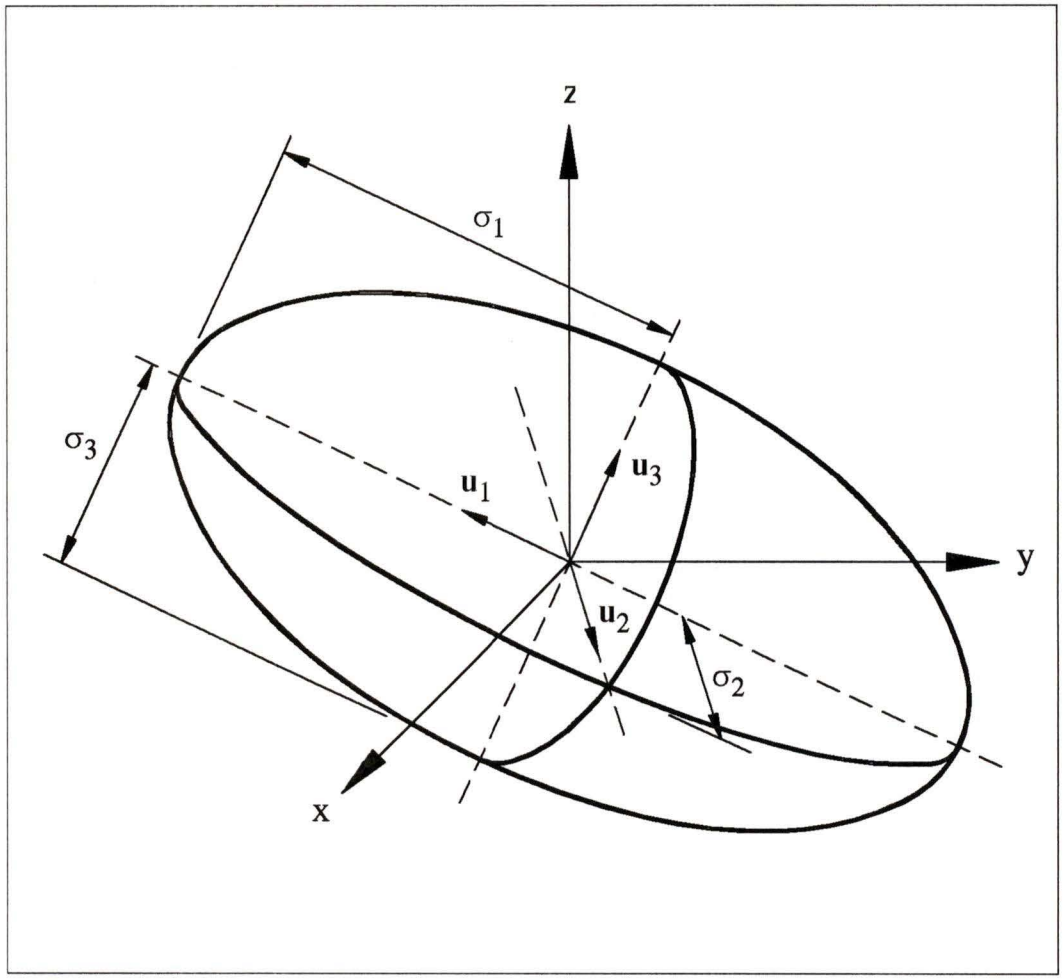

Figure 3.1: Ellipsoid with Associated Basis Vectors and Singular Values in three dimensions

The Force Ellipsoid

Analogous to the velocity transmission ratio, a *force transmission ratio* can be defined to characterize the force transmission characteristics of a manipulator in a given posture. The force transmission ratio for a desired task-space direction is defined as the ratio of the output wrench intensity in this direction in m-dimensional space to the magnitude of the n input wrench intensities at the joints required to generate it,

$$T_F = \frac{\| \mathbf{F} \|}{\| \boldsymbol{\tau} \|} \tag{3.7}$$

These input and output wrench intensities are related by the $m \times n$ ($n \geq m$) instantaneous transformation matrix $[\mathbf{N}]$.

$$\mathbf{F}_{m\times 1} = [\mathbf{N}]_{m\times n} \boldsymbol{\tau}_{n\times 1} \tag{3.8}$$

In the case where the manipulator has a serial-chain architecture, this transformation matrix is equivalent to the complemented, inverse transpose of the manipulator's Jacobian matrix $[\mathbf{J}^*]^{-T}$ (see equation (3.2)). If the manipulator has a parallel or hybrid structure, the transformation matrix is equivalent to the matrix $[\mathbf{K}]$ of equation (2.16). Performing a singular value decomposition of the matrix $[\mathbf{N}]$ gives

$$[\mathbf{N}] = [\mathbf{U}]\,[\boldsymbol{\Sigma}]\,[\mathbf{V}]^T = \begin{bmatrix} \mathbf{u}_1 & \cdots & \mathbf{u}_m \end{bmatrix} \begin{bmatrix} \sigma_1 & & \mathbf{0} \\ & \ddots & \\ \mathbf{0} & & \sigma_m \end{bmatrix} \begin{bmatrix} \mathbf{v}_1 & \cdots & \mathbf{v}_n \end{bmatrix}^T \tag{3.9}$$

The singular values σ_i gives the lengths, and the basis vectors $\mathbf{u}_i$ the directions, of the semi-axes of an ellipsoid $\mathcal{E}_F$ defined by

$$\mathcal{E}_F = \{\mathbf{F} \mid \mathbf{F} = [\mathbf{N}]\,\boldsymbol{\tau},\ \|\boldsymbol{\tau}\| = 1\} \tag{3.10}$$

This ellipsoid is termed the *force ellipsoid.* For a manipulator capable of sustaining or applying arbitrary forces and moments ($m = 6$) the force ellipsoid will be a hyperellipsoid in six dimensional space. An ellipsoid for the case when $m = 3$, such as for a manipulator required to produce only forces in three dimensions, is given in Figure 3.1. Similarly to the velocity ellipsoid, the distance from the centre of the force ellipsoid to its surface in any direction represents the force transmission ratio in the same direction in task space. In general, a large force ellipsoid indicates that the manipulator can generate large wrench intensities at the end effector with relatively small outputs from the actuators. Once again, this desirable effect of a large force transmission ratio must also be accompanied by a corresponding increase in the amplification of joint torque/force errors, resulting in a reduction in the resolution of force control capability.

Relationships Between Force and Velocity Ellipsoids

Table 3.1 summarizes the instantaneous transforms and associated matrices which determine the characteristics of the velocity and force ellipsoids for both open-chain and closed-chain manipulator types. For a given manipulator type, it is easily seen that the instantaneous transformation matrix associated with either the velocity or force ellipsoid is the complemented, inverse transpose of the instantaneous transform matrix associated with the other ellipsoid,

$$[\mathbf{N}] = [\mathbf{M}^*]^{-T} \quad \text{and} \quad [\mathbf{N}^*]^{-T} = [\mathbf{M}] \tag{3.11}$$

We would like to determine the relationships between the singular values and basis vectors of $[\mathbf{M}]$ and $[\mathbf{N}]$.

	Velocity Ellipsoid	Force Ellipsoid
Instantaneous Transformation	$\mathbf{V} = [\mathbf{M}]\,\dot{\mathbf{q}}$	$\mathbf{F} = [\mathbf{N}]\,\boldsymbol{\tau}$
Open-Chain Transformation Matrix	$[\mathbf{M}] = [\mathbf{J}]$	$[\mathbf{N}] = [\mathbf{J}^*]^{-T}$
Closed-Chain Transformation Matrix	$[\mathbf{M}] = [\mathbf{K}^*]^{-T}$	$[\mathbf{N}] = [\mathbf{K}]$

Table 3.1: Instantaneous transforms and associated matrices defining velocity and force ellipsoids

As given by equation (3.5), the singular value decomposition of $[\mathbf{M}]$ results in

$$[\mathbf{M}] = [\mathbf{U}]\,\mathrm{diag}\,(\sigma_1, \ldots, \sigma_m)\,[\mathbf{V}]^T \tag{3.12}$$

where diag$(\cdot)$ represents a diagonal matrix with the values in the parentheses on the main diagonal. Complementing the above decomposition gives

$$[\mathbf{M}^*] = [\mathbf{U}^*]\,\mathrm{diag}\,(\sigma_1, \ldots, \sigma_m)\,[\mathbf{V}]^T \tag{3.13}$$

and transposing gives

$$[\mathbf{M}^*]^T = [\mathbf{V}]\,\mathrm{diag}\,(\sigma_1, \ldots, \sigma_m)\,[\mathbf{U}^*]^T \tag{3.14}$$

finally, taking the inverse of the above results in

$$[\mathbf{M}^*]^{-T} = [\mathbf{U}^*]\,\mathrm{diag}\left(\frac{1}{\sigma_1}, \cdots, \frac{1}{\sigma_m}\right)[\mathbf{V}]^T = [\mathbf{N}] \tag{3.15}$$

Comparing the decompositions of $[\mathbf{M}]$ and $[\mathbf{M}] = [\mathbf{M}^*]^{-T}$ given by equations (3.12) and (3.15) shows that the singular values associated with the force ellipsoid are identical to the reciprocals of those associated with the velocity ellipsoid. Furthermore, the column space basis vectors of the force ellipsoid are in the same directions as those of the velocity ellipsoid if we associate forces with translational velocities and moments with angular velocities. This association is the inverse association normally attributed to screw quantities, the inversion being signified by the complement of $[\mathbf{U}]$ in the decomposition of equation (3.15). The inversion of subspaces is due to the reciprocity that exists between force and velocity screw systems.

The relations between the singular values and basis vectors of the velocity and force transformations described in the previous paragraph are consistent with the modelling of a manipulator as a mechanical transformer. Conservation of energy necessitates that an amplification in linear/angular velocity transmission must be accompanied by an identical reduction in force/moment transmission in the same direction in task space. This means that the direction of maximum velocity transmission ratio is also the direction of minimum force transmission ratio and vise versa. This inverse velocity-force relation also applies between angular velocities and moments.

3.1.3 Kinematic Dexterity Measures

In the discussion below, the Jacobian matrix for serial-chain manipulators will be used to describe the kinematic dexterity measures since the measures were first introduced to quantify the dexterity of this class of manipulators. However, the measures are universally applicable to all types of open and closed chain manipulators by simple substitution of the corresponding matrix describing the instantaneous kinematic transform being investigated.

The first kinematic dexterity measure is simply the determinant of the Jacobian matrix. This measure is only applicable in the case where the manipulator is non-redundant and the Jacobian matrix is square. Paul and Stevenson [40] used the determinant to evaluate the performance of nonredundant wrists. In particular, the determinant of the wrist's Jacobian matrix was used as a measure of the degree of closeness to singular points in the wrist's working range of motion.

Yoshikawa [60] extended the concept of the determinant to include cases where the manipulator is redundant and the Jacobian matrix is no longer square. By noting that the absolute value of the determinant of a square matrix is identical to the product of the singular values of the matrix, Yoshikawa defined what he termed a *manipulability* measure based on this same product. The product of the singular values can also be calculated as

$$w = \sigma_1 \sigma_2 \cdots \sigma_m = \sqrt{\det\left([\mathbf{J}]\,[\mathbf{J}]^T\right)} \tag{3.16}$$

Geometrically, this product is linearly proportional to the volume of the velocity ellipsoid, thereby giving a measure indicating the average velocity transmission ratio in all task space directions. In general, the larger the volume of the velocity ellipsoid, the larger the task space velocity for a given set of joint rates. If one of the singular values approaches zero the volume of the velocity ellipsoid, and hence the manipulability measure, also approach zero. The presence of a singularity is signaled by the value of the manipulability measure nearing zero. However, as pointed out by Forsythe and Moler [11], the value of the determinant or product of singular values is not a meaningful measure of the invertibility, or degree of ill-conditioning of a matrix. This limits the use of the determinant or manipulability measure to being an average measure of velocity transmission ratio and not a measure of closeness to a singularity.

A second kinematic dexterity measure is the ratio of the largest and smallest singular values of the Jacobian matrix,

$$\kappa = \frac{\sigma_{max}}{\sigma_{min}} = \frac{\sigma_1}{\sigma_m} \tag{3.17}$$

This ratio, which is termed the Euclidean *condition number* of the matrix, is commonly used by numerical analysts to quantify the sensitivity of linear systems and to sensibly deal with the concept of matrix rank while employing finite precision computations [12].

The concept of the condition number was first applied to manipulator design and analysis by Salisbury and Craig [48] to optimize the finger dimensions for an articulated hand. In this work the condition number of the Jacobian matrix was used as an accuracy measure bounding the relative amplification of errors between joint torques and finger-tip forces. However, as demonstrated by Chiu [7], the condition number is not a measure of accuracy in either the force or position control ability of an actuated mechanism. As shown in the previous section, the force and velocity transmission ratios determine the amplifications between inputs and desired outputs, and outputs due to errors at the inputs. The condition number is a measure of the sensitivity of a linear system to round-off errors during numerical inversion as demonstrated by Forsythe and Moler [11]. This form of error is generally of little interest to designers and analysts of robotic mechanisms.

In the context of manipulator kinematics, the condition number of the Jacobian matrix indicates the uniformity of the force and velocity transmission characteristics of the manipulator with respect to different task space directions. Geometrically, this is equivalent to the degree of roundness of the velocity and force ellipsoids. For example, if the condition number of the Jacobian matrix attains its minimum value

of one, all of the singular values are identical, the velocity and force ellipsoids are perfect spheroids, and the manipulator has uniform characteristics in all directions in task space in terms of the norms of joint and end effector forces and velocities. A manipulator configuration with a condition number of one is termed an *isotropic* [48] manipulator configuration due to this directional uniformity of instantaneous kinematic characteristics.

Klein and Blaho [25] reviewed the geometric and kinematic dexterity measures described above and proposed a new measure. Examining the determinant and condition number in terms of their singular values, they noted that both measures are critically dependent on the minimum singular value of the Jacobian matrix. Through further investigation they also found that for serial-chain manipulators the minimum singular value changes more radically near singularities than do the other singular values, consequently dominating the behaviour of the condition number and the determinant. This behavior of the minimum singular value motivated Klein and Blaho to suggest the minimum singular value as a measure of dexterity.

Geometrically, the minimum singular value of the Jacobian matrix is the minimum radius of the velocity ellipsoid signifying the minimum velocity transmission ratio from all task space directions. Therefore, the minimum singular value represents the maximum velocity the end effector can be moved in any arbitrary direction relative to the norm of the joint rates. Viewed in a different manner, the reciprocal of the minimum singular value places an upper bound on the joint velocities relative to the task space velocity. As a result of these characteristics, it is generally preferable that the manipulator be in a configuration which maximizes the minimum singular value.

Researchers have also proposed other dexterity measures based on the singular values of the Jacobian matrix. Among these are the arithmetic or geometric means of the singular values. The arithmetic mean of the singular values along with the condition number of the Jacobian matrix was employed by Asada and Cro Granito [4] as a dexterity measure used in optimizing the kinematic performance of three degree-of-freedom wrist joints. No geometric interpretation of the arithmetic mean of the singular values other than the fact that it represents the average length of the semi-axes of the velocity ellipsoid was given in the work.

Yoshikawa [62] suggested the geometric mean of the singular values as a dexterity measure,

$$w_{gm} = (\sigma_1 \sigma_2 \cdots \sigma_m)^{\frac{1}{m}} \tag{3.18}$$

This measure is equivalent to the radius of a spheroid whose volume is equal to that of the velocity ellipsoid. However, since the measure is simply the m'th root of Yoshikawa's original manipulability measure [60], optimizations or comparisons of different manipulator configurations based on this new measure would give the same results as those given by the original measure.

3.1.4 Unit and Frame Variability of Kinematic Dexterity

In the previous section several kinematic dexterity measures based upon the singular values of the manipulator's instantaneous transformation matrices were described. However, the variability of the singular values, and therefore the dexterity measures themselves, due to changes in units of measure and coordinate frames of reference were not considered. These important considerations require careful examination in order for the dexterity measures to have meaningful physical interpretations.

As demonstrated in Section 2.2, the instantaneous transformation matrices for any manipulator of general structure can be considered to be made up of rows or columns of screw coordinates describing the freedoms and constraints of the mechanism in a given configuration. The primary vectors of the screw coordinates[2] are unitless since they describe the direction of the screw axes. The secondary vectors have units of length because they describe the distance the screw axes are from the origin of the frame of reference along with the linear pitches of the screws. As a consequence of this mix of units associated with screw coordinates, the instantaneous transformation matrices also have elements with differing units. Some of the elements of the matrices will be unitless while others will be associated with units of length. This fact can also be verified by noting that the instantaneous mappings between joint and task spaces involve mappings between mixed unit quantities, the units differing only by length. For a dexterity measure based upon instantaneous transformation matrices to have physical meaning, the measure of length must be chosen to allow the "perceived cost" of angular versus translational velocities and forces versus moments to be reflected. Choosing a shorter measure of length emphasizes translational and moment related terms, while conversely a longer measure of length emphasizes rotational and force related terms. Most commonly the measure of length will be based upon a characteristic length of the manipulator such as the distance from the last joint to the tip of the end effector for a serial-chain manipulator.

The instantaneous transformation matrices of a manipulator can be expressed with respect to any desired frame of reference. This is accomplished by writing the screw coordinates upon which the transformation matrices are based with respect to the same desired frame of reference. A rotation of the frame of reference does not

[2]See Appendix A for an overview of screw quantities and screw coordinates

alter the singular values of an instantaneous transformation matrix since the associated screw transform is an orthogonal operator in this case. A purely translational displacement in the frame of reference location affects only the secondary vector of the screw coordinates comprising the instantaneous transformation matrices. Therefore, the singular values of the matrices and consequently the dexterity measures based upon them are affected by displacements in the origin of the frame of reference. This result demonstrates that kinematic dexterity measures are not frame invariant. Kinematic dexterity measures characterize the instantaneous ability of a manipulator to reposition and reorient the end effector of a manipulator about the origin of the chosen frame of reference. It is therefore essential to place the origin of the frame of reference at a point of significance in terms of the manipulation operations to be performed by the device being analyzed.

3.2 Singular Configurations

The consideration of singular configurations is of significant importance in the design of manipulators of any structure. Singular configurations are special configurations of a manipulator where the instantaneous transformations between joint space and end effector space become singular and therefore non-invertible. These transformations include both the transformations between joint rates and end effector velocities as well as the transformations between joint wrench intensities and end effector wrenches. Singular configurations of serial open-chain manipulators have been extensively studied and are generally well understood. In this case, the effect of a manipulator entering a singular configuration is that the manipulator suffers from a loss in instantaneous motion freedom at its end effector. In the case of a fully-parallel or hybrid manipu-

lator, the manipulator may lose or gain an instantaneous motion freedom at its end effector when in a singular configuration [16, 20]. The existence of two distinctly different types of singular configurations is a trait specific to closed-chain mechanisms and warrants further examination of their causes and characteristics.

3.2.1 Stationary Configurations

The first type of singular configuration for a closed-chain mechanism or manipulator is one in which the device loses an instantaneous motion freedom in task space. This type of singular configuration is termed a *stationary configuration* [20] due to the loss of motion capability.

Stationary singular configurations are caused by a degenerate alignment of the joints of an individual serial-chain branch of the closed chain. The joints of a branch define a screw system Ψ_{jt} of possible branch end velocities. In a non-degenerate configuration the order of Ψ_{jt} is six for a branch capable of spatial motion. In a degenerate configuration the order of Ψ_{jt} is less than six and a screw system Γ_{jt} reciprocal to Ψ_{jt} (order $\{\Gamma_{jt}\} = 6 -$ order $\{\Psi_{jt}\}$) will exist. Since the branch end is constrained to motions belonging to Ψ_{jt}, the degenerate branch, and therefore the manipulator, have lost one or more instantaneous motion freedoms. The branch end and the manipulator's end effector is no longer capable of instantaneous motions which would perform work if the end effector was subjected to a wrench acting on the screws of Γ_{jt}. Consequently, a wrench of arbitrary intensity acting on the screws of Γ_{jt} applied at the end effector requires no actuator outputs to equilibrate the applied load. The mechanical structure of the branch carries the load in place of the actuators. This type of singularity is identical to that encountered with a serial manipulator where the Jacobian matrix becomes rank deficient due to the joint screws

of the manipulator becoming linearly dependent.

The presence of stationary singular configurations also affects the behaviour of a manipulator in regions near the singular points. As a stationary configuration is approached, a reciprocal product $\mathbf{W}_k \chi \mathbf{S}_k$ associated with an active or passive joint k rapidly declines towards a zero value. Recall the following joint rate solution from Chapter 2:

$$\dot{q}_k = \frac{\mathbf{W}_k \chi \mathbf{V}}{\mathbf{W}_k \chi \mathbf{S}_k} \tag{3.19}$$

From this equation it can be seen that for an instantaneous end effector motion $\mathbf{V}$ which is not reciprocal to $\mathbf{W}_k$, $\dot{q}_k$ becomes exceedingly large. This may pose less of a problem if joint k is a passive joint. However, if joint k is an active joint, the motion may not be possible since $\dot{q}_k$ will be bounded to remain below a certain absolute value as determined by the characteristics of the actuator.

The instantaneous transformation matrices developed in Section 2.2 will also show traits illustrating the proximity of a stationary configuration if joint k is an active joint. The declining value of a reciprocal product $\mathbf{W}_k \chi \mathbf{S}_k$ results in the reciprocal product matrix $[\mathbf{B}]$ of equation (2.10) having an entry on its diagonal tending to infinity. As a consequence, $[\mathbf{K}^*]^T$ will have a singular value tending to infinity, demonstrating the possibility of large joint rates for some end effector motions. The declining reciprocal product value also influences the inverse static force solution of equation (2.19). Since $[\mathbf{K}^*]^T$ has a singular value tending to infinity, $[\mathbf{K}]^{-1}$ will have a singular value approaching zero. This demonstrates that for certain end effector loads, all joint wrench intensities required to equilibrate the load will tend toward zero values. In other words, load is essentially resisted by the mechanical structure of the manipulator and not by the actuators at the joints.

Finally, stationary singular configurations can be described as points where different solution branches of the inverse displacement problem described in Section 2.1.1 meet. Inverse displacement solution branch points occur along the workspace boundary of the manipulator branches and can also occur at positions within their workspaces depending upon branch structure. A manipulator at or near a stationary configuration can suffer from a discontinuity in joint rates due to the inverse displacement solution changing solution branches if steps are not taken to avoid it.

The non-uniqueness of manipulator inverse displacement solutions is caused by the multiplicity of branch inverse displacement solutions for each branch of the manipulator. Therefore, for certain manipulator architectures such as the Stewart platform, stationary singular configurations do not exist since the branches posses only a single inverse displacement solution for each branch end position.

3.2.2 Uncertainty Configurations

The second type of singular configuration is one in which the mechanism or manipulator gains an uncontrollable instantaneous motion freedom in task space. This type of singular configuration can only occur with closed-chain devices and is termed an *uncertainty configuration* [20].

For a manipulator to remain controllable, the end effector must be constrained in all translational and rotational directions in space when the actuators are locked in fixed positions. These constraints can either come from the physical structure of the device or from the actuators used to controllably alter the position and orientation of the end effector. In the case of a six degree-of-freedom manipulator, all constraints immobilizing the end effector must in general be provided by the actuators.

For a six degree-of-freedom hybrid manipulator, the screws representing the restraint directions available from the actuation of each active joint j are the screws $\mathbf{W}_j$ which are reciprocal to all joint screws in the branch except that associated with active joint j. These screws form the columns of the reciprocal screw matrix [**W**] as demonstrated in Section 2.2. The reciprocal screws must form a screw system Ψ_r of order six for the manipulator's end effector to remain fully constrained. In other words, the reciprocal screw matrix [**W**] must be of rank six. If the reciprocal screws become linearly dependent and form a system of five or less, the end effector will become capable of uncontrollable instantaneous motions belonging to the system of screws Γ_r reciprocal to Ψ_r even though the actuators remain locked in position. In such a circumstance the manipulator is said to be in an uncertainty configuration since the instantaneous motion the end effector may undergo is uncertain due to the lack of controllability.

Uncertainty configurations of closed-chain manipulators also affect the ability of the manipulator to sustain an arbitrary end effector loading. In order for a six degree-of-freedom hybrid manipulator to be capable of sustaining an end effector wrench **F**, **F** must belong to the system Ψ_r defined by the branch reciprocal screws $\mathbf{W}_j$. In a general configuration of the manipulator Ψ_r is of order six and spans the entire six-system of possible end effector wrenches allowing any arbitrary load (subject to the limits of actuation capability) to be carried. In an uncertainty configuration, the order of Ψ_r is reduced to five or less resulting in a system Γ_r reciprocal to Ψ_r. Any end effector load **F** not belonging to Ψ_r is unsustainable by the manipulator since the required restraining wrenches cannot be generated by the manipulator's actuators.

As a manipulator approaches an uncertainty configuration, the reciprocal screw matrix [**W**] becomes near singular by virtue of having a singular value near zero. This means that the inverse of the reciprocal screw matrix $[\mathbf{W}]^{-1}$ in the inverse static force solution of equation 2.19 has a singular value approaching infinity. Consequently, the joint wrench intensities for a wrench in the direction of the basis vector associated with this largest singular value will approach near infinite values as well. In essence this means that a manipulator operating near an uncertainty configuration is also incapable of supporting arbitrary loads at its end effector.

Finally, uncertainty configurations can be described as points where different solution branches of the forward displacement problem described in Section 2.1.2 meet. Consequently, a manipulator being near an uncertainty configuration can result in a forward displacement solution giving an end effector position and orientation on an improper solution branch. This incorrect result is only detectable through the examination of passive joint displacements from an inverse displacement analysis for all joints in the hybrid manipulator. If the incorrect forward displacement result is not detected, the displacement solution may proceed further down the incorrect solution branch as the manipulator continues to move. This can be disastrous for certain applications such as when a closed-chain or hybrid device is used as a master controller in master-slave teleoperation. In such an application the slave manipulator would move in seemingly random directions as the master controller is manipulated by the operator after the master controller's forward displacement solution has switched solution branches.

In conclusion of this section, it can be observed that the two different types of singular configurations of a hybrid manipulator can result in different portions of the instantaneous transforms becoming singular. In a stationary configuration the inverse of the reciprocal product matrix can become singular[3], while in an uncertainty configuration the reciprocal screw matrix becomes singular. Table 3.2 shows these results along with a summary of the instantaneous kinematic characteristics of a manipulator while being in each of the singular configuration types.

	SINGULARITY TYPE	
	STATIONARY	UNCERTAINTY
Singular Matrices	$[\mathbf{B}]^{-1} \rightarrow [\mathbf{K}]^{-1}, [\mathbf{K}^*]^{-T}$	$[\mathbf{W}] \rightarrow [\mathbf{K}], [\mathbf{K}^*]$
Motion Characteristics $\dot{\mathbf{q}} = [\mathbf{B}][\mathbf{W}^*]^T\mathbf{V}$ $= [\mathbf{K}^*]^T\mathbf{V}$	$\mathbf{V} = \mathbf{0}$ for some $\dot{\mathbf{q}}$	$\dot{\mathbf{q}} = \mathbf{0}$ for some $\mathbf{V}$
	$\dot{\mathbf{q}}$ nonexistent for some $\mathbf{V}$	$\mathbf{V}$ undetermined given $\dot{\mathbf{q}}$
Force Characteristics $\mathbf{F} = [\mathbf{W}][\mathbf{B}]\boldsymbol{\tau}$ $= [\mathbf{K}]\boldsymbol{\tau}$	$\boldsymbol{\tau} = \mathbf{0}$ for some $\mathbf{F}$	$\mathbf{F} = \mathbf{0}$ for some $\boldsymbol{\tau}$
	$\mathbf{F}$ undetermined given $\boldsymbol{\tau}$	$\boldsymbol{\tau}$ nonexistent for some $\mathbf{F}$

Table 3.2: Characteristics of hybrid manipulator singular configurations

[3]Note that the inverse of the reciprocal product matrix $[\mathbf{B}]^{-1}$ becomes singular as $\mathbf{W}_k \chi \mathbf{S}_k$ tends to zero for an actuated joint. Although not reflected in $[\mathbf{B}]^{-1}$, $\mathbf{W}_k \chi \mathbf{S}_k$ tending to zero for a passive joint also results in a stationary configuration.

Chapter 4

Stewart Platform Optimization

4.1 The Stewart Platform and its Modelling

The Stewart platform is a closed-chain fully-parallel manipulator having an end effector with six active degrees of freedom. This form of manipulator was first introduced by Stewart [51] in 1965 as an aircraft simulator drive mechanism. Today, the Stewart platform is almost exclusively used for all flight and other motion simulators. However, many researchers are beginning to investigate its use as a general manipulation device as noted in the introduction of this thesis.

4.1.1 Architecture and Geometric Model

The Stewart platform is comprised of two rigid bodies connected together by six actuated prismatic joints (legs). The stationary rigid body is referred to as the base and the moving rigid body is referred to as the platform. The base and platform are most commonly constructed such that the six actuator attachment points on each of the rigid bodies lie in a plane as depicted in Figure 4.1. In order to allow full six degree-of-freedom motion of the platform the linear actuators are connected to the platform by way of spherical joint groups and to the base by way of universal joints.

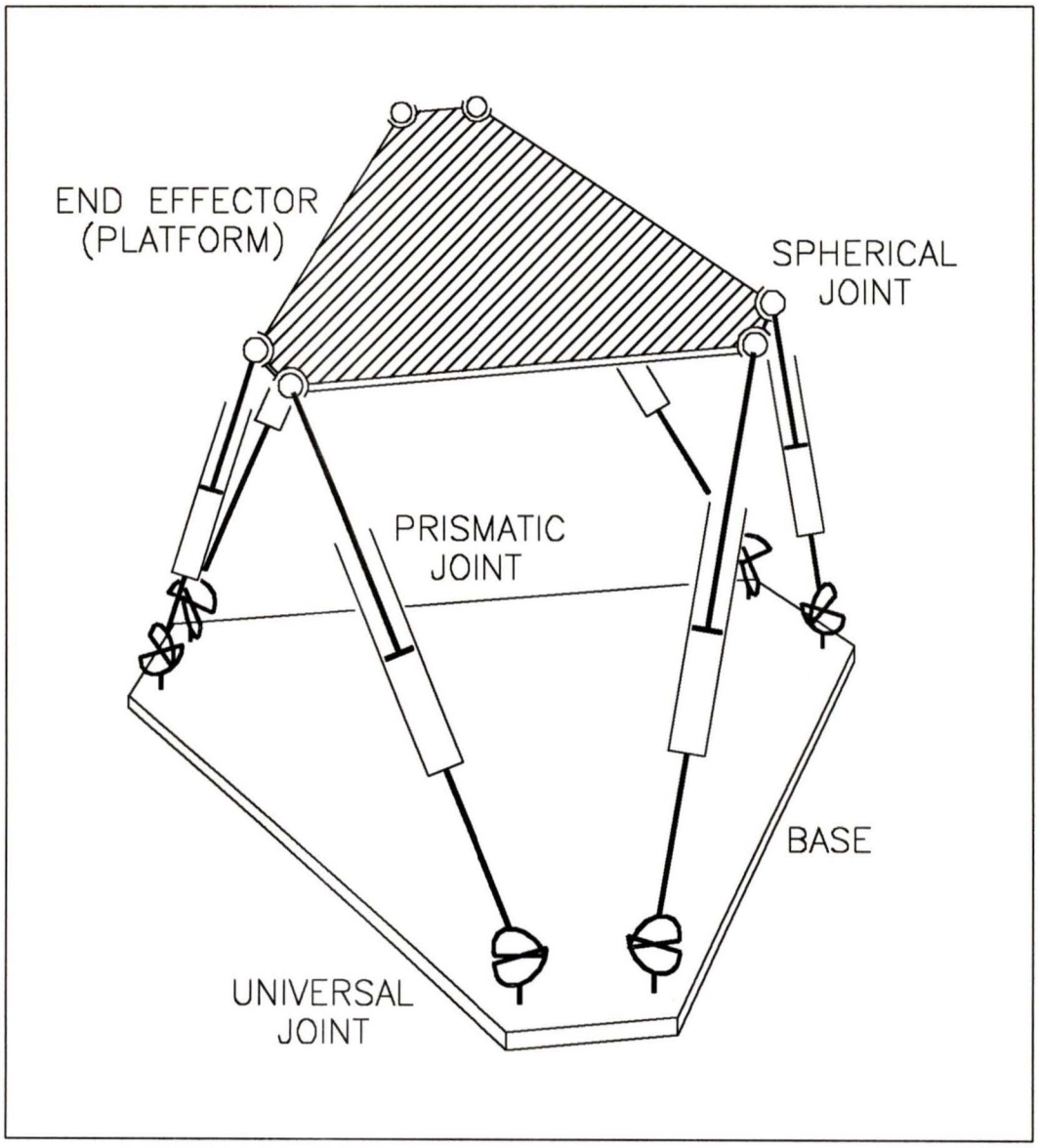

Figure 4.1: Architecture of the Stewart platform

By definition, the specific tasks to be performed by a manipulator are varied and are not known before its design and construction. This variability of tasks suggests the manipulator should have properties which are as homogeneous as possible. Therefore, as an initial step in design, the architecture of the manipulator should posses the highest degree of geometric symmetry possible. In order to achieve this symmetry, only architectures of the Stewart platform where the six actuator attachment points at the base and at the platform form semi-regular hexagonal planes are considered. With this architecture, the base and platform actuator attachment points can be considered to be distributed along the periphery of circles as illustrated in Figure 4.2. The base attachment points lie at the centres of the universal joints located at the base of each branch. The platform attachment points are at the centres of the spherical joints at the base distal end of each branch. The following geometric parameters describing the architecture of the manipulator arise out of this symmetric construction:

- r_b, the radius of the base circle which determines the size of the base.
- r_p, the radius of the platform circle which determines the size of the platform.
- ϕ_b, the half separation angle between adjacent actuator attachment points on the base.
- ϕ_p, the half separation angle between adjacent actuator attachment points on the platform.

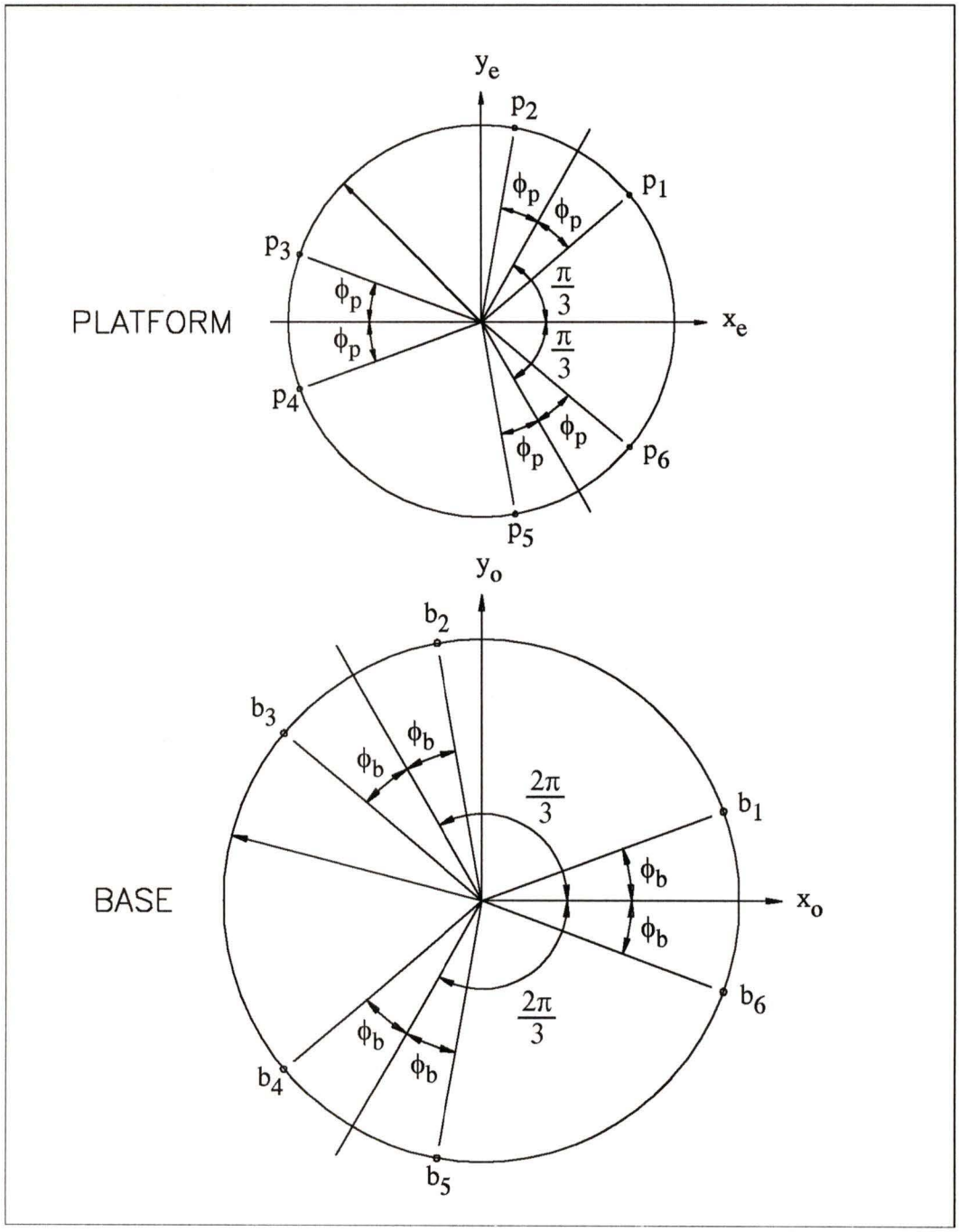

Figure 4.2: Base and platform actuator attachment points for a Stewart platform

4.1.2 Instantaneous Kinematic Modelling

The fully-parallel architecture of the Stewart platform represents one extreme of possible six degree of freedom hybrid manipulator architectures where only one joint in each of its six branches is actuated. Therefore, the instantaneous kinematic equations developed in Section 2.2 for a hybrid manipulator of general structure are applicable to the Stewart platform. To apply these results we require expressions for the reciprocal screws $\mathbf{W}_i$ and reciprocal products $\mathbf{W}_i \chi \mathbf{S}_i$ associated with each of the manipulator's actuated joints. These quantities make up the reciprocal screw and the reciprocal product matrices upon which the instantaneous transformations are based.

Each of the actuated prismatic joints of the Stewart platform can be represented by an infinite pitch screw along the sliding direction of the joint. The corresponding unit screw coordinates of the active joints are

$$\mathbf{S}_i = \left\{ \begin{array}{c} \mathbf{0} \\ \mathbf{l}_i \end{array} \right\} \quad ; \quad i = 1, \ldots, 6 \tag{4.1}$$

where $\mathbf{l}_i$ is a unit vector in the sliding direction of the prismatic joint. The vector $\mathbf{l}_i$ can be found by applying the inverse displacement solution of equation 2.3 in Section 2.1.1. Letting the orientation of the coordinate frames at the base of the branch be the same as that of the base frame (i.e., ${}^{o}[\mathbf{R}]_{b_i}$ is an identity matrix) the position of the branch end with respect to its base is

$${}^{b_i}\mathbf{p}_i = {}^{o}\mathbf{e} - {}^{o}\mathbf{b}_i + {}^{o}[\mathbf{R}]_e \, {}^{e}\mathbf{p}_i \tag{4.2}$$

where ${}^{o}\mathbf{b}_i$ and ${}^{e}\mathbf{p}_i$ are determined from the geometry of Figure 4.2. From ${}^{b_i}\mathbf{p}_i$, the actuated prismatic joint displacement and sliding direction with respect to the base frame are

$$q_i = \| {}^{b_i}\mathbf{p}_i \| \quad ; \quad {}^{o}\mathbf{l}_i = \frac{{}^{b_i}\mathbf{p}_i}{q_i} \tag{4.3}$$

The screw $\mathbf{W}_i$ reciprocal to all joints in each branch except for the actuated prismatic joint can be found by considering the screw systems formed by the passive spherical and universal joints. Reciprocal to a system of screws forming a spherical joint Ψ_{sph} is the three-system of all zero pitch screws passing through the centre of the spherical joint. Reciprocal to a system of screws forming a universal joint Ψ_{uni} is a four-system of screws. Reciprocal to both Ψ_{sph} and Ψ_{uni} is the zero pitch screw passing through the centres of both joint groups. Assuming the sliding directions of the prismatic joints pass through the respective centres of the spherical and universal joints in the same branch, the required reciprocal screws are

$$\mathbf{W}_i = \left\{ \begin{array}{c} \mathbf{l}_i \\ \mathbf{l}_{o_i} \end{array} \right\} \quad ; \quad i = 1, \ldots, 6 \tag{4.4}$$

where $\mathbf{l}_i$ are as defined in equation 4.3 with respect to the base frame and $\mathbf{l}_{o_i}$ is the moment of the screw axes about the origin of the frame of reference. These screw coordinates for the required reciprocal screws correspond to the normalized Plücker coordinates of the lines of action of the prismatic joints. The moment ${}^{o}\mathbf{l}_{o_i}$ can be expressed with respect to the base frame as

$${}^{o}\mathbf{l}_{o_i} = ({}^{o}[\mathbf{R}]_{e}\, {}^{e}\mathbf{p}_i) \times {}^{o}\mathbf{l}_i \tag{4.5}$$

Finally, we require expressions for the reciprocal products $\mathbf{W}_i \chi \mathbf{S}_i$ in the reciprocal product matrix. Forming the reciprocal product for each linear actuator gives

$$\mathbf{W}_i \chi \mathbf{S}_i = \left\{ \begin{array}{c} \mathbf{l}_i \\ \mathbf{l}_{o_i} \end{array} \right\} \chi \left\{ \begin{array}{c} \mathbf{0} \\ \mathbf{l}_i \end{array} \right\} = \mathbf{l}_i \cdot \mathbf{l}_i = \| \mathbf{l}_i \|^2 = 1 \tag{4.6}$$

Since the reciprocal products are equal to unity, the reciprocal product matrix $[\mathbf{B}]$ is an identity matrix and the instantaneous transformation matrix $[\mathbf{K}]$ is identical to the reciprocal screw matrix $[\mathbf{W}]$.

In summary, the inverse velocity and forward static force solutions for the Stewart platform are as follows:

Inverse Velocity Solution

$$\dot{\mathbf{q}} = \begin{bmatrix} \mathbf{W}_1^{*T} \\ \vdots \\ \mathbf{W}_6^{*T} \end{bmatrix} \mathbf{V} = [\mathbf{W}^*]^T \mathbf{V} = [\mathbf{K}^*]^T \mathbf{V} \tag{4.7}$$

Forward Static Force Solution

$$\mathbf{F} = \begin{bmatrix} \mathbf{W}_1 & \cdots & \mathbf{W}_6 \end{bmatrix} \boldsymbol{\tau} = [\mathbf{W}]\boldsymbol{\tau} = [\mathbf{K}]\boldsymbol{\tau} \tag{4.8}$$

where $\mathbf{W}_i$ are the normalized Plücker coordinates of the lines of action of the prismatic joints as previously described.

4.2 Stewart Platform Configuration Optimization

4.2.1 Objective and Stewart Platform Application

Configuration optimization is a local optimization which involves finding the manipulator architecture and end effector position and orientation which minimizes (or maximizes) the desired local performance measure. Since closed-chain manipulators like the Stewart platform are most suited to applications requiring relatively small workspaces and orientational freedoms of the end effector, there is little purpose in optimizing the manipulator configuration based upon geometric dexterity measures. Kinematic dexterity measures can be used to find manipulator configurations which provide optimum instantaneous kinematic characteristics. This is the approach that will be taken in the remainder of this work.

The condition number of the forward static force transformation matrix $[\mathbf{K}]$ will be used as an initial performance measure in optimizing the configuration of the Stewart

platform. Minimizing the condition number results in a manipulator with the highest degree of instantaneous kinematic isotropy for both force and velocity transmission since $[\mathbf{K}]$ and $[\mathbf{K}^*]^T$ have identical singular values (Section 3.1.2). The use of other kinematic dexterity measures will be discussed in Section 4.2.5.

As discussed in Section 3.1.4, the coordinate frame of reference used when calculating the elements of $[\mathbf{K}]$ affects the resulting values of kinematic dexterity measures. Configurations resulting from the minimization of the condition number will provide optimal dexterity at the end effector point coincident with the reference frame origin. As a logical point to begin with, the reference frame will be considered to be located at the centre of the platform plane as illustrated in Figure 4.2. In Section 4.2.6 the results are extended for a more general class of reference locations which are off the platform plane.

The Stewart platform is a six degree-of-freedom device and is therefore capable of generating or sustaining wrenches of arbitrary pitch at its end effector by forces produced at its linear actuators. Since a wrench of arbitrary pitch involves both units of force and units of moment, the force transformation matrix $[\mathbf{K}]$ will have elements with different units. The elements of $[\mathbf{K}]$ differ only by units of length. This can be verified by the fact that the primary vectors of the reciprocal screw coordinates which make up each of the columns of $[\mathbf{K}]$ are unitless, while the secondary vectors of the reciprocal screw coordinates have units of length. As noted in Section 3.1.4, the choice of length measure can be used to scale the relative importance of the force (angular velocity) related terms to that of the moment (linear velocity) related terms. To achieve this scaling a characteristic length can be chosen for the device and all quantities associated with length scaled with respect to it. If the radius of the platform is chosen as the desired characteristic length for the Stewart platform, the relative

importance or weighting of the force versus moment (angular versus linear velocity) terms will be equivalent[1]. Using the radius of the platform as a characteristic length of the manipulator (i.e., $r_p = 1$ length unit), yields the following nine independent parameters as the variables of the optimization:

- r_b, ϕ_b, ϕ_p, as defined earlier, describe the architecture of the manipulator.
- x_e, y_e, z_e define the position of the centre of the platform with respect to the centre of the base (${}^o\mathbf{e}$).
- α, β, γ (roll, pitch, yaw angles about x_o, y_o, z_o, respectively) define the orientation of the platform with respect to the base (${}^o[\mathbf{R}]_e$).

Note that each of the above length parameters (r_b, x_e, y_e, z_e) are normalized (represent ratios) with respect to the platform radius.

4.2.2 Local Optimization Results

The Simplex method of Nelder and Mead [37] was used to find the manipulator configuration(s) which minimize the condition number of the force transformation matrix $[\mathbf{K}]$. Depending on the initial values of the nine optimization variables, different optimal configurations of the Stewart platform were found. Manipulators having these configurations all had identical objective function values of $\kappa \approx 1.4142$. This objective function value is shown to be exactly $\kappa = \sqrt{2}$ in Section 4.2.3. All configurations

[1]This equivalency can be observed by examining the form of the Stewart platform force transformation matrix given by equation (4.12) of Section 4.2.3. This transformation matrix is based on using r_p as a characteristic length and a platform-plane centred frame of reference. Comparing the first three elements of any column (terms related to forces) to the last three elements of any column (terms related to moments) we see both always have unit magnitude.

with this minimum condition number were found to have $x_e = y_e = \alpha = \beta = \gamma = 0$, i.e., the platform was parallel to and only vertically displaced from the base.

Three configurations typifying the family of optimal configurations are depicted in Figure 4.3. In all cases the sliding directions of the linear actuators are tangent to the platform circle when projected onto a horizontal plane (e.g., the base plane). Furthermore, by noting the associated base radii and platform heights, it can be shown that the legs are angled at 45 degrees to the vertical for all optimum configurations. These conditions which define the entire family of locally optimum Stewart platform configurations can be expressed by the following relations:

$$x_e = y_e = \alpha = \beta = \gamma = 0 \tag{4.9}$$

$$r_b^2 = r_p^2 + z_e^2 = 1 + z_e^2 \tag{4.10}$$

$$\phi_b + \phi_p = \frac{\pi}{3} - \arccos\left(\frac{r_p}{r_b}\right) = \frac{\pi}{3} - \arccos\left(\frac{1}{r_b}\right) \tag{4.11}$$

These relations were found by considering the geometries of the configurations and applying simple geometric principles.

The conditions of equation (4.9) assign zero values to five of the nine variables of the optimization problem. This reduces the number of free variables to four, namely r_b, ϕ_b, ϕ_p, and z_e. The next condition (4.10) relates r_b and z_e, leaving only one of the two as a free variable (e.g., r_b) and only three free variables in total. The final condition (4.11) relates ϕ_b and ϕ_p to r_b leaving only one of the half separation angles as a free variable (e.g., ϕ_p). Therefore, these conditions in effect leave only two of the variables of the optimization as free variables. Both of these free variables can take on an infinite number of values while still maintaining the optimality of the manipulator configuration.

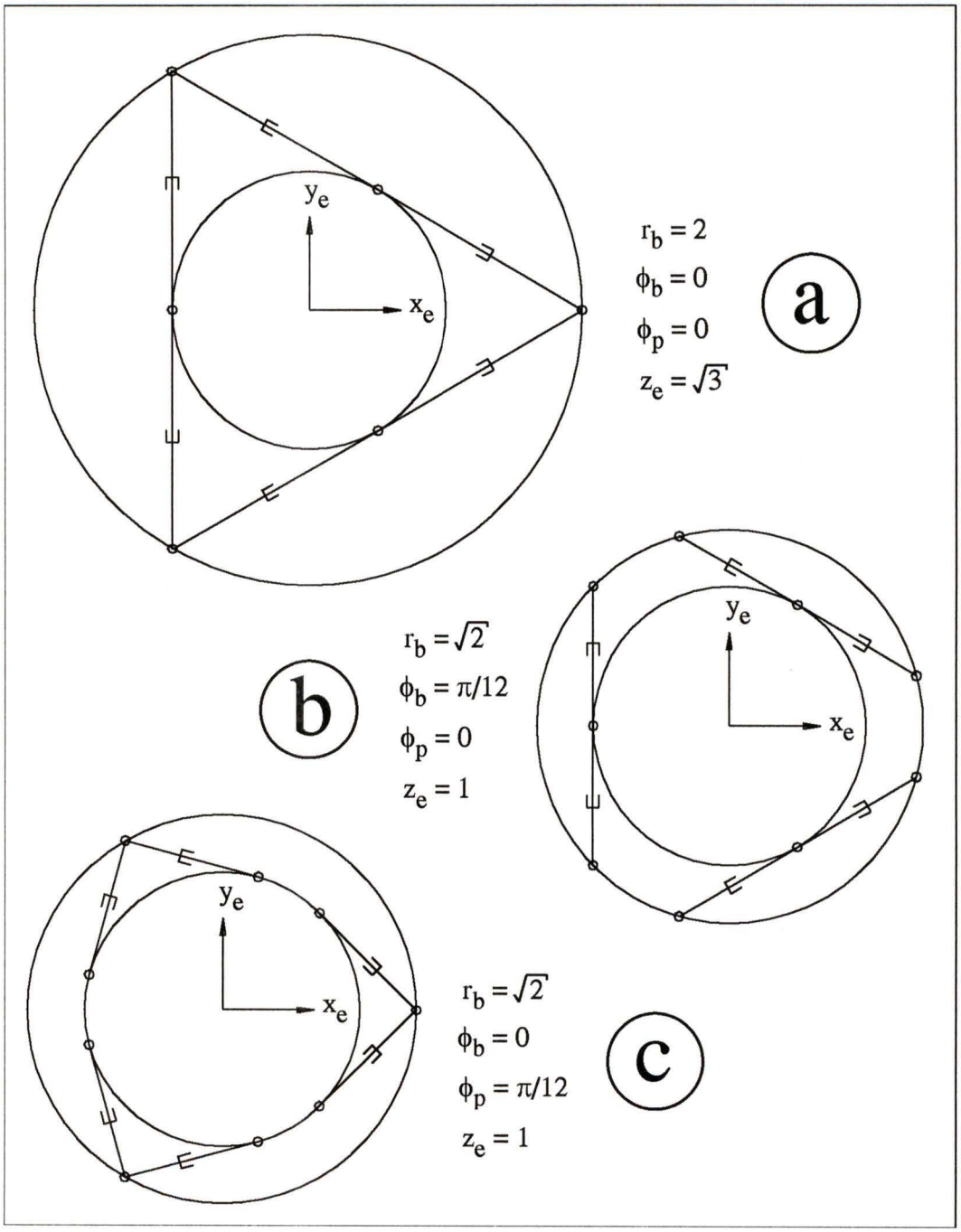

Figure 4.3: Typical optimal configurations of the Stewart platform (Top Views)

The first of our chosen free variables r_b allows the base size along with the platform height to be expanded or contracted for any fixed value of the second variable ϕ_p. In order to maintain optimality of the configurations the actuator separation angle in the base ϕ_b must be altered according to (4.11), and r_b and z_e must still related by (4.10). This variation is illustrated in configurations (a) and (b) of Figure 4.3. Since the legs are angled at 45 degrees to the vertical for all locally optimal configurations, the directions of each of the six legs will remain the same for all optimal configurations with the same platform actuator separation angle, ϕ_p. This results in their Plücker line coordinates, and hence their force transformation matrices [**K**], being identical. Since both the force and velocity instantaneous kinematic transformations are based upon the matrix [**K**], the two configurations can be termed *instantaneous kinematic equivalents* (Pittens and Podhorodeski [43]).

The second free variable, ϕ_p, allows the legs to be redistributed around the platform in a symmetric manner for fixed values of r_b and z_e. For the configurations to maintain optimality, ϕ_b and ϕ_p must sum to the fixed value given by (4.11). This second type of variation is illustrated in configurations (b) and (c) of Figure 4.3.

In combination with a uniform scaling of manipulator dimensions, there are effectively three free choices in the design of Stewart platforms possessing configurations with optimal dexterity. In other words, the conditions of (4.9), (4.10), and (4.11) define a three parameter family of Stewart platforms with optimal dexterity (Pittens and Podhorodeski [44]).

4.2.3 Independence of Singular Values with Respect to ϕ_p

The entire family of locally optimal configurations have identical singular values of their instantaneous transformation matrices. It is easy to see that configurations which are instantaneous kinematic equivalents will have identical singular values since their transformation matrices are identical. However, it is not evident that configurations with differing platform actuator separation angles will have the same singular values. This property is now rigorously demonstrated.

By considering the Plücker line coordinates of the prismatic joints and scaling using the platform radius as a characteristic length, the force transformation matrix $[\mathbf{K}]$ for any manipulator configuration satisfying (4.9) through (4.11) (i.e., a locally optimum configuration) can be written as

$$[\mathbf{K}] = \frac{1}{\sqrt{2}} \begin{bmatrix} -s\left(\frac{\pi}{3} - \phi_p\right) & s\left(\frac{\pi}{3} + \phi_p\right) & -s\left(\pi - \phi_p\right) \\ c\left(\frac{\pi}{3} - \phi_p\right) & -c\left(\frac{\pi}{3} + \phi_p\right) & c\left(\pi - \phi_p\right) \\ 1 & 1 & 1 \\ s\left(\frac{\pi}{3} - \phi_p\right) & s\left(\frac{\pi}{3} + \phi_p\right) & s\left(\pi - \phi_p\right) \\ -c\left(\frac{\pi}{3} - \phi_p\right) & -c\left(\frac{\pi}{3} + \phi_p\right) & -c\left(\pi - \phi_p\right) \\ 1 & -1 & 1 \end{bmatrix}$$

$$\begin{bmatrix} -s\left(\pi - \phi_p\right) & s\left(\frac{\pi}{3} + \phi_p\right) & -s\left(\frac{\pi}{3} - \phi_p\right) \\ -c\left(\pi - \phi_p\right) & c\left(\frac{\pi}{3} + \phi_p\right) & -c\left(\frac{\pi}{3} - \phi_p\right) \\ 1 & 1 & 1 \\ -s\left(\pi - \phi_p\right) & -s\left(\frac{\pi}{3} + \phi_p\right) & -s\left(\frac{\pi}{3} - \phi_p\right) \\ -c\left(\pi - \phi_p\right) & -c\left(\frac{\pi}{3} + \phi_p\right) & -c\left(\frac{\pi}{3} - \phi_p\right) \\ -1 & 1 & -1 \end{bmatrix} \tag{4.12}$$

where $s(\cdot)$ and $c(\cdot)$ represent the sine and cosine functions, respectively.

Using the sum and difference trigonometric identities, the above matrix can be rewritten as

$$[\mathbf{K}] = \frac{1}{\sqrt{2}} \begin{bmatrix} -\frac{\sqrt{3}}{2}c\phi_p + \frac{1}{2}s\phi_p & \frac{\sqrt{3}}{2}c\phi_p + \frac{1}{2}s\phi_p & -s\phi_p \\ \frac{1}{2}c\phi_p + \frac{\sqrt{3}}{2}s\phi_p & -\frac{1}{2}c\phi_p + \frac{\sqrt{3}}{2}s\phi_p & -c\phi_p \\ 1 & 1 & 1 \\ \frac{\sqrt{3}}{2}c\phi_p - \frac{1}{2}s\phi_p & \frac{\sqrt{3}}{2}c\phi_p + \frac{1}{2}s\phi_p & s\phi_p \\ -\frac{1}{2}c\phi_p - \frac{\sqrt{3}}{2}s\phi_p & -\frac{1}{2}c\phi_p + \frac{\sqrt{3}}{2}s\phi_p & c\phi_p \\ 1 & -1 & 1 \end{bmatrix}$$

$$\begin{bmatrix} -s\phi_p & \frac{\sqrt{3}}{2}c\phi_p + \frac{1}{2}s\phi_p & -\frac{\sqrt{3}}{2}c\phi_p + \frac{1}{2}s\phi_p \\ c\phi_p & \frac{1}{2}c\phi_p - \frac{\sqrt{3}}{2}s\phi_p & -\frac{1}{2}c\phi_p - \frac{\sqrt{3}}{2}s\phi_p \\ 1 & 1 & 1 \\ -s\phi_p & -\frac{\sqrt{3}}{2}c\phi_p - \frac{1}{2}s\phi_p & -\frac{\sqrt{3}}{2}c\phi_p + \frac{1}{2}s\phi_p \\ c\phi_p & -\frac{1}{2}c\phi_p + \frac{\sqrt{3}}{2}s\phi_p & -\frac{1}{2}c\phi_p - \frac{\sqrt{3}}{2}s\phi_p \\ -1 & 1 & -1 \end{bmatrix} \tag{4.13}$$

Post-multiplying the above matrix by its transpose results in the following diagonal matrix:

$$[\mathbf{K}]\,[\mathbf{K}]^T = \begin{bmatrix} \frac{3}{2} & 0 & 0 & 0 & 0 & 0 \\ 0 & \frac{3}{2} & 0 & 0 & 0 & 0 \\ 0 & 0 & 3 & 0 & 0 & 0 \\ 0 & 0 & 0 & \frac{3}{2} & 0 & 0 \\ 0 & 0 & 0 & 0 & \frac{3}{2} & 0 \\ 0 & 0 & 0 & 0 & 0 & 3 \end{bmatrix} \tag{4.14}$$

Note that the product $[\mathbf{K}]\,[\mathbf{K}]^T$ is independent of ϕ_p. Since the singular values of $[\mathbf{K}]$ are identical to the square roots of the positive eigenvalues of $[\mathbf{K}]\,[\mathbf{K}]^T$, the singular values are also independent of ϕ_p. The normalized eigenvectors of $[\mathbf{K}]\,[\mathbf{K}]^T$ are the column space basis vectors associated with each of these singular values. Therefore, the force transmission ratios represented by the singular values and their associated task space directions are as follows for an optimum Stewart platform configuration:

$$
\begin{aligned}
x,y \text{ force} &\rightarrow T_{F_{\mathrm{f},x}} = T_{F_{\mathrm{f},y}} = \sigma_{\mathrm{f},x} = \sigma_{\mathrm{f},y} = \sqrt{\tfrac{3}{2}} \\
z \text{ force} &\rightarrow T_{F_{\mathrm{f},z}} = \sigma_{\mathrm{f},z} = \sqrt{3} \\
x,y \text{ moment} &\rightarrow T_{F_{\mathrm{m},x}} = T_{F_{\mathrm{m},y}} = \sigma_{\mathrm{m},x} = \sigma_{\mathrm{m},y} = \sqrt{\tfrac{3}{2}} \\
z \text{ moment} &\rightarrow T_{F_{\mathrm{m},z}} = \sigma_{\mathrm{m},z} = \sqrt{3}
\end{aligned}
$$

Furthermore, the condition number of the force transformation matrix [**K**] is

$$\kappa = \frac{\sigma_{max}}{\sigma_{min}} = \sqrt{2} \tag{4.15}$$

The above singular values and directions demonstrate that the manipulator requires $\sqrt{2}$ times joint effort (measured by the norm of the vector $\boldsymbol{\tau}$) to produce a force and/or moment in the x-y plane as it does to produce a force and/or moment in the z-direction. As a consequence of work-energy relations (Section 3.1.2), the singular values also demonstrate that $\sqrt{2}$ times as much joint effort (measured by the norm of the vector $\dot{\mathbf{q}}$) is required to translate and/or rotate in the z-direction as it does to translate and/or rotate in any direction in the x-y plane.

4.2.4 Architectural Limitations

The relations of (4.9), (4.10) and (4.11) define the family of optimum Stewart platform configurations. These relations also place limits on the values the architectural parameters can obtain in order to preserve optimality of the configuration. The limits derived from these relations correspond to actual physical limitations on the architectural parameters of the manipulator. Examining relation (4.10), and requiring that z_e remain real valued, demonstrates that the base radius must remain greater than the platform radius ($r_b = r_p$ results in $z_e = 0$, an uncertainty configuration of the manipulator). This limit on r_b restricts the sum of ϕ_b and ϕ_p to be less than $\pi/3$ by relation (4.11).

In addition to the architectural limitations inferred by the relations defining the family of optimum manipulator configurations, there is a second physical limitation that the manipulator's legs do not cross and interfere with one another at the optimal configuration. This requires that the actuator separation angles remain greater than or equal to zero. As a consequence of this requirement and relation (4.11), the base radius is limited to be less than or equal to twice that of the platform. Table 4.1 summarizes the architectural limitations for locally optimal Stewart platform manipulators.

Architectural Parameter	Limitation	Cause
Leg Separation Angles	$\phi_b \geq 0\,,\ \ \phi_p \geq 0$	interference among legs
	$\phi_b + \phi_p < \pi/3$	z_e remain real valued
Base Radius	$r_p < r_b \leq 2r_p$	z_e real, leg interference

Table 4.1: Architectural limitations for optimal Stewart platform configurations

4.2.5 Performance Measure Considerations

The configuration optimization performed in Section 4.2.2 was based on using the condition number of the manipulator's force transformation matrix as the desired performance measure. Performing local configuration optimizations using any other performance measure referred to in the Section 3.1.3 resulted in the same solutions governed by (4.9) through (4.11). This occurs as a result of the singular values being identical in all cases and these singular values simultaneously optimizing each of these objectives. The performance measures and the resulting optimum objective function values are as follows:

Condition Number

$$\text{Minimize} \quad f_{obj} = \frac{\sigma_{max}}{\sigma_{min}} \qquad \Rightarrow \qquad f_{obj,opt} = \sqrt{2}$$

Determinant

$$\text{Maximize} \quad f_{obj} = \prod_{i=1}^{6} \sigma_i \qquad \Rightarrow \qquad f_{obj,opt} = \frac{27}{4}$$

Minimum Singular Value

$$\text{Maximize} \quad f_{obj} = \sigma_{min} \qquad \Rightarrow \qquad f_{obj,opt} = \sqrt{\frac{3}{2}}$$

Arithmetic Mean Singular Value

$$\text{Maximize} \quad f_{obj} = \frac{1}{6}\sum_{i=1}^{6} \sigma_i \qquad \Rightarrow \qquad f_{obj,opt} = \frac{\sqrt{2}+1}{\sqrt{3}}$$

Geometric Mean Singular Value

$$\text{Maximize} \quad f_{obj} = \left(\prod_{i=1}^{6} \sigma_i\right)^{\frac{1}{6}} \qquad \Rightarrow \qquad f_{obj,opt} = \left(\frac{27}{4}\right)^{\frac{1}{6}}$$

Note that these results retain the reference frame location at the centre of the platform plane.

4.2.6 Reference Location Considerations

As mentioned in Sections 3.1.4 and 4.2.1, the optimal configurations of a manipulator are a function of the choice of instantaneous reference frame location. The configuration optimization of Section 4.2.2 considered a specific reference location at the centre of the platform plane. This means that the point on the end effector with optimal dexterity corresponds to the centre of the platform. In this section, the optimization results are shown to be easily extended for a more general class of reference locations.

Consider a Stewart platform where the desired reference point is vertically displaced a distance h from the centre of the platform plane as depicted in Figure 4.4. Next consider a *virtual platform* parallel to the plane of the platform and having it's centre located at the reference point. This virtual platform is shown in Figure 4.4 with a dotted outline. Temporarily ignoring the platform plane and considering the virtual platform plane in its place, it is easy to see that the same optimal configurations described by relations (4.9) to (4.11) would be achieved. The virtual platform with radius r_e and actuator separation angle ϕ_e would take the place of the actual platform with radius r_p and actuator separation angle ϕ_p. Additionally the distance from the base to the virtual platform, z_e, would now be equal to the distance from the base to the actual platform plus the reference point displacement ($z_e = z_p + h$). Using these substitutions, the relations describing the family of optimal configurations for the case where the reference point is vertically displaced from the centre of the platform plane can be rewritten as:

$$x_e = y_e = \alpha = \beta = \gamma = 0 \tag{4.16}$$

$$r_b^2 = r_e^2 + z_e^2 = 1 + z_e^2 \tag{4.17}$$

$$\phi_b + \phi_r = \tfrac{\pi}{3} - \arccos\left(\tfrac{r_e}{r_b}\right) = \tfrac{\pi}{3} - \arccos\left(\tfrac{1}{r_b}\right) \tag{4.18}$$

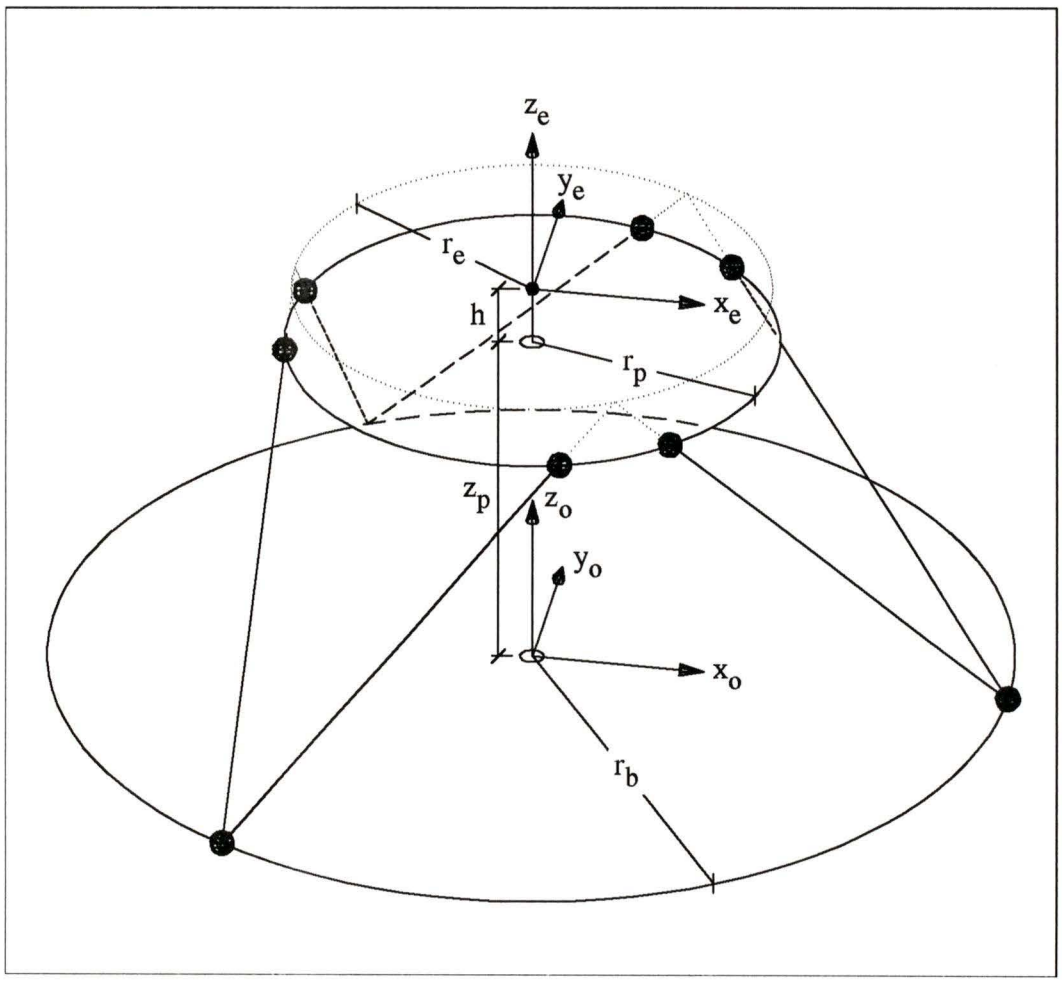

Figure 4.4: Optimal Stewart platform configuration with vertical reference frame offset

Note that the radius of the virtual platform, r_e, becomes the characteristic length which weights forces and moment as well as translational and rotational velocities equally. Using the substitutions given in the previous paragraph, the material presented in Sections 4.2.2 through 4.2.5 remains relevant to the case where the reference location is vertically displaced. Finally, it is important to note that the material presented in Section 4.2.4 places limits on distance the reference point can be above (or below) the platform plane in order that the same family of optimal configurations remain applicable.

The platform radius, height, and actuator separation angles are related to those in the virtual platform by

$$r_p^2 = r_e^2 + h^2 \tag{4.19}$$

$$z_p = z_e - h \tag{4.20}$$

$$\phi_p = \phi_e + \arccos\left(\frac{h}{r_p}\right) \tag{4.21}$$

The results given above apply only to cases where the reference point remains centrally located and only vertically displaced from the platform plane.

4.3 Stewart Platform Architecture Optimization

As presented in Section 4.2, configuration optimization results in the definition of a family of optimum configurations for the Stewart platform. A method using considerations based upon global performance measures can be employed to isolate a single optimum Stewart platform architecture. The results of the configuration optimization allow the number of architectural design parameters required for an optimization based upon global performance measures to be reduced to two. That is, the search for a best architecture considering global characteristics can be constrained to the family of optimal configurations defined by varying r_b and ϕ_p within the limits set out in Section 4.2.4. This allows selection of an architecture with optimal local characteristics and best overall performance.

4.3.1 Objective and Stewart Platform Application

Overview of Global Performance Measures

Two classes of global performance measures have been proposed in the literature which could be used to find an optimum Stewart platform architecture. The first being the volume of the manipulator's workspace and the second being based upon "integrals" of local performance measures over some portion of the manipulator's workspace.

The determination of the workspace volume of parallel and hybrid manipulators is not a trivial task, and to date has only been performed using numerical methods. Traditionally, the volume of the Stewart Platform's and other closed-chain manipulator's workspaces are determined using methods based upon complete discretiza-

tions of Cartesian space and ascertaining whether or not each point belongs to the reachable space of the device [10, 32, 58]. In later work, Gosselin [15] developed an algorithm based upon geometrical principles for determining the workspace volume of six degree of freedom parallel manipulators with reduced computational requirements. Using this method, the workspace volumes of the locally optimum Stewart platforms for a given set of linear actuator displacement limits could be compared to select a unique optimum manipulator architecture. However, if the workspace volume of the manipulator was of primary importance, a serial-chain manipulator architecture might be more suited to the task. Furthermore, if the characteristics of parallel-chain manipulators are deemed highly desirable and the application requires a larger workspace size, the Stewart platform could simply be scaled up or be fitted with larger displacement linear actuators to give the required operational volume. For these reasons the workspace volume will not be investigated as a global performance measure in determining an optimum Stewart platform architecture.

The dexterity or manipulability measures introduced in Chapter 3 can also be extended to represent global performance measures through integration over a specified region of the manipulator's workspace. Asada and Cro Granito [4], as well as Kokkinis and Stoughton [26], integrated local performance measures based on the singular values of the Jacobian matrix over specified ranges of the workspace. Gosselin and Angeles [17] defined a performance index termed the *global conditioning index* which represents an average conditioning measure over the entire workspace of a manipulator. This conditioning measure was arrived at by integrating the reciprocal of the condition number over the workspace and then normalizing the result by dividing by the volume of the workspace. Finally, Singh and Rastegar [50] considered distributions of end effector positions and averaged the Jacobian matrix singular values

associated with these positions to result in the definition of a *global velocity ellipsoid.* This ellipsoid can be used to give a global measure of any local performance measure related to the singular values of the manipulator's Jacobian matrix.

Any of the above integration based methods could be used to isolate a unique optimum Stewart platform architecture(s). However, the methods are computationally expensive, especially for six degree-of-freedom manipulators where the integral inside the two dimensional optimization algorithm will be six dimensional. Furthermore, the numerical results of such an optimization are difficult to interpret since they provide no information on how the manipulator can be expected to perform in different directions or different portions of the workspace. These difficulties involved with integration based methods lead to the introduction of a new alternative method of quantifying the global performance of a manipulator. This new method, which is based upon gradients of local dexterity measures, retains directional performance information while also significantly reducing the computational effort required for the measures evaluation.

Gradient Based Global Dexterity Measures: Dexterity Gradients

The proposed global dexterity measure utilizes spatial gradients of a local kinematic dexterity measure about an optimum manipulator configuration. These gradients will be termed *dexterity gradients.* The position of the local optimum at which the gradients are calculated coincides with the point in the manipulator's workspace about where the manipulator would normally operate. In this manner, the proposed measure provides a first-order approximation to the characteristics of the manipulator at points in its normal operational region near the local optimum. Low numerical val-

ues of the measure signify shallow dexterity gradients away from the local optimum point indicating that the performance of the manipulator remains close to optimal at points proximal to the optimum point. Similarly, high numerical values of the proposed measure signify steep dexterity gradients and poor performance of the manipulator at positions displaced from the optimum point. Since gradient measures are only first-order approximations, the measures are only valid when quantifying the global dexterity of a manipulator which uses a portion of its workspace during normal operation. This is commonly the case for applications where parallel-chain manipulators are employed.

The dexterity gradients at the optimum point are functions of the task space directions along which the gradients are calculated. This allows dexterity gradients in different task space directions to be compared to give information concerning how the manipulator can be expected to perform in different regions of the manipulator's workspace. For architectural optimization purposes, a single number quantifying the global dexterity of a manipulator must be determined. This can be accomplished by averaging the dexterity gradients from all task space directions. Normally this would require a considerable amount of numerical computation. However, since the gradients are calculated at a local optimum point, the symmetry of these configurations allows a great deal of simplification to occur. In Section 4.2.3 it was shown that the symmetry of the optimal configurations results in equivalent instantaneous kinematic characteristics for motions in any direction in the x-y plane. Through further examination it was found that this configuration symmetry also results in the following symmetries related to the dexterity gradients at a local optimum:

1. As was the case for the instantaneous kinematic characteristics, the dexterity gradients along any direction in the x-y plane are equivalent.

2. The dexterity gradient in any direction, including those out of the x-y plane, is independent of the angle of rotation about the z axis. In other words, the dexterity gradients are identical for all directions having the same elevation angle from the x-y plane. This means that only directions in a single half-plane with one edge bounded by the z axis need be considered.

3. For any given line in task space passing through an optimum configuration, the dexterity gradients at the optimum point are identical in both directions along the line.

All of these symmetries apply equally to both translational and rotational related directions.

Taking into account all of the above observations, only translational and rotational directions lying in a single quadrant of a vertical plane containing the z axis need be considered to quantify the global dexterity of a manipulator using dexterity gradients. Therefore, the space of interest has reduced in dimension from six to four. Since three coordinates are required to describe any direction in four dimensional space, a three dimensional integration must be performed to compute the directionally averaged dexterity gradient quantifying the global dexterity of the manipulator.

In the following work, directions in the first quadrant of the x-z plane are used as representative directions in the four dimensional space of interest. These directions include combinations of x and z translations as well as x and z rotations (roll and yaw). Using these directions, the computation of the average dexterity gradient for the Stewart platform proceeds as follows.

Let θ_t and θ_r be angles in the x-z plane representing possible translational and rotational directions, respectively. Furthermore, let θ_w be an angle from which a translational/rotational weighting factor can be calculated. These three angles allow a unit vector representing any direction $\mathcal{D}$ in the four dimensional task space of interest to be defined as

$$\begin{aligned} \mathcal{D}_x &= \cos\theta_t \cos\theta_w \\ \mathcal{D}_y &= \sin\theta_t \cos\theta_w \\ \mathcal{D}_{roll} &= \cos\theta_r \sin\theta_w \\ \mathcal{D}_{yaw} &= \sin\theta_r \sin\theta_w \end{aligned} \tag{4.22}$$

Gradients, or slopes, of a desired local dexterity measure f_{obj} can be computed along these directions. This must be performed numerically since directional derivatives of kinematic dexterity measures can not be expressed in a closed form. Finally, gradients from all possible directions can be integrated and then normalized to give the required average dexterity gradient,

$$\text{Grad}_{avg} = \frac{8}{\pi^3} \int_{\theta_w=0}^{\theta_w=\frac{\pi}{2}} \int_{\theta_r=0}^{\theta_r=\frac{\pi}{2}} \int_{\theta_t=0}^{\theta_t=\frac{\pi}{2}} \frac{d}{d\mathcal{D}}(f_{obj})\, d\theta_t\, d\theta_r\, d\theta_w \tag{4.23}$$

4.3.2 Global Optimization Results

Similar to the configuration optimization performed in Section 4.2, the gradient of the forward static force transformation matrices condition number was used as a local dexterity measure in optimizing the architectural design of the Stewart platform. Dexterity gradients at all feasible optimum manipulator configurations were determined by numerically calculating the following limit:

$$\text{Grad}\,(\kappa) = \lim_{\Delta p \to 0} \frac{\kappa - \kappa_{opt}}{\Delta p} \tag{4.24}$$

where κ is the condition number at a position displaced a distance Δp from the optimum point in the desired direction, and κ_{opt} is the condition number at the optimum configuration ($\kappa_{opt} = \sqrt{2}$). The radius of the platform r_p was used as the characteristic length of the manipulator to equally weight translational and rotational related quantities (Section 4.2.1), while the base radius r_b and the platform actuator half separation angle ϕ_p were used as the two free variables describing the family of optimal configurations. The remaining non-zero variables describing the optimal configuration can be found from r_b and ϕ_p through the following relations derived from equations (4.10) and (4.11) in Section 4.2.2:

Platform Height

$$z_e = \sqrt{r_b^2 - 1} \tag{4.25}$$

Base Actuator Half Separation Angle

$$\phi_b = \frac{\pi}{3} - \arccos\left(\frac{1}{r_b}\right) - \phi_p \tag{4.26}$$

To begin with, condition number gradients at the optimal configurations of the Stewart platform were calculated along directions coinciding with the primary axes of the manipulator as modelled in Section 4.1.1. These directions correspond with the directions of the principle axes of the manipulator's velocity and force ellipsoids which characterize the instantaneous kinematic properties of the device. The dexterity gradients along these directions can be used to give insights into the expected performance of the manipulator in different regions of its workspace.

The surface and contour plots of Figure 4.5 give the condition number gradients calculated along the horizontal direction (any translational direction in the x-y, or platform, plane) for optimal configurations of the Stewart platform. Similarly, Figures 4.6 and 4.7 respectively give the condition number gradients along the vertical (z translation) and roll/pitch (rotation about any line passing through the platform centre and lying in the x-y, or platform, plane) directions. In each of the gradient plots, a line separating valid and invalid Stewart platform architectures is included. This line is described by the following relation,

$$\phi_p = \frac{\pi}{3} - \arccos\left(\frac{1}{r_b}\right) \tag{4.27}$$

which corresponds to all optimum configurations with $\phi_b = 0$. Architectures beyond this dividing line are invalid due to the requirement that $\phi_b < 0$ which implies that the optimal manipulator configurations possess crossed leg pairs.

Examining the horizontal and vertical translational condition number gradients of Figures 4.5 and 4.6 it can be seen that both plots have identical shapes; the only difference being that the vertical gradient is four times as large as the corresponding horizontal gradient for all points. The significance of this number and the identical shapes is not known at the present.

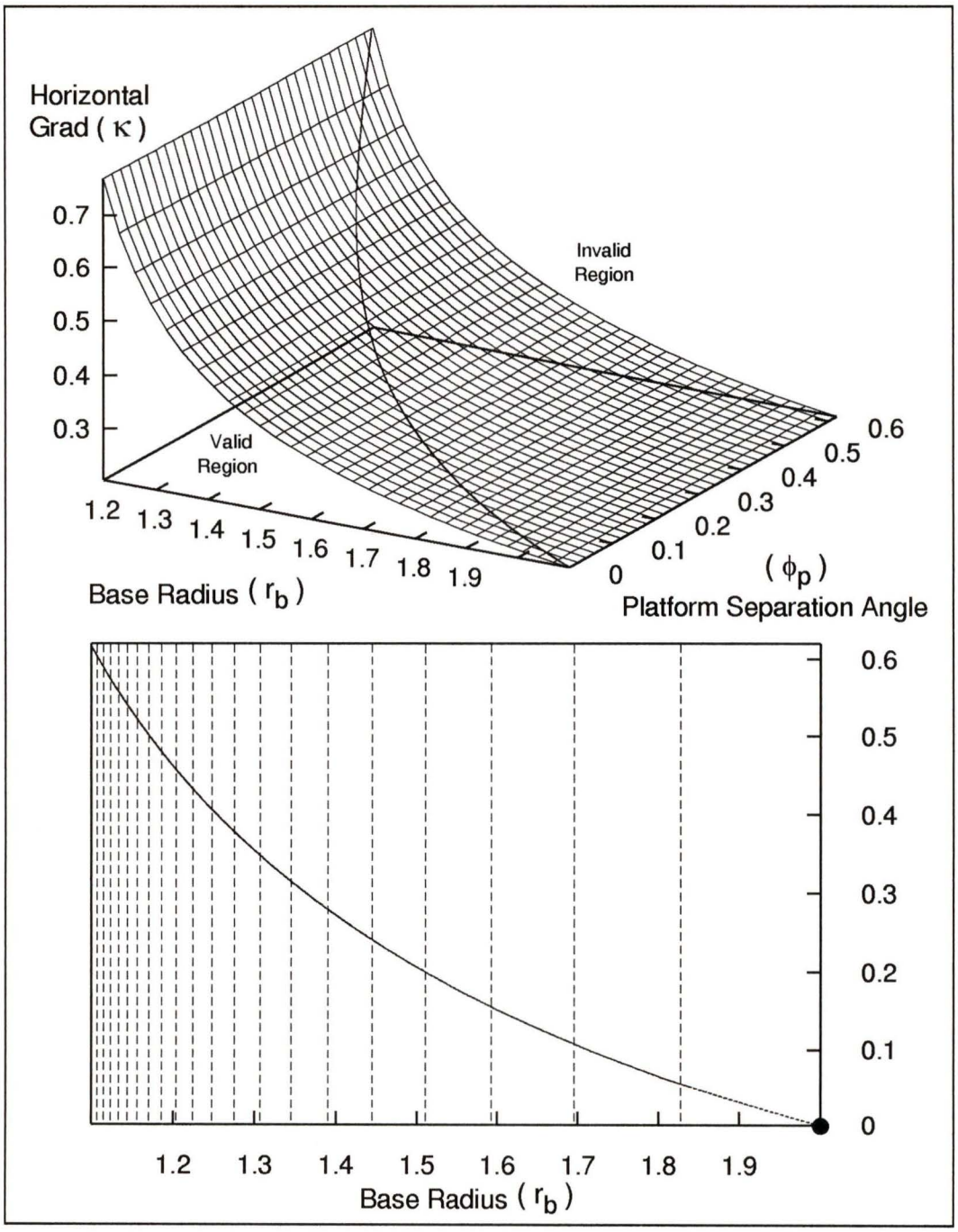

Figure 4.5: Surface and Contour Plot of Horizontal Condition Number Gradients for Locally Optimal Stewart Platforms

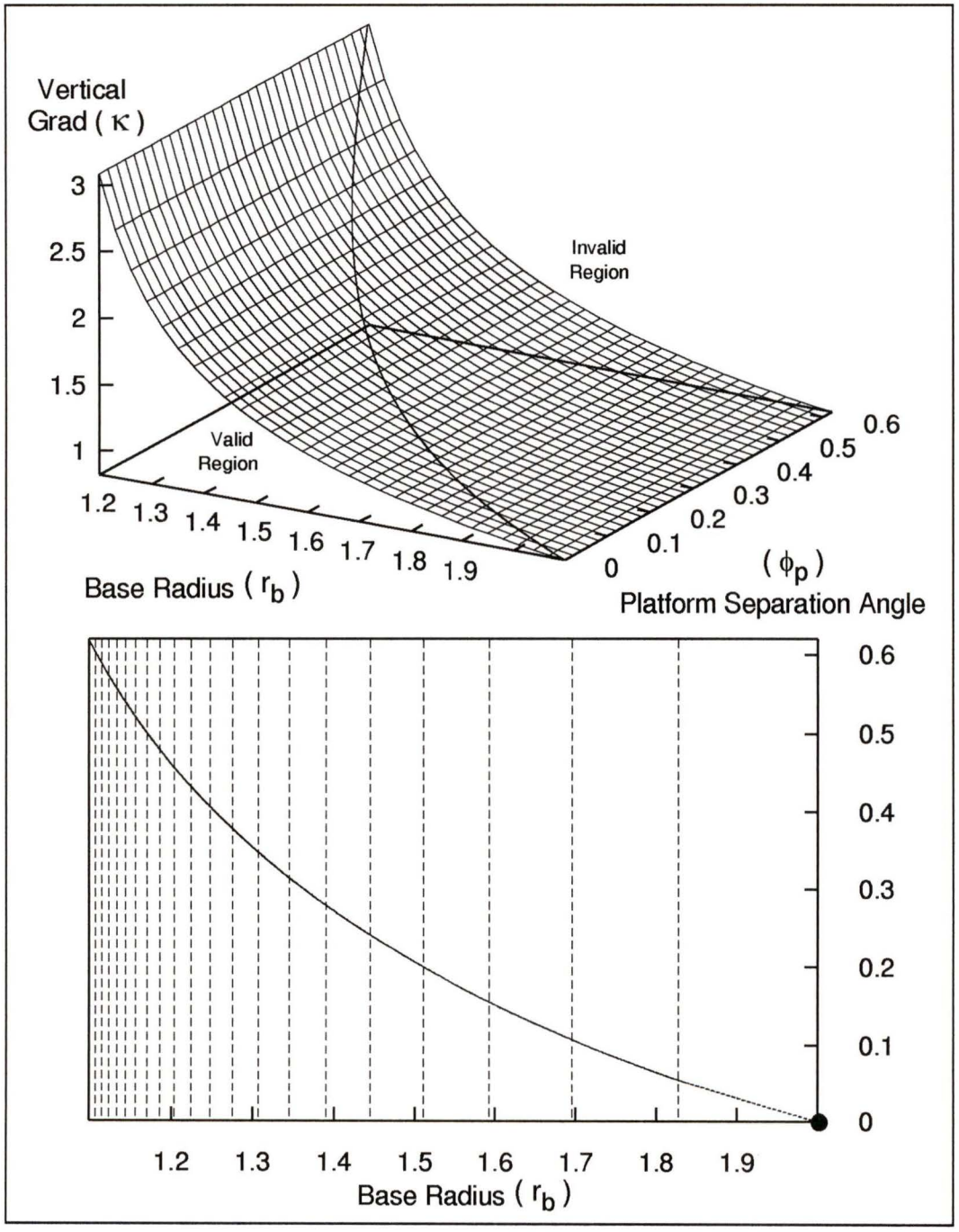

Figure 4.6: Surface and Contour Plot of Vertical Condition Number Gradients for Locally Optimal Stewart Platforms

Further examination of Figures 4.5 and 4.6 shows that gradients in horizontal and vertical directions are independent of the platform separation angle ϕ_p. Gradients in the horizontal direction are independent of ϕ_p as a result of the symmetry of the optimum configurations at which the gradients are calculated. This symmetry is not broken by varying ϕ_p due to the manner in which ϕ_p is defined (Section 4.1.1). However, the vertical gradients are independent of ϕ_p even for configurations where the legs are randomly distributed about the platform circle. The vertical gradients are only functions of the leg lengths and their angles to the platform plane which are solely determined by the base radius r_b for all optimal configurations. As the legs become shorter in length, the uncertainty configuration in which the base and platform plane become coincident is more closely approached with the same vertical movement. This is the factor causing the vertical gradient to have its quickly rising value as the base radius approaches that of the platform (i.e., $r_b = 1$). A similar factor with different uncertainty configurations causes the horizontal gradient to have the same characteristic.

The architectures with the minimum condition number gradients within the valid region are marked on each of the gradient contour plots with a solid round symbol. The minimum horizontal gradient occurs with a Stewart platform architecture where $r_b = 2$ and $\phi_p = 0$. The condition number gradient at this point is 0.2041 $\left(\approx \frac{1}{2\sqrt{6}}\right)$. The minimum vertical gradient of 0.8165 $\left(\approx \sqrt{\frac{2}{3}}\right)$ occurs with the same manipulator architecture.

The roll/pitch condition number gradients for optimal configurations of the Stewart platform are given by the surface and contour plots of Figure 4.7. The roll/pitch gradient characteristics differ substantially from those of the horizontal and vertical gradients as evidenced by the deep grooved shape of the roll/pitch gradient plot.

The plots show a larger dependence of the gradients on the platform separation angle ϕ_p than the base radius r_b. This is the opposite behaviour when compared to the horizontal and vertical gradients where the gradients are independent of ϕ_p. The condition number gradient plots in Figure 4.7 also show that there is no single manipulator architecture having a minimum roll/pitch gradient. Any point at the bottom of the plot's "groove" possesses the minimum roll/pitch gradient of 0.3536 $\left(\approx \frac{1}{2\sqrt{2}}\right)$, the curve at the grooves bottom being described by the following function:

$$\phi_p = \frac{\pi}{6} - \frac{1}{3}\arccos\left(\frac{1}{r_b}\right) \tag{4.28}$$

The Stewart platform architecture with the minimum roll/pitch gradient and the maximum possible base radius occurs when $\phi_p = \frac{\pi}{12}$, $\phi_b = 0$ and $r_b = \sqrt{2}$. This point is marked on the contour plot with a solid round symbol.

The yaw condition number gradients calculated at optimal configurations of the Stewart platform were found to be zero in all cases. With the aid of material presented later in this work, this behaviour can be readily explained. When a small yaw motion is imparted to the platform, the leg pairs meeting at the platform effectually remain at the same angles of 90 degrees with respect to one another as measured around the periphery of the platform circle. In other words, the sum of the angles of the legs to the vertical for each leg pair remains equal to 90 degrees. This means that the leg pairs, and therefore the associated zero pitch reciprocal screws, are in effect simply being rotated about a horizontal line passing through the centre of the platform and the midpoint between the actuator attachment points on the platform. As will be shown in Section 5.3, this movement of the reciprocal screw pairs does not affect the kinematic dexterity of the manipulator. Therefore, the yaw gradient of any optimal configuration of the Stewart platform will be zero for all kinematic dexterity measures.

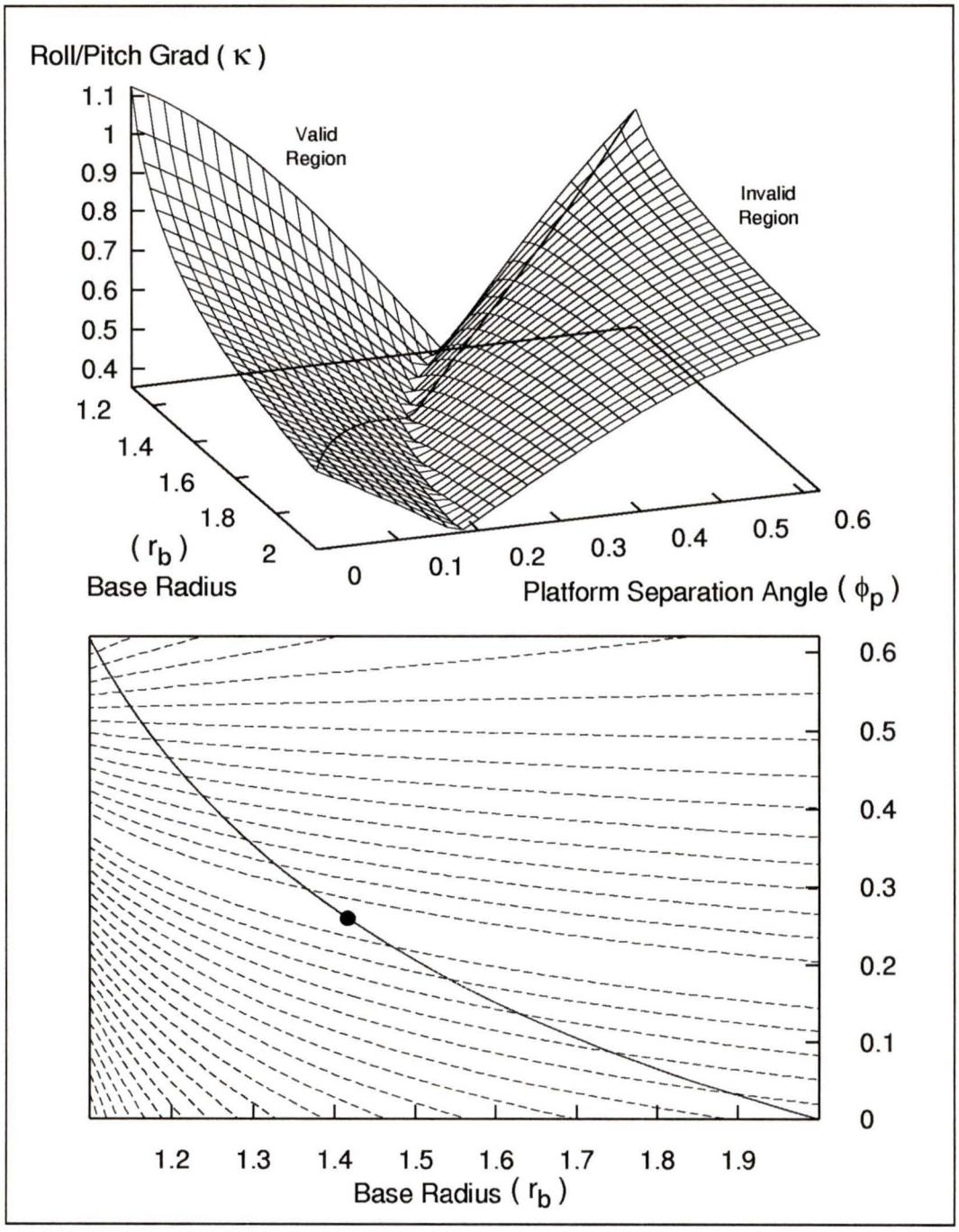

Figure 4.7: Surface and Contour Plot of Roll/Pitch Condition Number Gradients for Locally Optimal Stewart Platforms

The gradient plots of Figures 4.5, 4.6, and 4.7 give indications of preferred architectures for the Stewart platform but do not include gradients calculated along arbitrary directions. The directionally averaged condition number gradients for optimal configurations of the manipulator were calculated using the method outlined at the end of the previous section (Section 4.3.1) and the results are given in the surface and contour plots of Figure 4.8. From these plots it can be seen that the behaviour of the horizontal and vertical gradients highly influences the average gradient due to the fact that the plot has the same general shape. The influence of the roll/pitch gradient can also be seen by the slight depression running along the surface of the plot in the general direction of varying r_b. The minimum point on the average gradient plot occurs at $r_b = 2$ and $\phi_p = 0.2084$ with a directionally averaged gradient of 0.4795. However, this manipulator architecture is not practical since the legs of the manipulator must cross to achieve the optimum configuration. Among manipulator architectures with non-interfering legs, the Stewart platform with a base radius equal to twice that of the platform's ($r_b = 2$) and all actuator attachment points occurring in concurrent pairs at the base and platform ($\phi_b = 0, \phi_p = 0$) possesses the minimum average condition number gradient of 0.5216. This architecture is the optimum Stewart platform architecture when the condition number and its gradient is used as the desired performance measures. This optimum point is marked with a solid round symbol on the contour plot of Figure 4.8.

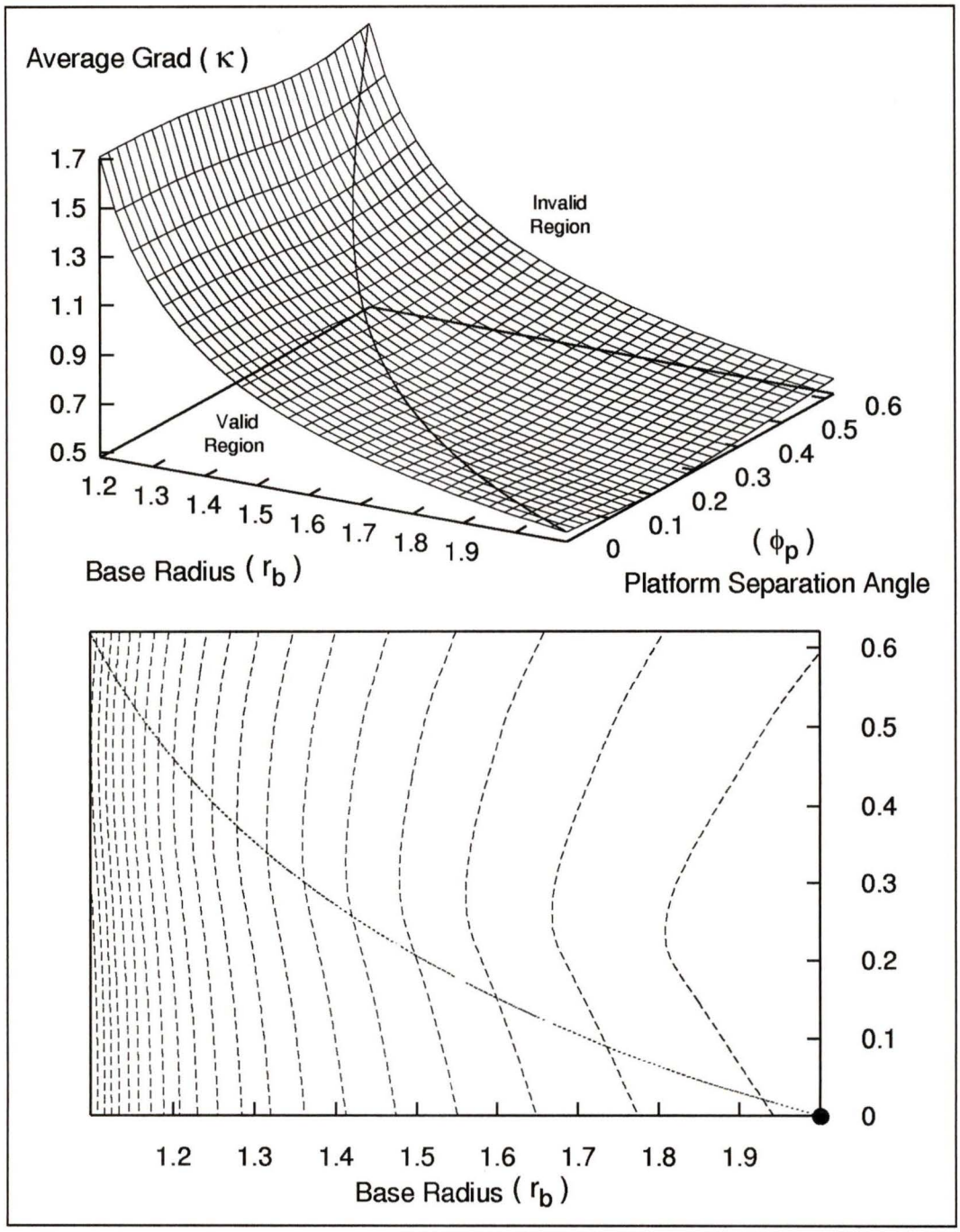

Figure 4.8: Surface and Contour Plot of Directionally Averaged Condition Number Gradients for Locally Optimal Stewart Platforms

4.3.3 Performance Measure Considerations

Kinematic dexterity measures other than the condition number can also be used to form gradient based global dexterity measures. The remaining kinematic dexterity measures introduced in Chapter 3 where examined for their suitability in the architectural optimization of the Stewart platform using dexterity gradients. It was found that the determinant, the arithmetic mean singular value, and the geometric mean singular value were ineffective when used as the local kinematic dexterity measure in a gradient based method. This is because the gradients of these dexterity measures were found to have zero values in all directions when calculated for optimum Stewart platform configurations. The minimum singular value, however, did produce non-zero gradients and was investigated further.

Similar to the previous section, minimum singular value gradients in directions along the manipulator's primary axes were calculated and plotted for optimum configurations of the Stewart platform. Comparing the results with those using gradients of the condition number showed the plots to be identical except that each of the gradient values were simply scaled by a fixed value for each of the corresponding plots. The horizontal and roll/pitch gradients of the minimum singular value were 0.8660 $\left(\approx \frac{\sqrt{3}}{2}\right)$ times those of the condition number, and the vertical gradients of the minimum singular value were 0.4330 $\left(\approx \frac{\sqrt{3}}{4}\right)$ times those of the condition number. The yaw gradients of the minimum singular value were zero for all optimal configurations, as was the case with gradients of the condition number.

The directionally averaged minimum singular value gradients were also calculated and plotted for optimum configurations of the Stewart platform, the results being presented in the surface and contour plots of Figure 4.9. Comparing these plots to those

for the average condition number gradient (Figure 4.8), the plots can be seen to be identical in general shape with only minor differences. The first difference being that the minimum singular value gradients are scaled down by a near constant value of approximately 0.56 (range of 0.53 to 0.60) compared to the condition number gradients. The second difference being that the minimum singular value plot has a slightly more pronounced depression running along the surface of the plot in the general direction of varying r_b caused by the roll/pitch gradient characteristics. However, both plots indicate the same manipulator architecture with $r_b = 2$, $\phi_b = 0$, and $\phi_p = 0$ as being optimum.

To conclude this chapter, Figure 4.10 illustrates a Stewart platform possessing the optimal architectural design. The characteristics of this optimum Stewart platform architecture at its optimum position and orientation are summarized in Table 4.2.

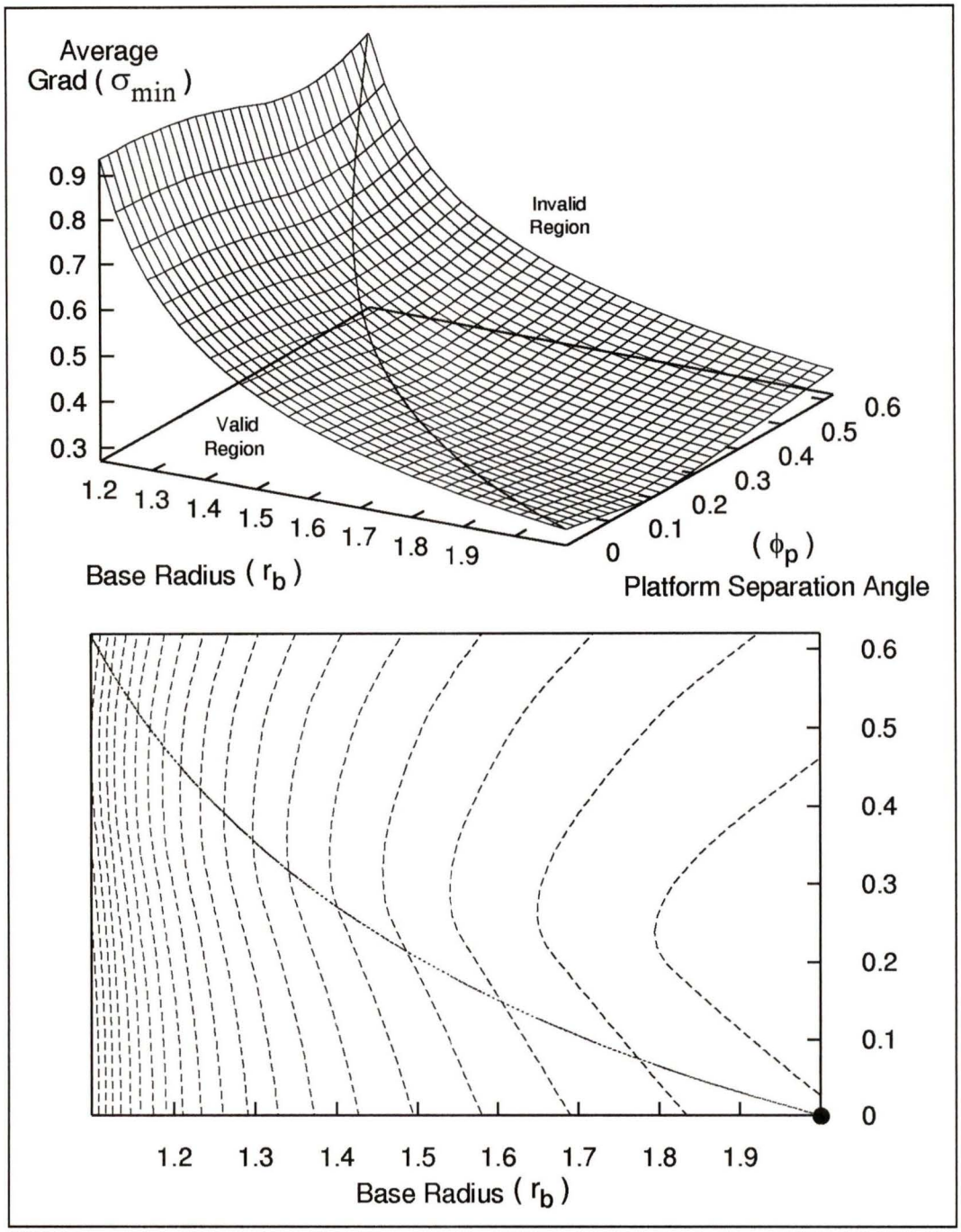

Figure 4.9: Surface and Contour Plot of Directionally Averaged Minimum Singular Value Gradients for Locally Optimal Stewart Platforms

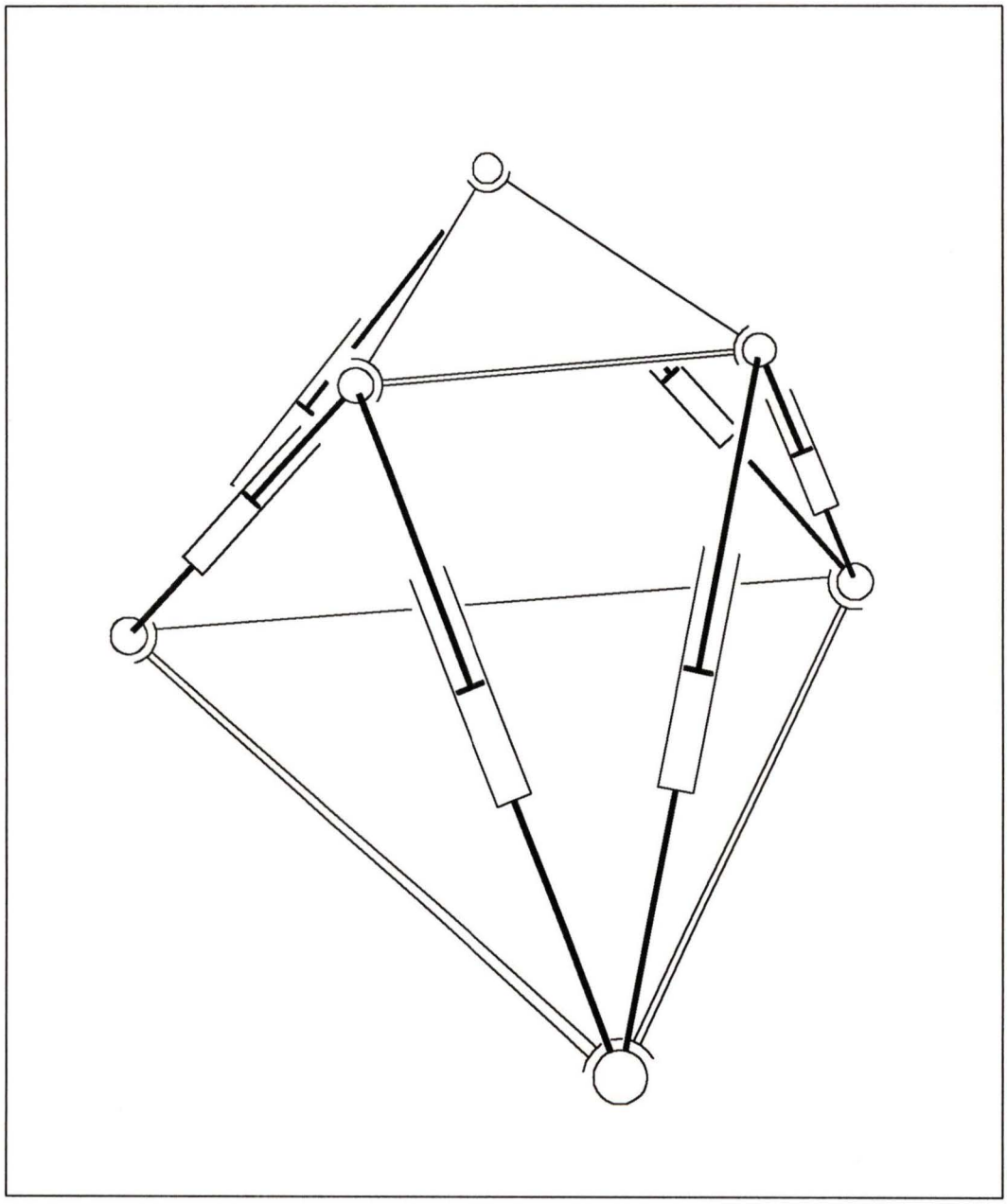

Figure 4.10: Stewart Platform with Optimal Architectural Design

CHARACTERISTIC	PARAMETER	VALUE(S)
Configuration	Architecture	$r_b = 2r_p,\ \phi_b = \phi_p = 0$
	Position	$x_e = y_e = 0,\ z_e = \sqrt{3}$
	Orientation (roll, pitch, yaw)	$\alpha = \beta = \gamma = 0$
Kinematic Dexterity	Condition Number	$\kappa = \frac{\sigma_{max}}{\sigma_{min}} = \sqrt{2}$
	Determinant	$\prod \sigma_i = \frac{27}{4}$
	Minimum Singular Value	$\sigma_{min} = \sqrt{\frac{3}{2}}$
	Arithmetic Mean Singular Value	$\frac{1}{6}\sum \sigma_i = \frac{\sqrt{2}+1}{\sqrt{3}}$
	Geometric Mean Singular Value	$(\prod \sigma_i)^{\frac{1}{6}} = \left(\frac{27}{4}\right)^{\frac{1}{6}}$
Dexterity Gradients	Horizontal Gradients	$\text{Grad}(\kappa) = 0.2041 \approx \frac{1}{2\sqrt{6}}$ $\text{Grad}(\sigma_{min}) = 0.1768 \approx \frac{1}{4\sqrt{2}}$
	Vertical Gradients	$\text{Grad}(\kappa) = 0.8165 \approx \sqrt{\frac{2}{3}}$ $\text{Grad}(\sigma_{min}) = 0.3536 \approx \frac{1}{2\sqrt{2}}$
	Roll/Pitch Gradients	$\text{Grad}(\kappa) = 0.5577$ $\text{Grad}(\sigma_{min}) = 0.4830$
	Yaw Gradients	$\text{Grad}(\kappa) = \text{Grad}(\sigma_{min}) = 0$
	Average Gradients	$\text{Grad}(\kappa)_{avg} = 0.5216$ $\text{Grad}(\sigma_{min})_{avg} = 0.3048$
	All Other Dexterity Gradients	$\text{Grad} = 0$

Table 4.2: Characteristics of the Optimum Stewart Platform Architecture at its Optimum Position and Orientation

Chapter 5

Hybrid Manipulator Optimization

The configuration and architectural optimization of the Stewart platform manipulator carried out in the previous chapter presents a groundwork for optimizing the architecture and configuration of a broader class of manipulator structures, namely hybrid manipulators.

5.1 6 DOF Hybrid Manipulators[1]

The hybrid class of manipulator structures encompasses an extremely large number of possible architectures. This holds true even when limiting the scope to only those manipulator structures capable of six degree-of-freedom (DOF) force and motion tasks with no joint or actuation redundancy, as is the case in this work. Therefore, at many stages in the optimization procedure, simplifications based on preferred attributes of hybrid manipulators and its branches are made to reduce the number of structures considered to a manageable number.

[1]The results of this section were presented at the 22'nd ASME Biennial Mechanisms Conference, Sept. 1992 [45].

5.1.1 Enumeration of Potential 6 DOF Hybrid Structures

Recall that a hybrid manipulator consists of serial branches acting in parallel on a common end effector. To be capable of six DOF force and motion tasks, the hybrid structure must have a minimum of six independent actuated joints distributed amongst its parallel-acting serial-branches. Each of the serial branches is comprised of passive and actuated joints. To have an active role in driving the hybrid structure each branch must have at least one actuated joint. Furthermore, for the end effector to have full six DOF capability, the end of each branch must be capable of six DOF motion. A branch capable of providing six DOF end motion and having no joint redundancy will have a total of six independent passive and active joint DOF.

In summary, the considered six DOF hybrid structures will consist of serial branches having six joint freedoms with at least one joint actuated and having a total of six actuated joints in the hybrid structure. The number of branches and the number of actuated joints in each branch for all potential non-redundant six DOF hybrid structures are enumerated in Table 5.1.

The one and six branch chains of Table 5.1 correspond to the cases of strictly-serial and fully-parallel chain manipulators, respectively. These extremes can be considered to be limiting cases of hybrid manipulators. That is, the strictly-serial chain corresponds to no passive joints and the fully-parallel chain corresponds to a manipulator structure with the minimum of one joint actuated in each branch. The remaining entries in Table 5.1 describe possible structures for hybrid manipulation devices having more than one branch, and with more than one joint actuated in at least one of its branches.

Number of Branches In Parallel	Number of Actuated Single-Freedom Joints in Each Branch
1	6
2	1,5
	2,4
	3,3
3	1,1,4
	1,2,3
	2,2,2
4	1,1,1,3
	1,1,2,2
5	1,1,1,1,2
6	1,1,1,1,1,1

Table 5.1: Enumeration of 6 DOF Hybrid Manipulator Structures

5.1.2 Preferred Attributes of Hybrid Manipulators

Several attributes can be considered preferred for a hybrid manipulator structure. These preferred attributes are related to issues of structural stiffness, dynamic performance, symmetry of branch actuation, kinematic simplicity, branch interference, and workspace size. In this section, the hybrid manipulator structures enumerated in Table 5.1 are evaluated according to these criteria.

As previously described, symmetry of branch actuation has advantages for manipulators expected to perform arbitrary manipulation tasks. Furthermore, branch symmetry is advantageous in terms of device production costs. Examining the hybrid structures of Table 5.1, three of the structures posses the potential of symmetrical

branch geometries, namely the "2-3,3", the "3-2,2,2", and the "6-1,1,1,1,1,1" ("number of branches–actuated joints per branch") structures.

The occurrence of branch interference is heavily influenced by the number of branches in the chain and tends to be a major factor limiting the accessible work volume. Of the chains with the potential of possessing symmetric actuation, the fully-parallel configuration "6-1,1,1,1,1,1" is at a serious disadvantage in terms of branch interference.

Actuation of only base proximal joints allows passive joint groups to be placed at the end of the branches. As a consequence, manipulated masses of the branches are reduced and dynamic performance is enhanced. Furthermore, having a passive spherical group of joints at the branch end allows the branch end to sustain only pure forces due to end effector loading. Of the chains with symmetric actuation potential, the "2-3,3" structure cannot employ passive spherical joints at both branch ends since the end effector would no longer be fully constrained. In this case one or both of the branches must sustain a moment caused by end effector loading. This requirement reduces the stiffness of the structure. The "3-2,2,2" structure can employ spherical joints at the branch ends, eliminating moment loading of the branches while simultaneously minimizing the manipulated mass associated with motions of the end effector.

From the above discussion, the three branch, two actuated joints per branch structure ("3-2,2,2") is seen to be potentially advantageous as a basic non-redundantly actuated six DOF hybrid manipulator structure. The remainder of this work concentrates on this manipulator structure.

5.2 Kinematically Simple Branch Structures[2]

In this section, kinematically simple branch structures suitable for use in six degree-of-freedom hybrid manipulators are identified. Through elimination of fundamentally degenerate and equivalent branch types, five unique branch structures employing revolute joints are shown to exist.

5.2.1 Definition of the Kinematically Simple Class

As discussed in the previous section, grouping the last three joint DOF of each branch as a passive spherical joint is advantageous in terms of manipulator stiffness and dynamic capabilities. Therefore, all branch structures under consideration will employ a passive spherical joint at the branch end. Furthermore, since linear actuators and linear passive joints are generally more complicated, bulky, and less efficient than their rotary counterparts, only revolute joints are considered in this investigation.

Construction and kinematic modeling of the branches is simplified if unnecessary offsets of the branch links are eliminated and if the joint directions are successively parallel or at right angles. Furthermore, to avoid joint redundancy and to maintain six DOF end effector motion capability, successive joints cannot be parallel unless separated by a length. The requirement of a passive spherical end joint combined with the avoidance of unnecessary offsets and the constraint of successively parallel or perpendicular joint directions defines a kinematically simple class of branch structures.

[2]The results of this section were presented at the 22'nd ASME Biennial Mechanisms Conference, Sept. 1992 [45].

5.2.2 The Unique Kinematically Simple Branch Structures

As a consequence of the kinematically simple requirements, the branch structures are comprised of a main-arm consisting of three joints, and a passive spherical (three joint) group at the branch end. To have the ability of six DOF branch end motion, the main-arm joints must not intersect at a common point. Avoiding unnecessary offsets, the three main-arm joints are dispersed amongst a fixed shoulder and an elbow. That is, there are either two joints at the shoulder and one at the elbow or vice versa. Figure 5.1 illustrates the potential joint directions at the shoulder and at the elbow. Considering permutations of the possible joint distributions and directions yields

$$2\left[\left(\frac{3!}{(3-2)!}\right)(3)\right] = 36$$

potential branch layouts for the kinematically simple class. However, many of these 36 layouts are degenerate or are kinematically equivalent.

Placing two of the main-arm joints at the shoulder results in the elbow joint being constrained to lie on a spherical surface of fixed radius. That is, the main-arm consists of a revolute joint constrained to a surface generated by the pointer mechanism of the first two joints (pointer-revolute branch structure). Placing one revolute joint at the shoulder and two joints at the elbow results in a pointing mechanism at the elbow constrained to lie on a circle of fixed radius generated by the shoulder joint (revolute-pointer branch structure).

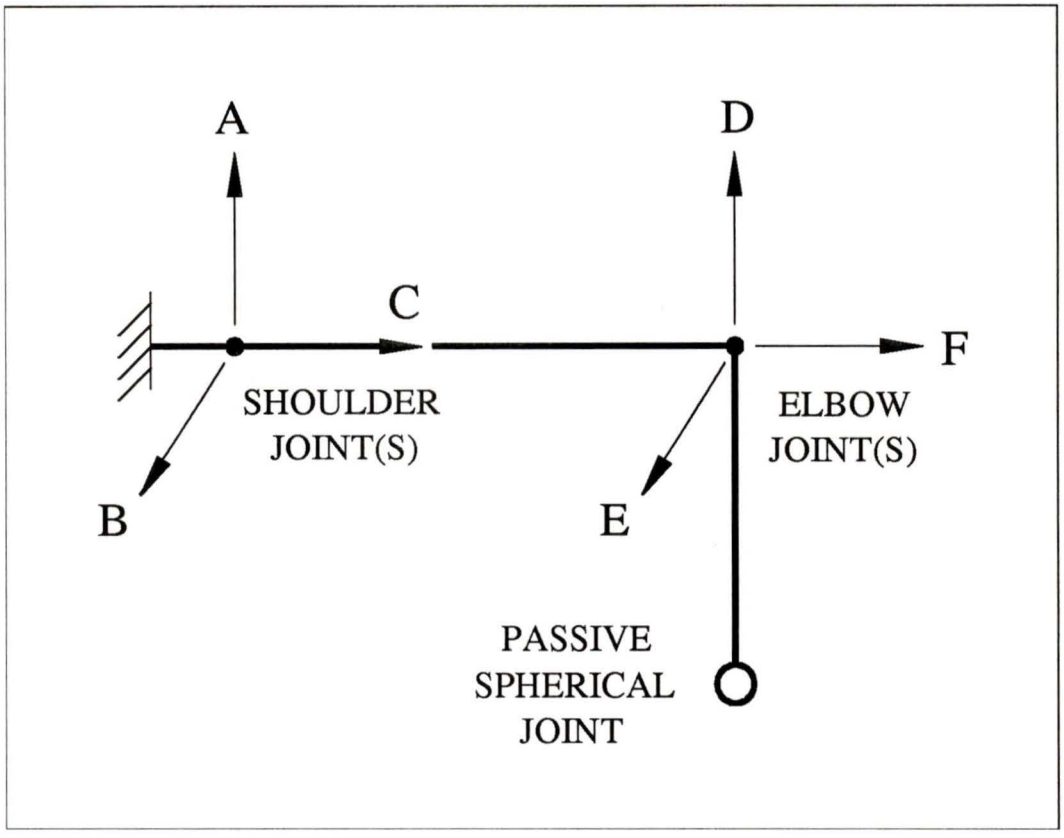

Figure 5.1: Kinematically Simple Branch Joint Directions

Pointer-Revolute Main-Arm Structures

Degenerate Layouts

Examining Figure 5.1 it is easily seen that the single elbow joint cannot be in the 'D' direction (along the direction of the second link). With an elbow in this direction the final four joints of the branch intersect at a common point, i.e., the elbow joint is not independent of the degrees of freedom supplied by the passive spherical joint. The resulting branch structures would be equivalent to a pointer with a spherical joint

at the branch end, a device capable of producing only five DOF motions. This is verified by the fact that a zero pitch screw passing through the centre of the shoulder joints and the centre of the passive spherical joint is reciprocal to all joint screws in the branch, regardless of the branch joint displacements. This means that the branch is incapable of producing motions which would perform work if the branch end is subject to a wrench acting on this reciprocal screw (i.e., the branch end cannot translate along the line passing through the centre of the shoulder joints and the centre of the passive spherical joint).

An elbow joint in the 'F' direction also results in a branch structure capable of only five degrees of freedom. The pointer at the shoulder of the branch allows positioning of the elbow joint at any point on a fixed sphere. Since an elbow joint in the 'F' direction remains normal to the surface of this sphere, the branch structure only permits the end spherical joint to be positioned at any point on a slightly larger fixed spherical surface (2 DOF positioning). The same reciprocal screw as described for the elbow joint in the 'D' direction applies to this case with the elbow joint in the 'F' direction, further verifying the lack of six DOF capability for the branch.

Since pointer-revolute branch structures with elbow joints in the 'D' or 'F' directions result in degenerate layouts, the elbow joint must be in the 'E' direction. The directions of the two shoulder joints remain unrestricted. Taking all permutations of shoulder joint directions results in six plausible kinematically simple pointer-revolute branch structures. Figure 5.2 shows these six branch structures.

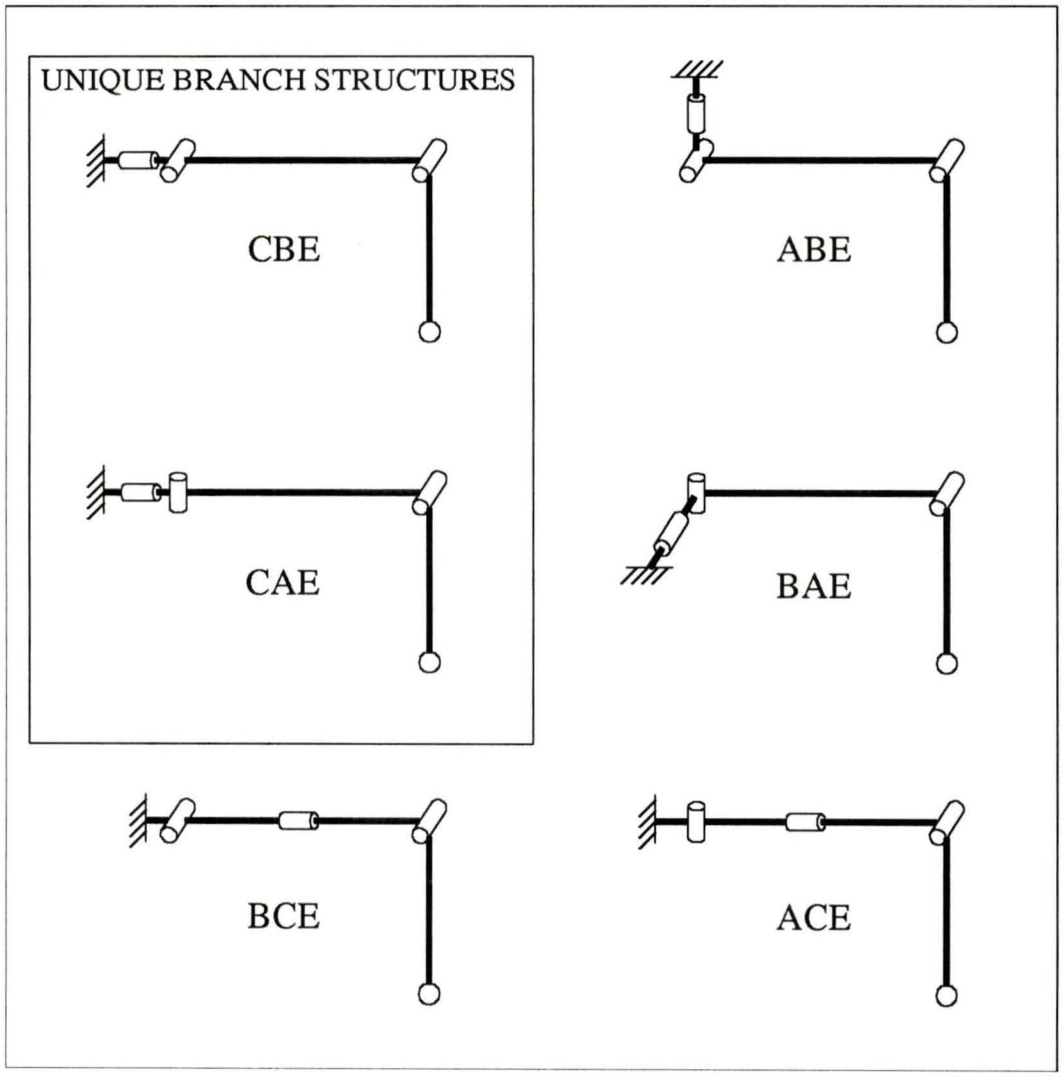

Figure 5.2: Kinematically Simple Pointer-Revolute Branches

Equivalent Branches

Rotating the second joint of the 'CBE' branch structure in Figure 5.2 by 90 degrees and comparing the resulting configuration to the 'ABE' structure shows that the structures are identical except that branches are mounted at different angles. The branches can be considered to be identical since the mounting orientation of the branches has not been considered at this point. Similarly, if the second joint of the 'CAE' structure is rotated by 90 degrees a structure identical to the 'BAE' structure results. Furthermore, rotating joint 2 of the 'BCE' structure by 90 degrees demonstrates that it is identical to the 'ACE' structure. However, these two structures are actually revolute-pointer structures since the elbows of these branches are constrained to lie on a circle of fixed radius. The second joint forms part of a pointing mechanism at the elbow of the branch, not one at the shoulder of the branch. Therefore, these branch structures will reappear as revolute-pointer structures and will be dealt with at that time. Taking these equivalencies into account, there are only two unique kinematically simple pointer-revolute branch structures typified by the 'CBE' and 'CAE' structures of Figure 5.2.

Revolute-Pointer Branch Structures

Degenerate Layouts

Examining the joint directions of Figure 5.1 it can be seen that the second elbow joint for revolute-pointer main-arms cannot be in the 'D' direction. This degeneracy is the same as that considered for the pointer-revolute main-arm structures although the reciprocal screw direction illustrating the degeneracies of the resulting layouts will depend on the remaining main-arm joint directions. The 'AED', 'AFD', 'CED', and 'CFD' structures have zero pitch reciprocal screws passing through the centres of the elbow and spherical joints. The 'BED' structure has a zero pitch reciprocal screw passing through the centre of the spherical joint parallel to the remaining main-arm joint axes. Finally, the 'BDF' structure has a zero pitch reciprocal screw passing through the centre of the shoulder joint and the centre of the passive spherical joint.

The single shoulder joint cannot be in the 'C' direction. A shoulder joint in the 'C' direction would only cause rotation of the elbow pointer-mechanism about its own centre resulting in a device capable of only five DOF motions. A screw passing through the centre of the elbow joints and the centre of the passive spherical joint is reciprocal to all joint screws regardless of joints displacements, verifying the degeneracy of the branch structure.

Eliminating all structures corresponding to the above degenerate cases yields eight plausible permutations of kinematically simple revolute-pointer branch structures. These eight structures are depicted in Figure 5.3.

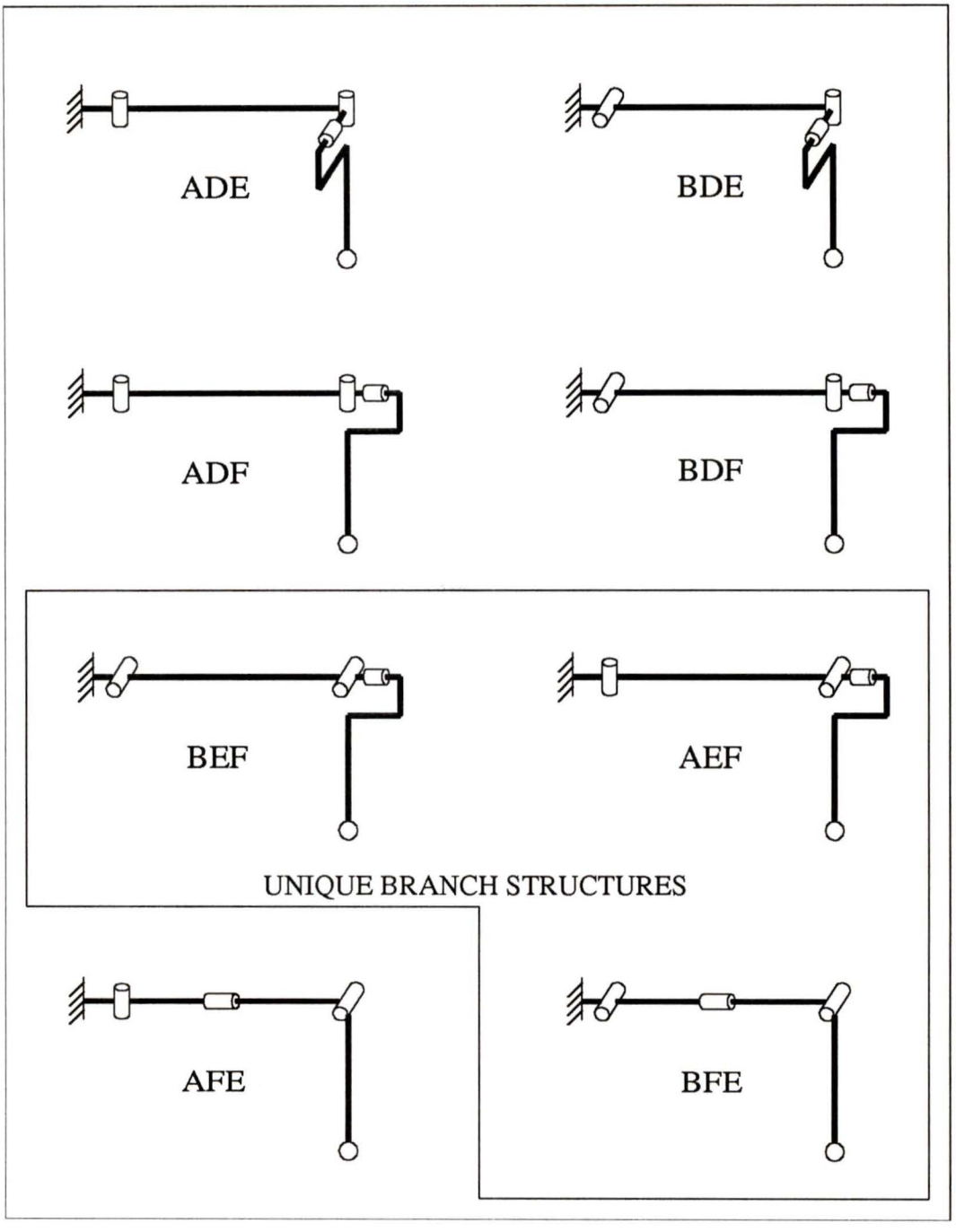

Figure 5.3: Kinematically Simple Revolute-Pointer Branches

Equivalent Branches

Rotating the second joint of the 'ADE' structure by 90 degrees and comparing the resulting configuration to the 'ADF' structure in Figure 5.3 shows that the structures are identical. Similarly, if the third joint of the 'ADF' structure is rotated by 90 degrees a branch identical to the 'BEF' structure results. Therefore, these three revolute-pointer branch structures are equivalent, all being typified by the 'BEF' structure. Similarly, the 'BDE', 'BDF' and 'AEF' structures can be shown to be equivalent, all being typified by the 'AEF' branch structure. Finally, rotating joint 2 of the 'AFE' structure by 90 degrees demonstrates that it is identical to the 'BFE' structure. These latter two structures can be observed to be identical to the 'ACE' and 'BCE' structures of Figure 5.2 which were found to belong to the revolute-pointer type of branch structures being presently considered. Taking these equivalencies into account, there are only three unique kinematically simple revolute-pointer branch structures typified by the 'BEF', 'AEF' and 'BFE' structures of Figure 5.3.

The Unique Branch Structures

Combining the unique branch structures found for both the pointer-revolute and revolute-pointer structure types, there are five unique branch structures belonging to the kinematically simple class. These five unique structures are highlighted in Figures 5.2 and 5.3. If these branches are to be used to construct non-redundantly actuated six DOF hybrid manipulators consisting of three branches (3-2,2,2 hybrid structures), there are fifteen possible actuated kinematically simple branch structures that can be employed. These fifteen actuated branch structures are derived from the five unique branches by considering combinations of actuated main-arm joints.

5.3 Configuration Optimization of Hybrid Manipulators

The configuration optimizations in this work are based on kinematic dexterity measures related to the instantaneous kinematic transformations of the manipulator under study. These instantaneous kinematic transformations are functions of the reciprocal screws associated with each of the actuated joints and the reciprocal product scalar quantities weighting each of these reciprocal screws (Section 2.2). As was shown in Chapter 4 for the Stewart platform, there can exist different manipulator configurations having identical associated reciprocal screws and reciprocal products. These manipulator configurations were termed instantaneous kinematic equivalents.

Since manipulators of varying architecture can possess identical reciprocal screws and reciprocal screw products, the configuration optimization procedure for hybrid manipulators will be carried out in a different manner than that previously employed for the Stewart platform. Instead of first picking a specific type of manipulator structure and then finding configurations in which the associated reciprocal screws and reciprocal products optimize the desired kinematic dexterity measure, the reciprocal screws and reciprocal products which optimize dexterity can first be found and then manipulator configurations can be "fitted" to these screws and products. Each of these manipulator configurations will be instantaneous kinematic equivalents of one another. This method of configuration optimization will be employed to optimize the configuration of hybrid manipulators since there are many different manipulator structures to consider for optimization.

5.3.1 Reciprocal Screws for Kinematically Simple Hybrid Manipulators

The work contained in Sections 5.1 and 5.2 reduced the number of hybrid manipulator structures to be further studied and optimized by considering preferred attributes for hybrid devices. It was found that structures with three identical branches, the branches being one of five possible kinematically simple types and having the same two joints being actuated in each branch, have advantages which make them preferable to other six DOF hybrid structures. In order to optimize the configurations of hybrid manipulators based on these structures, the types of reciprocal screws associated with the structures must be first be determined.

Recall from Section 2.2 that the reciprocal screws which make up the reciprocal screw matrix for the manipulator are screws which are reciprocal to all joint screws in the branch except that associated with the actuated joint of interest. Considering the class of kinematically simple branch structures defined in the previous section, the reciprocal screws for all branches in the class must be reciprocal to the screws associated with the passive spherical joint at each of the branch ends.

The joint screws associated with a spherical group of joints belong to the three-system of all zero pitch screws passing through the centre of the spherical joint [20], Ψ_{sph}. Reciprocal to Ψ_{sph} is the same three-system of zero pitch screws passing through the centre of the spherical joint. Therefore, the reciprocal screws associated with the actuated joints of the kinematically simple branches must all be zero-pitch screws passing through the centre of the branch's passive spherical joint. The direction of each of the reciprocal screws is determined by the locations and directions of the zero-pitch joint screws describing the main-arm joints other than the actuated joint under

consideration. For a zero-pitch screw to be reciprocal to another zero-pitch screw, the screws must intersect or be parallel (intersect at infinity) [20]. Considering this, and the different cases of possible main-arm joint actuation, yields all reciprocal screw quantities potentially required. Figure 5.4 illustrates the joint screws and reciprocal screws associated with the main-arm joints of the five unique kinematically simple branches.

5.3.2 Objective and Hybrid Manipulator Application

Knowing that the reciprocal screws for kinematically simple branches consist of zero-pitch screws passing through the centre of the passive spherical joints at their branch ends, assembled manipulator structures can now be considered for configuration optimization purposes. The manipulators under consideration are symmetric devices with three branches supporting the platform. Therefore, the branch attachment points on the platform occur at uniform 120 degree intervals at the same distance from the platform centre. The reciprocal screws used in defining the instantaneous kinematic transformations occur in pairs at these branch attachment points since there are two actuated joints in each of the branches. To maintain the symmetry of the configuration, each branch's reciprocal screw corresponding to the same actuated joint will have identical directions with respect to the radial, tangential, and normal directions of the platform. This symmetry of reciprocal screw directions is illustrated in Figure 5.5 along with angular coordinates used in defining the directions of the reciprocal screws with respect to the platform's radial, tangential, and normal directions.

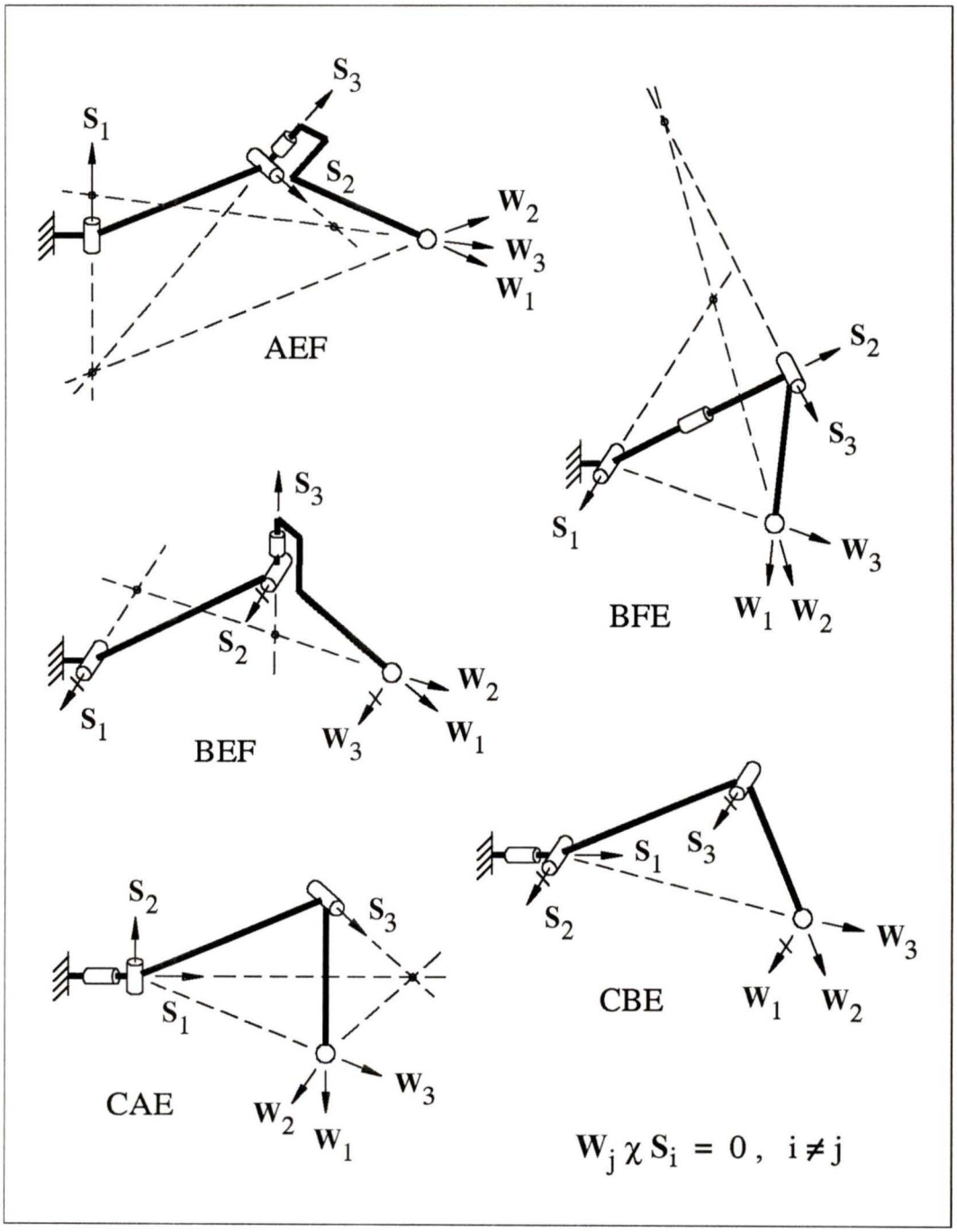

Figure 5.4: Main-Arm Joint Screws and Associated Reciprocal Screws for Kinematically Simple Branches

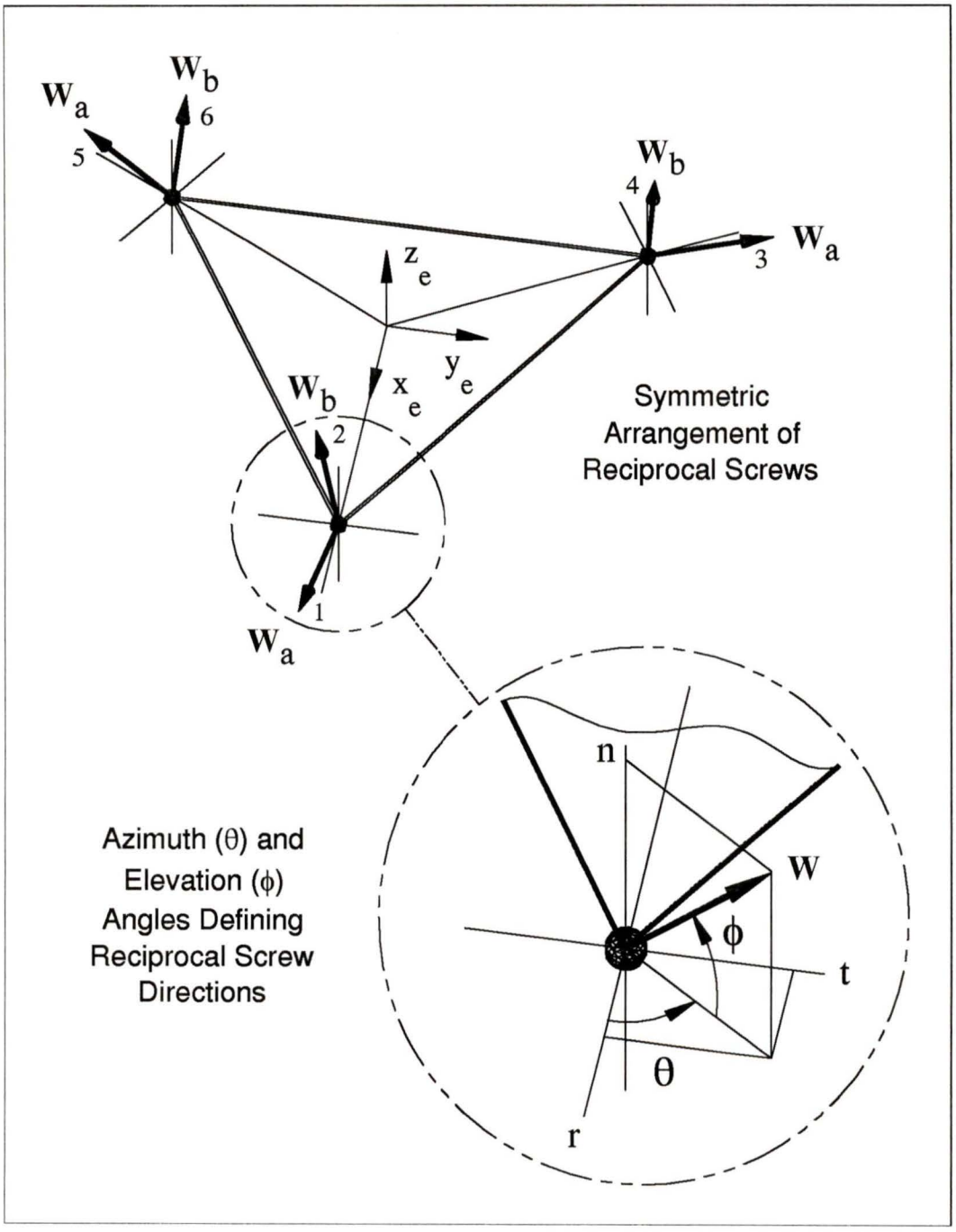

Figure 5.5: Reciprocal Screws Directions for Symmetric Configurations of Hybrid Manipulators

The two reciprocal screws $\mathbf{W}_a$ and $\mathbf{W}_b$ at each of the branch attachment points can have different reciprocal product scalar weighting factors, w_a and w_b, in addition to differing directions. These weighing factors are defined in terms of the reciprocal products as

$$\mathrm{w}_a = \frac{1}{\mathbf{W}_a \chi \mathbf{S}_a} \quad ; \quad \mathrm{w}_b = \frac{1}{\mathbf{W}_b \chi \mathbf{S}_b} \tag{5.1}$$

where $\mathbf{S}_a$ and $\mathbf{S}_b$ are the joint screws associated with $\mathbf{W}_a$ and $\mathbf{W}_b$, respectively. Using these weighting factors and the reciprocal screw geometry in Figure 5.5, the six weighted reciprocal screws defining the columns of the force transformation matrix [**K**] can be written with respect to the end effector (platform centred) frame as

$$^e\mathbf{W}_1 = \mathrm{w}_a \{ r_a,\ t_a,\ n_a\ ;\ 0,\ -n_a,\ t_a \}^T \tag{5.2}$$

$$^e\mathbf{W}_2 = \mathrm{w}_b \{ r_b,\ t_b,\ n_b\ ;\ 0,\ -n_b,\ t_b \}^T \tag{5.3}$$

$$^e\mathbf{W}_3 = \mathrm{w}_a \left\{ -\frac{1}{2}r_a - \frac{\sqrt{3}}{2}t_a,\ \frac{\sqrt{3}}{2}r_a - \frac{1}{2}t_a,\ n_a\ ;\ \frac{\sqrt{3}}{2}n_a,\ \frac{1}{2}n_a,\ t_a \right\}^T \tag{5.4}$$

$$^e\mathbf{W}_4 = \mathrm{w}_b \left\{ -\frac{1}{2}r_b - \frac{\sqrt{3}}{2}t_b,\ \frac{\sqrt{3}}{2}r_b - \frac{1}{2}t_b,\ n_b\ ;\ \frac{\sqrt{3}}{2}n_b,\ \frac{1}{2}n_b,\ t_b \right\}^T \tag{5.5}$$

$$^e\mathbf{W}_5 = \mathrm{w}_a \left\{ -\frac{1}{2}r_a + \frac{\sqrt{3}}{2}t_a,\ -\frac{\sqrt{3}}{2}r_a - \frac{1}{2}t_a,\ n_a\ ;\ -\frac{\sqrt{3}}{2}n_a,\ \frac{1}{2}n_a,\ t_a \right\}^T \tag{5.6}$$

$$^e\mathbf{W}_6 = \mathrm{w}_b \left\{ -\frac{1}{2}r_b + \frac{\sqrt{3}}{2}t_b,\ -\frac{\sqrt{3}}{2}r_b - \frac{1}{2}t_b,\ n_b\ ;\ -\frac{\sqrt{3}}{2}n_b,\ \frac{1}{2}n_b,\ t_b \right\}^T \tag{5.7}$$

where

$$r_a = \cos\theta_a \cos\phi_a \quad ; \quad r_b = \cos\theta_b \cos\phi_b \tag{5.8}$$

$$t_a = \sin\theta_a \cos\phi_a \quad ; \quad t_b = \sin\theta_b \cos\phi_b \tag{5.9}$$

$$n_a = \sin\phi_a \quad ; \quad n_b = \sin\phi_b \tag{5.10}$$

Note that the above reciprocal screw coordinates utilize the platform radius as a characteristic length of the manipulator, thereby weighting the force and moment terms equally.

From the above definitions of $\mathbf{W}_1$ through $\mathbf{W}_6$ it can be seen that six scalar quantities: $\theta_a, \phi_a, \theta_b, \phi_b, \mathrm{w}_a$, and w_b are required to uniquely define the force transformation matrix [**K**] for symmetric manipulator configurations. These quantities become the variables of the configuration optimization problem. However, for kinematic performance measures other than the condition number, leaving w_a and w_b as independent optimization variables will lead to meaningless results with both of the weighting factors tending to infinity. This would occur since the measures are not invariant of a uniform scaling in the singular values of [**K**] as would occur by scaling w_a and w_b by a uniform amount. To avoid this problem, only w_b is used as an optimization variable and w_a is calculated from w_b as

$$\mathrm{w}_a = \sqrt{2 - \mathrm{w}_b{}^2} \quad ; \quad 0 \leq \mathrm{w}_b \leq \sqrt{2} \tag{5.11}$$

This maintains a uniform weighting among the pairs of reciprocal screws allowing all previously introduced kinematic dexterity measures to be investigated.

5.3.3 Optimization Results

The Simplex method of Nelder and Mead [37] was used to find reciprocal screw directions and weightings which optimize each of the kinematic dexterity measures. Many optima having the same objective function values were found for each measure, the optima being geometrically related for a given dexterity measure. These optimum solutions for each kinematic dexterity measure are discussed in detail in subsequent paragraphs. Stated numerical values of the objective functions and relations among the optimization variables will be verified in the analyses of Sections 5.3.4 and 5.3.6.

Determinant

Using the determinant of the force transformation matrix [**K**] as the desired dexterity measure results in a family of optimal reciprocal screw directions with equal objective function values of $\frac{27}{4}$. The family of optimal weighted reciprocal screws can be described by the following relations among the directions and weightings of the reciprocal screw pairs at each branch mounting point on the platform:

$$w_a = w_b = 1 \tag{5.12}$$

$$\theta_a = \theta_b = \frac{\pi}{2} \tag{5.13}$$

$$| \phi_a - \phi_b | = \frac{\pi}{2} \tag{5.14}$$

From the above relations it can noted that only one parameter is required to differentiate among the members of the family of solutions with equal determinant values. This single parameter being the rotational angle of the perpendicular screw pairs about the radial line from the centre of the platform to each branch mounting point. The elevation angle for the first of the reciprocal screw pair ϕ_a can be used as this parameter if ϕ_b is maintained at $\phi_b = \phi_a + \frac{\pi}{2}$.

Geometric Mean Singular Value

The geometric mean singular value of [**K**] is simply the sixth root of the determinant of [**K**]. Therefore, the same family of solutions described above for the determinant apply to the case when optimizations are based on using the geometric mean singular value as a dexterity measure. The maximum geometric mean singular value for the optimal reciprocal screw directions and weightings is $\left(\frac{27}{4}\right)^{\frac{1}{6}}$.

Arithmetic Mean Singular Value

Using the arithmetic mean singular value of the force transformation matrix [**K**] as the desired dexterity measure results in the same family of optimal reciprocal screw directions and weightings as the determinant and geometric mean singular value. The maximum arithmetic mean singular value corresponding to all members of the family of solutions is $\frac{\sqrt{2}+1}{\sqrt{3}}$.

Minimum Singular Value

Using the minimum singular value of the force transformation matrix [**K**] as a dexterity measure in the optimization problem results in a two-parameter family of optimal solutions with equal objective function values of $\sqrt{\frac{3}{2}}$. This two-parameter family encompasses the one-parameter family of optimal solutions from the formerly investigated dexterity measures. The relations among the optimization variables for all members of the two-parameter family are

$$w_a = w_b = 1 \tag{5.15}$$

$$\frac{\pi}{4} \leq \theta_a = \theta_b \leq \frac{\pi}{2} \tag{5.16}$$

$$| \phi_a - \phi_b | = \frac{\pi}{2} \tag{5.17}$$

The first parameter describing the family of optimal solutions is identical to the parameter used in describing the one-parameter family of solutions found for the formerly investigated dexterity measures. As previously noted, the elevation angle ϕ_a can be used as this parameter while maintaining $\phi_b = \phi_a + \frac{\pi}{2}$. The second parameter is the azimuth angle of both reciprocal screws ($\theta_a = \theta_b$) at each branch attachment point.

Condition Number

Finally, using the condition number of the force transformation matrix [**K**] as the desired dexterity measure results in two distinct families of solutions. All members of both families have equal objective function values of $\sqrt{2}$. The first family is identical to that which occurred when using the minimum singular value. The second family is characterized by solutions with the following values of and limits on the optimization variables value:

$$\phi_a = 0 \quad ; \quad \phi_b = \frac{\pi}{2} \tag{5.18}$$

$$\frac{1}{\sqrt{2}} \leq \frac{w_b}{w_a} \leq 1 \tag{5.19}$$

$$\frac{1}{\sqrt{2}} \frac{w_b}{w_a} \leq \sin\theta_a \leq \frac{w_b}{w_a} \quad \Rightarrow \quad \frac{\pi}{4} \leq \theta_a \leq \frac{\pi}{2} \tag{5.20}$$

The limits on w_b/w_a and θ_a described by the above relations are illustrated in the plot of Figure 5.6. As labeled on the plot, any point inside the bounding lines represents reciprocal screw directions and weightings resulting in optimal dexterity as quantified by the condition number of the force transformation matrix.

Comparison Of Optimum Solutions

Comparing the optimum solutions from the different kinematic dexterity measures, it can be noted that the one-parameter family of solutions found using the determinant (and both types of mean singular values) is common to all optimal solutions. Therefore, this one-parameter family of optimum reciprocal screw directions and weightings will be taken as preferred and will be further investigated for use in determining the optimal configurations of hybrid manipulators.

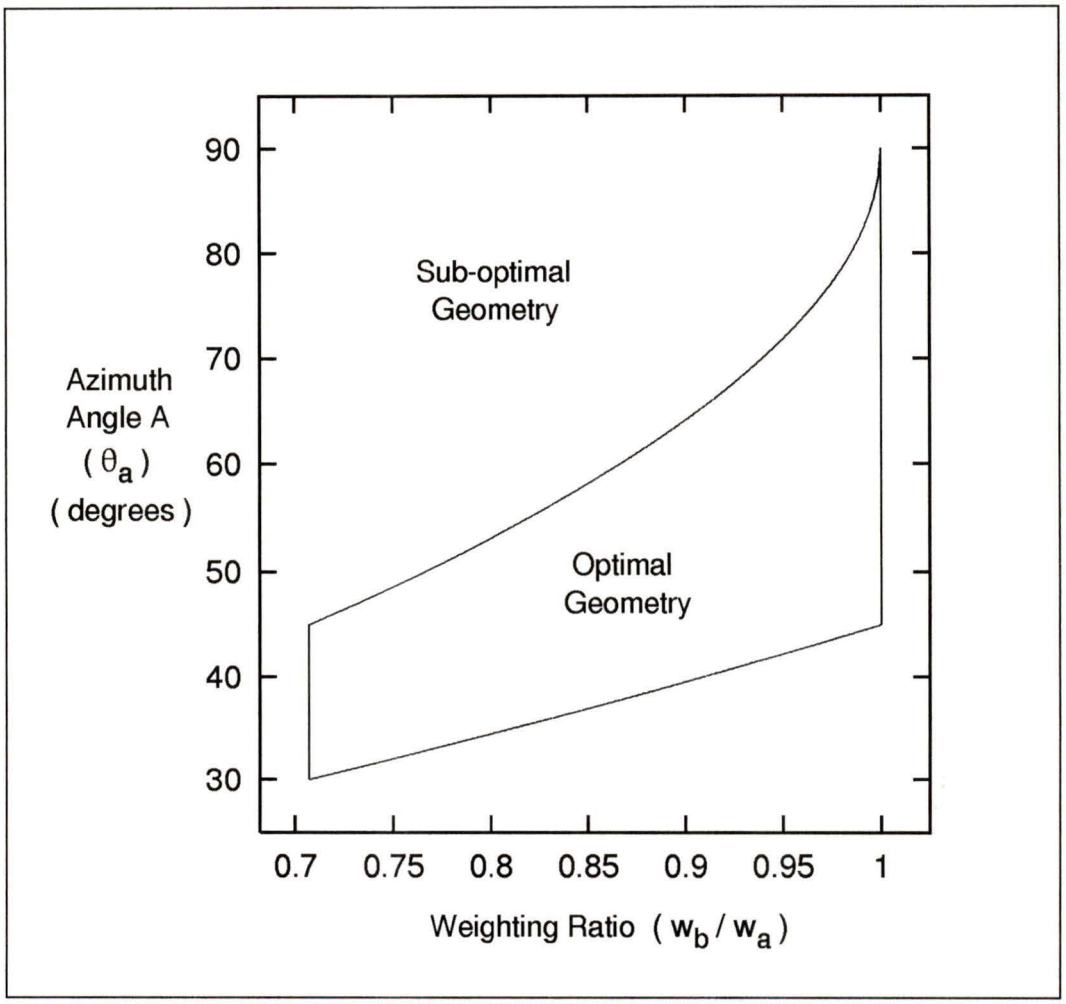

Figure 5.6: Limits on Horizontal Reciprocal Screw Directions and Reciprocal Screw Weighting Ratios for Minimum Condition Number

5.3.4 Independence of Singular Values with Respect to ϕ_a

In the previous section, a one-parameter family of reciprocal screw directions and weightings was found which simultaneously optimizes all considered kinematic dexterity measures. Since these dexterity measures are expressible in terms of the singular values of the force transformation matrix [**K**], it is natural to assume that the singular values are identical for all members of the family of optimal solutions. This property is now rigorously demonstrated.

The family of optimal solutions under considerations is described by the relations (5.12), (5.13), and (5.14) among the optimization variables. As previously noted, utilizing the elevation angle ϕ_a as a free parameter and maintaining $\phi_b = \phi_a + \frac{\pi}{2}$ allows all members of the family of optimal solutions to be described. Using this relation among the elevations angles, the values $\mathrm{w}_a = \mathrm{w}_b = 1$ and $\theta_a = \theta_b = \frac{\pi}{2}$ from relations (5.12) and (5.13) respectively, and the reciprocal screw coordinates defined in relations (5.2) through (5.7), the force transformation matrix for any member of the optimum family of solutions can be written as

$$[\mathbf{K}] = \begin{bmatrix} 0 & 0 & -\frac{\sqrt{3}}{2}C_{\phi_a} & \frac{\sqrt{3}}{2}S_{\phi_a} & \frac{\sqrt{3}}{2}C_{\phi_a} & -\frac{\sqrt{3}}{2}S_{\phi_a} \\ C_{\phi_a} & -S_{\phi_a} & -\frac{1}{2}C_{\phi_a} & \frac{1}{2}S_{\phi_a} & -\frac{1}{2}C_{\phi_a} & \frac{1}{2}S_{\phi_a} \\ S_{\phi_a} & C_{\phi_a} & S_{\phi_a} & C_{\phi_a} & S_{\phi_a} & C_{\phi_a} \\ 0 & 0 & \frac{\sqrt{3}}{2}S_{\phi_a} & \frac{\sqrt{3}}{2}C_{\phi_a} & -\frac{\sqrt{3}}{2}S_{\phi_a} & -\frac{\sqrt{3}}{2}C_{\phi_a} \\ -S_{\phi_a} & -C_{\phi_a} & \frac{1}{2}S_{\phi_a} & \frac{1}{2}C_{\phi_a} & \frac{1}{2}S_{\phi_a} & \frac{1}{2}C_{\phi_a} \\ C_{\phi_a} & -S_{\phi_a} & C_{\phi_a} & -S_{\phi_a} & C_{\phi_a} & -S_{\phi_a} \end{bmatrix} \tag{5.21}$$

where S_{ϕ_a} and C_{ϕ_a} represent the sine and cosine of ϕ_a, respectively.

Post-multiplying the matrix by its transpose results in the following diagonal matrix:

$$[\mathbf{K}]\,[\mathbf{K}]^T = \begin{bmatrix} \frac{3}{2} & 0 & 0 & 0 & 0 & 0 \\ 0 & \frac{3}{2} & 0 & 0 & 0 & 0 \\ 0 & 0 & 3 & 0 & 0 & 0 \\ 0 & 0 & 0 & \frac{3}{2} & 0 & 0 \\ 0 & 0 & 0 & 0 & \frac{3}{2} & 0 \\ 0 & 0 & 0 & 0 & 0 & 3 \end{bmatrix} \tag{5.22}$$

Note that the product $[\mathbf{K}]\,[\mathbf{K}]^T$ is independent of ϕ_a. Since the singular values of $[\mathbf{K}]$ are identical to the square roots of the positive eigenvalues of $[\mathbf{K}]\,[\mathbf{K}]^T$, the singular values are also independent of ϕ_a.

The fact that the singular values, and therefore the instantaneous kinematic characteristics of associated manipulator configurations, are independent of ϕ_a can be predicted by examining the geometry of the reciprocal screws defining $[\mathbf{K}]$. Since all reciprocal screws are of zero pitch with equal weightings ($\mathrm{w}_a = \mathrm{w}_b = 1$), and each pair of reciprocal screws at the branch attachment points on the platform are orthogonal to one another ($\phi_b = \phi_a + \frac{\pi}{2}$), the pairs of reciprocal screws form orthonormal groups multiplied by a common scaling factor of $\sqrt{2}$. The scaled orthonormal reciprocal screw pairs can be independently rotated by any angle about their common normal (described by varying ϕ_a and maintaining $\phi_b = \phi_a + \frac{\pi}{2}$) without altering the instantaneous kinematic ability the reciprocal screws and associated singular values of $[\mathbf{K}]$ represent[3].

[3]Dividing all reciprocal screws by the common vector magnitude of $\sqrt{2}$ results in each orthogonal reciprocal screw pair forming orthonormal basis vectors for subspaces of $\mathbf{R}^6$ (6 dimensional vector space). Rotating the orthogonal reciprocal screw pairs simply results in a different orthonormal bases describing the same subspaces. Therefore, the singular values of the matrix $[\mathbf{K}]$ composed of the three pairs of these scaled orthonormal basis vectors in $\mathbf{R}^6$ must be independent of their rotations.

Furthermore, note that the matrix $[\mathbf{K}]\,[\mathbf{K}]^T$ of equation (5.22) is identical to that found when analyzing the family of optimum configurations of the Stewart platform (equation (4.14) in Section 4.2.3). Therefore, the instantaneous kinematic characteristics of hybrid manipulators utilizing the optimum reciprocal screw directions and weightings are identical to those of the optimum Stewart platform configurations. This result is expected since the reciprocal screw directions and weightings of optimal Stewart platform configurations where the actuator attachment points at the platform meet in pairs ($\phi_p = 0$) belong to the one-parameter family of optimal solutions found in the previous section, namely a member where $\phi_a = \frac{\pi}{4}$ and $\phi_b = \frac{3\pi}{4}$. Therefore, the optimal configurations of three-branch hybrid manipulators have the following singular values and kinematic dexterity measure values associated with the manipulators force transformation matrix:

Singular Values

$$\sigma_{\mathrm{f},x} = \sigma_{\mathrm{f},y} = \sigma_{\mathrm{m},x} = \sigma_{\mathrm{m},y} = \sqrt{\frac{3}{2}} \quad ; \quad \sigma_{\mathrm{f},z} = \sigma_{\mathrm{m},z} = \sqrt{3}$$

Determinant

$$f_{obj} = \prod_{i=1}^{6} \sigma_i = \frac{27}{4}$$

Geometric Mean Singular Value

$$f_{obj} = \left(\prod_{i=1}^{6} \sigma_i \right)^{\frac{1}{6}} = \left(\frac{27}{4} \right)^{\frac{1}{6}}$$

Arithmetic Mean Singular Value

$$f_{obj} = \frac{1}{6} \sum_{i=1}^{6} \sigma_i = \frac{\sqrt{2}+1}{\sqrt{3}}$$

Minimum Singular Value

$$f_{obj} = \sigma_{min} = \sqrt{\frac{3}{2}}$$

Condition Number

$$f_{obj} = \frac{\sigma_{max}}{\sigma_{min}} = \sqrt{2}$$

5.3.5 Selection of a Unique Optimum Solution

Having established that the singular values describing the instantaneous kinematic characteristics of associated manipulator configurations are independent of ϕ_a for the one-parameter family of optimal solutions, a potentially preferred member of the family represented by a specific value of ϕ_a can now be isolated. Reexamining the families of optimal reciprocal screw directions and weightings found in Section 5.3.3, it can be seen that the reciprocal screw geometry described by

$$w_a = w_b = 1 \tag{5.23}$$

$$\theta_a = \frac{\pi}{2} \quad ; \quad \theta_b = 0 \tag{5.24}$$

$$\phi_a = 0 \quad ; \quad \phi_b = \frac{\pi}{2} \tag{5.25}$$

belongs to the one-parameter family of optimal solutions previously discussed, therefore simultaneously optimizes all kinematic dexterity measures. However, this reciprocal screw geometry has the additional benefit of maintaining directional uniformity of the velocity and force transmission ratios (as quantified by the condition number of $[\mathbf{K}]$) for some changes in the reciprocal screw directions and weightings.

Referring back to Figure 5.6, the reciprocal screw weightings, w_a and w_b, and the azimuth angle of the horizontal reciprocal screw θ_a can be varied over ranges inside the bounding lines on the plot without altering the condition number of $[\mathbf{K}]$. In terms of the performance of actual manipulators, this means that a manipulator with an optimum configuration having reciprocal screws described by the geometry of (5.23), (5.24), and (5.25) has the potential of maintaining the directional uniformity of its instantaneous kinematic characteristics while the manipulator is displaced from the optimum position. Based on this argument, a manipulator configuration with equally weighted reciprocal screws, one reciprocal screw at each branch attachment point

on the platform being vertical, and the other being in the platform plane tangent to the platform circle, can be considered to be the unique optimum manipulator configuration.

5.3.6 Singular Values for Symmetric Three-Branch Manipulators

A unique optimum set of reciprocal screw directions and weightings has been isolated as a result of the work contained in Sections 5.3.3 through 5.3.5. However, the limits on the reciprocal screw geometric parameters found in Section 5.3.3 for different kinematic dexterity measures remains to be verified. This verification will be carried out by examining the reciprocal screw geometry in order to determine expressions for the singular values of the force transformation matrix as functions of the variables describing the reciprocal screw geometry.

Recall that using the condition number as a performance objective in optimizing the reciprocal screw geometry resulted in two distinct families of solutions. The first of these families had equally weighted perpendicular screws with no constraints on the actual values ϕ_a and ϕ_b could take; just that the difference between the two angles be $\frac{\pi}{2}$ to keep the screws perpendicular. The second family of reciprocal screw geometries optimizing the condition number has members with unequally weighted screws and requires that one screw be vertical (e.g., $\phi_b = \frac{\pi}{2}$) and the other screw be horizontal ($\phi_a = 0$). Fortunately, setting $\phi_a = 0$ and $\phi_b = \frac{\pi}{2}$ does not exclude investigating the limits on the reciprocal screw geometric parameters for all other dexterity measures. This occurs since these elevation angles belong to the one-parameter family of optimal solutions common to all the kinematic dexterity measures.

We can now examine the reciprocal screw geometry for the case when $\phi_a = 0$ and $\phi_b = \frac{\pi}{2}$ to determine expressions for the singular values of the force transformation

matrix. This geometry is depicted in Figure 5.7 where the vertical reciprocal screws $\mathbf{W}_b$ and the z-axis of the end effector frame z_e are normal to the plane of the paper (platform plane). The primary axes of the force and velocity ellipsoids coincide with the axes of the end effector frame due to the symmetry of the reciprocal screw geometry. Recalling that the singular values of the force transformation matrix $[\mathbf{K}]$ are the force transmission ratios along the primary axes of the force ellipsoid (i.e., $T_F = \|\mathbf{F}\|/\|\boldsymbol{\tau}\|$), the singular values can be derived by considering the reciprocal wrench intensities required to generate forces/moments along each of the primary axes.

First consider the generation of a horizontal unit force $\mathbf{F}_h$ at the centre of the platform at an angle ψ to the x_e-axis. This force is generated solely by wrenches acting on the horizontal reciprocal screws $\mathbf{W}_a$ and therefore the force and moment balance equations reduce to

X Force

$$\cos\psi = \mathrm{w}_a \left\{ \tau_1 \cos\theta_a + \tau_3 \cos\left(\theta_a + \frac{2}{3}\pi\right) + \tau_5 \cos\left(\theta_a + \frac{4}{3}\pi\right) \right\} \tag{5.26}$$

Y Force

$$\sin\psi = \mathrm{w}_a \left\{ \tau_1 \sin\theta_a + \tau_3 \sin\left(\theta_a + \frac{2}{3}\pi\right) + \tau_5 \sin\left(\theta_a + \frac{4}{3}\pi\right) \right\} \tag{5.27}$$

Z Moment

$$0 = \mathrm{w}_a \left\{ \tau_1 \sin\theta_a + \tau_3 \sin\theta_a + \tau_5 \sin\theta_a \right\} \tag{5.28}$$

where τ_i is the magnitude of torque generated by revolute actuator i associated with reciprocal screw $\mathbf{W}_i$. Also note the platform radius r_p is being used as a characteristic length (i.e., $r_p = 1$) to weight forces and moments equally.

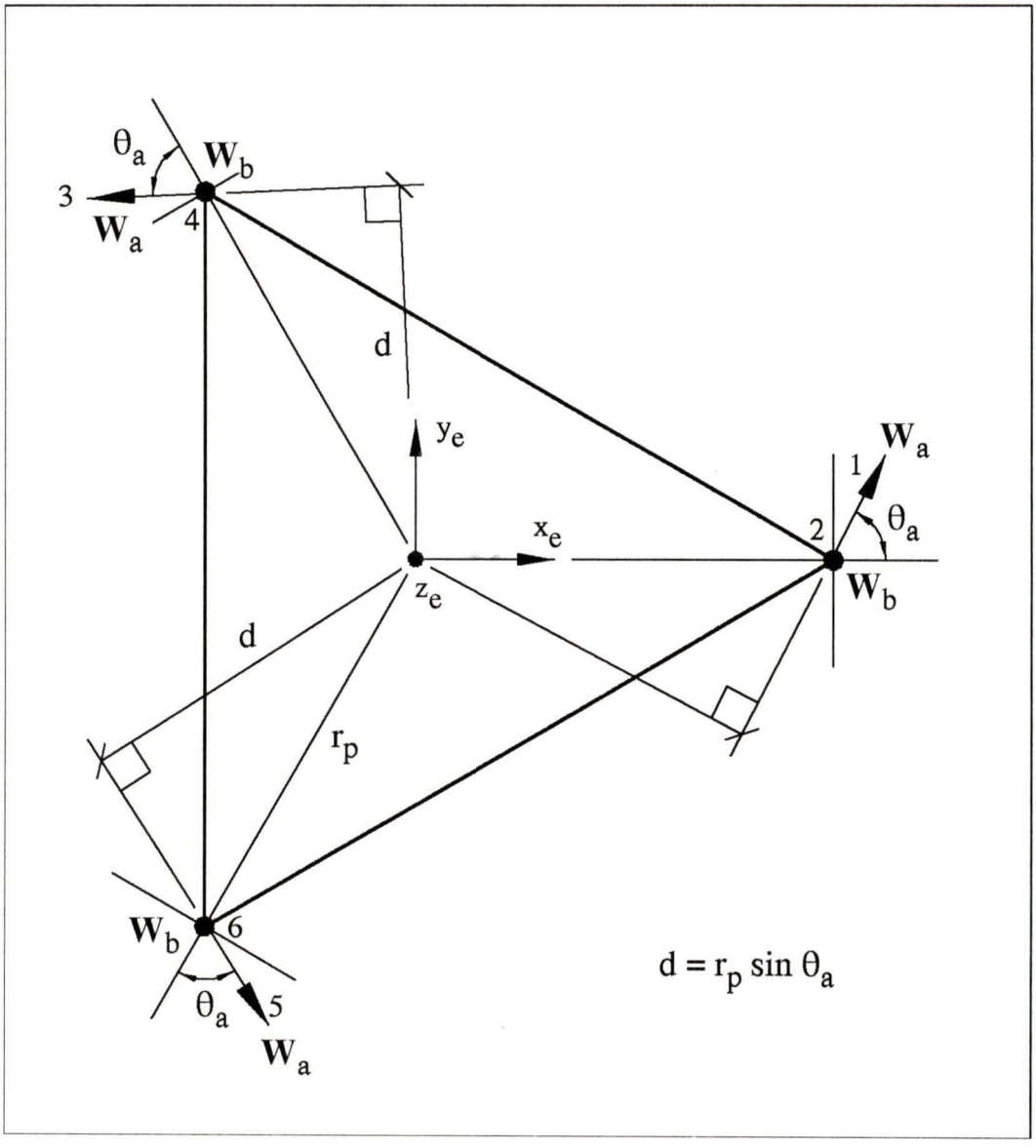

Figure 5.7: Reciprocal Screw Geometry for $\phi_a = 0$, $\phi_b = \frac{\pi}{2}$ (Top View)

It can be shown that the solution to (5.26), (5.27), and (5.28) is

$$\tau_1 = \frac{2}{3\mathrm{w}_a}\cos(\theta_a - \psi) \tag{5.29}$$

$$\tau_3 = \frac{2}{3\mathrm{w}_a}\cos\left(\theta_a - \psi + \frac{2}{3}\pi\right) \tag{5.30}$$

$$\tau_5 = \frac{2}{3\mathrm{w}_a}\cos\left(\theta_a - \psi + \frac{4}{3}\pi\right) \tag{5.31}$$

and therefore the singular values representing the force transmission ratios in the horizontal direction of force are

$$\sigma_{\mathrm{f},x} = \sigma_{\mathrm{f},y} = T_{F_{f,h}} = \frac{\|\mathbf{F}_h\|}{\|\boldsymbol{\tau}\|} = \frac{1}{\sqrt{\frac{2}{3\mathrm{W}_a^2}}} = \sqrt{\frac{3}{2}}\,\mathrm{w}_a \tag{5.32}$$

Next, consider the generation of a vertical unit force $\mathbf{F}_v$ at the centre of the platform. This force is generated by equal wrench intensities acting on the vertical reciprocal screws $\mathbf{W}_b$ as shown in the following force balance:

$$\|\mathbf{F}_v\| = 1 = \mathrm{w}_b(\tau_2 + \tau_4 + \tau_6) \;\rightarrow\; \tau_2 = \tau_4 = \tau_6 = \frac{1}{3\mathrm{w}_b} \tag{5.33}$$

Therefore the singular value in the vertical direction of force is

$$\sigma_{\mathrm{f},z} = T_{F_{f,v}} = \frac{\|\mathbf{F}_v\|}{\|\boldsymbol{\tau}\|} = \frac{1}{\sqrt{\frac{1}{3\mathrm{W}_b^2}}} = \sqrt{3}\,\mathrm{w}_b \tag{5.34}$$

Similarly, a unit vertical moment $\mathbf{M}_v$ is generated by equal wrench magnitudes acting on the horizontal reciprocal screws $\mathbf{W}_a$ as shown in the following moment balance:

$$\|\mathbf{M}_v\| = 1 = \mathrm{w}_a\sin\theta_a(\tau_1 + \tau_3 + \tau_5) \;\rightarrow\; \tau_1 = \tau_3 = \tau_5 = \frac{1}{3\mathrm{w}_a\sin\theta_a} \tag{5.35}$$

Therefore the singular value in the vertical direction of moment is

$$\sigma_{\mathrm{m},z} = T_{F_{m,v}} = \frac{\|\mathbf{M}_v\|}{\|\boldsymbol{\tau}\|} = \frac{1}{\sqrt{\frac{1}{3\mathrm{W}_a^2\sin^2\theta_a}}} = \sqrt{3}\,\mathrm{w}_a\sin\theta_a \tag{5.36}$$

Finally, consider the generation of a horizontal unit moment $\mathbf{M}_h$ at an angle ψ to the x_e-axis. This moment is generated solely by wrenches acting on the vertical reciprocal screws $\mathbf{W}_b$ as shown in the following moment and force balance equations:

X Moment

$$\cos\psi = \mathrm{w}_b\left(\frac{\sqrt{3}}{2}\tau_4 - \frac{\sqrt{3}}{2}\tau_6\right) \tag{5.37}$$

Y Moment

$$\sin\psi = \mathrm{w}_b\left(-\tau_2 + \frac{1}{2}\tau_4 + \frac{1}{2}\tau_6\right) \tag{5.38}$$

Z Force

$$0 = \mathrm{w}_b\left(\tau_2 + \tau_4 + \tau_6\right) \tag{5.39}$$

It can be shown that the solution to these equations is

$$\tau_2 = \frac{1}{\mathrm{w}_b}\left(\frac{1}{3}\sin\psi - \frac{1}{\sqrt{3}}\cos\psi\right) \tag{5.40}$$

$$\tau_4 = \frac{1}{\mathrm{w}_b}\left(\frac{1}{3}\sin\psi + \frac{1}{\sqrt{3}}\cos\psi\right) \tag{5.41}$$

$$\tau_6 = -\frac{2}{3\mathrm{w}_b}\cos\psi \tag{5.42}$$

and therefore the singular values in the horizontal direction of moment are

$$\sigma_{\mathrm{m},x} = \sigma_{\mathrm{m},y} = T_{F_{m,h}} = \frac{\|\mathbf{M}_h\|}{\|\boldsymbol{\tau}\|} = \frac{1}{\sqrt{\frac{2}{3\mathrm{w}_b^2}}} = \sqrt{\frac{3}{2}}\,\mathrm{w}_b \tag{5.43}$$

Verification of Optimization Results

Having developed expressions for the singular values of [**K**], each kinematic dexterity measure can now be examined to verify the limits on the optimization variables found in Section 5.3.3. During these verifications remember that w_a and w_b are not independent, but are related by

$$\mathrm{w}_a = \sqrt{2 - \mathrm{w}_b{}^2} \quad ; \quad 0 \le \mathrm{w}_b \le \sqrt{2} \tag{5.44}$$

Determinant

Using the expressions for the singular values in terms of the optimization variables, the determinant of [**K**] is

$$\prod_{i=1}^{6} \sigma_i = \frac{27}{4} \mathrm{w}_a^3 \mathrm{w}_b^3 \sin\theta_a \tag{5.45}$$

which has a maximum value of $\frac{27}{4}$ when $\mathrm{w}_a = \mathrm{w}_b = 1$ and $\theta_a = \frac{\pi}{2}$ verifying the optimization results of Section 5.3.3. Figure 5.8 demonstrates this maximum point (marked with dot) and the behaviour of the determinant as a function of the reciprocal screw geometry.

Geometric Mean Singular Value

The geometric mean singular value is simply the sixth root of the determinant. Therefore, the same optimum reciprocal screw geometry as was found for the determinant results. The behaviour of the geometric singular value as a function of the reciprocal screw directions and weightings will also be similar to that of Figure 5.8 except with shallower slopes away from the optimum point.

Arithmetic Mean Singular Value

The arithmetic mean singular value of [**K**] can now be written as

$$\frac{1}{6}\sum_{i=1}^{6} \sigma_i = \mathrm{w}_a \left(\frac{1}{\sqrt{6}} + \frac{1}{2\sqrt{3}} \sin\theta_a \right) + \mathrm{w}_b \left(\frac{1}{\sqrt{6}} + \frac{1}{2\sqrt{3}} \right) \tag{5.46}$$

which also has a maximum value when $\mathrm{w}_a = \mathrm{w}_b = 1$ and $\theta_a = \frac{\pi}{2}$ as shown in the surface and contour plots of Figure 5.9. The maximum arithmetic mean singular value is $\frac{\sqrt{2}+1}{\sqrt{3}}$, which agrees with previous results.

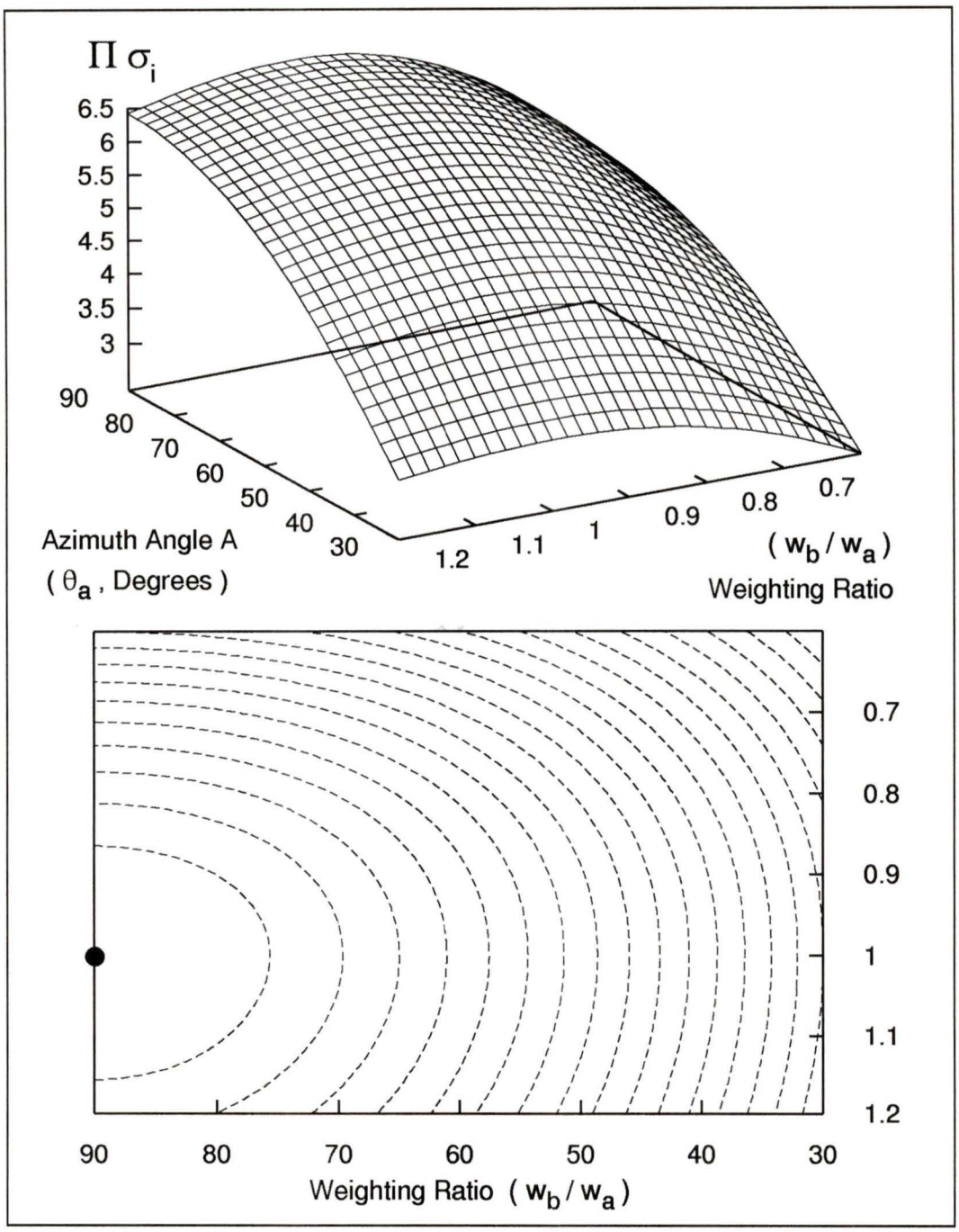

Figure 5.8: Surface and Contour Plot of Determinant vs. Horizontal Reciprocal Screw Direction and Reciprocal Screw Weighting Ratio

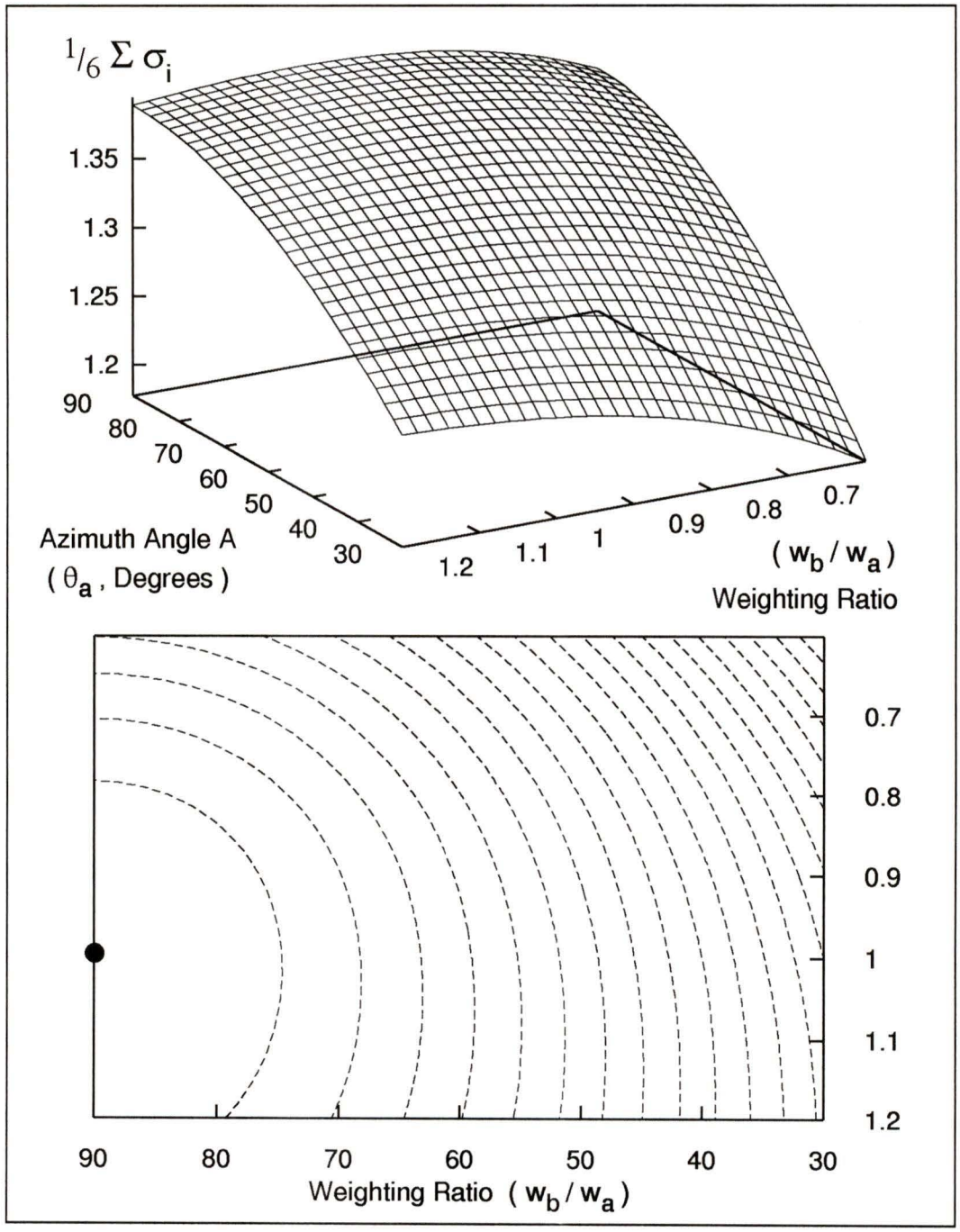

Figure 5.9: Surface and Contour Plot of Arithmetic Mean Singular Value vs. Horizontal Reciprocal Screw Direction and Reciprocal Screw Weighting Ratio

Minimum Singular Value

A closed form expression for the minimum singular value of [**K**] cannot be written. However, expressions for the singular values can be examined and conclusions can be drawn knowing that the goal is to maximize the minimum singular value. Examining equations (5.32) and (5.43), the first conclusion is that the minimum singular value can never be greater than $\sqrt{\frac{3}{2}}$ since the values of w_a and w_b cannot simultaneously be greater than unity. This means that all optimum reciprocal screw geometries, as quantified by the minimum singular value, have $w_a = w_b = 1$. Knowing the minimum singular value has a maximum of $\sqrt{\frac{3}{2}}$, examination of equation (5.36) shows that the the value of θ_a cannot be less than $\frac{\pi}{4}$ otherwise this singular value will become the smallest with a value less than the optimum. Therefore, θ_a can have any value between $\frac{\pi}{4}$ and $\frac{\pi}{2}$ while still maintaining the optimum minimum singular value. These results, which agree with those found in the optimization of Section 5.3.3, can easily be seen in the surface and contour plots of Figure 5.10. The dots on the contour plot mark the limits on θ_a for maintaining an optimum reciprocal screw geometry.

Condition Number

Since the condition number is the ratio of the largest and smallest singular values of [**K**], a closed form expression for the condition number cannot be written. However, knowing the minimum value of the condition number for optimum reciprocal screw geometries is $\sqrt{2}$ from Section 5.3.4, limits on the optimization variables such that this value is not exceeded can be found.

The lower and upper limits on the ratio of reciprocal screw weighting factors will be investigated first. Examining equations (5.32) and (5.43) it can be seen that if

w_b/w_a is less than $\frac{1}{\sqrt{2}}$ then the condition number of $[\mathbf{K}]$ will be

$$\kappa = \frac{\sigma_{max}}{\sigma_{min}} \geq \frac{\sigma_{\mathrm{f},x} = \sigma_{\mathrm{f},y}}{\sigma_{\mathrm{m},x} = \sigma_{\mathrm{m},y}} \geq \sqrt{2} \tag{5.47}$$

Similarly, from equations (5.32) and (5.34) it can be seen that if w_b/w_a is greater than one then the condition number is

$$\kappa = \frac{\sigma_{max}}{\sigma_{min}} \geq \frac{\sigma_{\mathrm{f},z}}{\sigma_{\mathrm{f},x} = \sigma_{\mathrm{f},y}} \geq \sqrt{2} \tag{5.48}$$

Therefore, the ratio of reciprocal screw weighting factors must lie between the following limits

$$\frac{1}{\sqrt{2}} \geq \frac{w_b}{w_a} \geq 1 \tag{5.49}$$

which agrees with the results found in Section 5.3.3.

Knowing the limits on the reciprocal screw weighting factor ratios, the limits on the horizontal reciprocal screw's azimuth angle θ_a can now be investigated. For the condition number to remain at its optimal value of $\sqrt{2}$ the singular value in the vertical direction of moment $\sigma_{\mathrm{m},z}$ must lie in the range

$$\sigma_{min} = \sigma_{\mathrm{m},x} = \sigma_{\mathrm{m},y} = \sqrt{\frac{3}{2}} w_b \leq \sigma_{\mathrm{m},z} = \sqrt{3} w_a \sin\theta_a \leq \sigma_{max} = \sigma_{\mathrm{f},z} = \sqrt{3} w_b \tag{5.50}$$

or

$$\frac{1}{\sqrt{2}} \frac{w_b}{w_a} \leq \sin\theta_a \leq \frac{w_b}{w_a} \tag{5.51}$$

Note that the above equation is only valid for w_b/w_a in the range defined by (5.49). Equation (5.51) agrees with relation found from the optimization results of Section 5.3.3 and completes the verification of limits on the optimization variables. The surface and contour plots of Figure 5.11 shows the behaviour of the condition number for different reciprocal screw geometries. The boundary defined by relations (5.49) and (5.51) is clearly seen on the plots with the corners of the boundary being marked with dots on the contour plot.

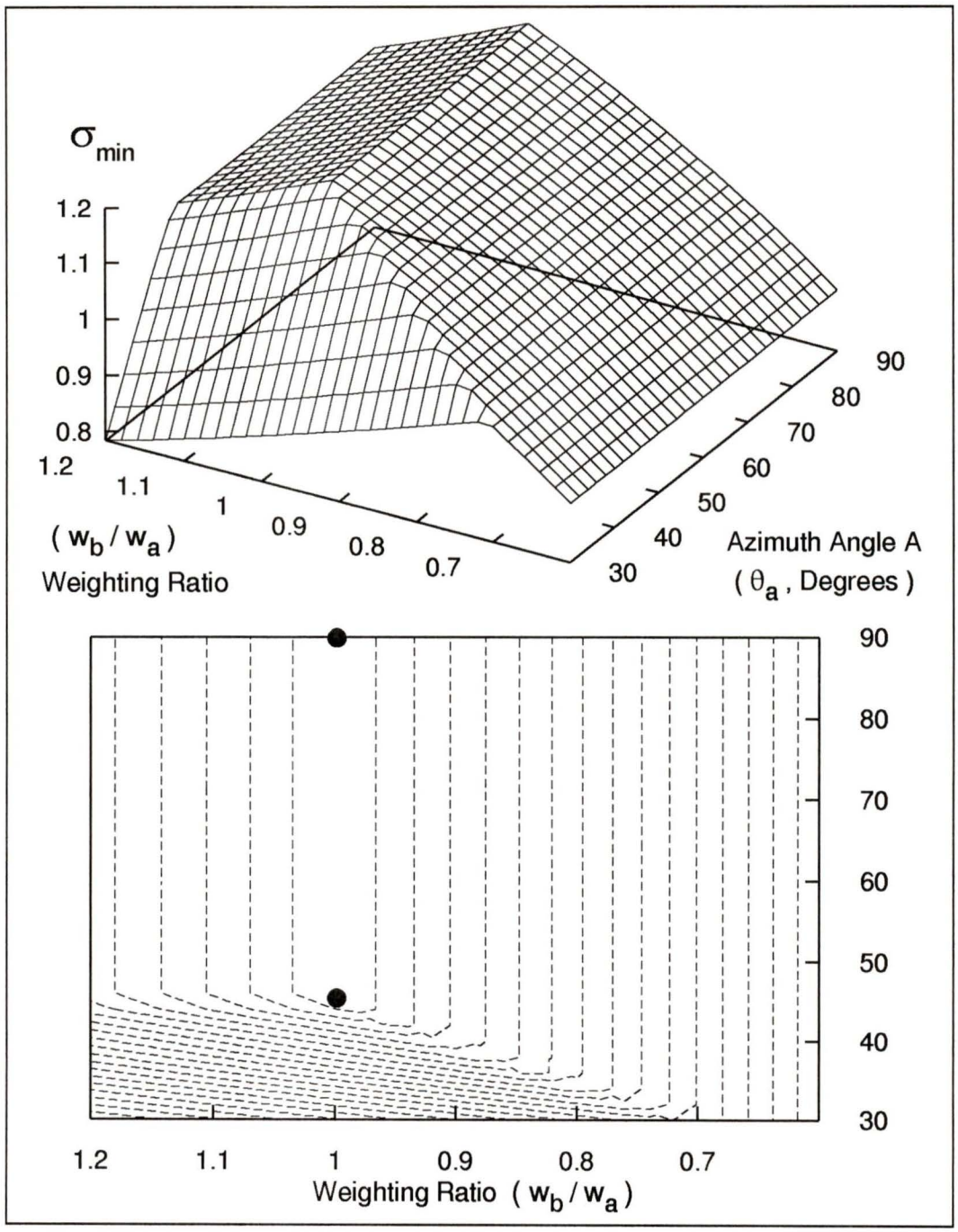

Figure 5.10: Surface and Contour Plot of Minimum Singular Value vs. Horizontal Reciprocal Screw Direction and Reciprocal Screw Weighting Ratio

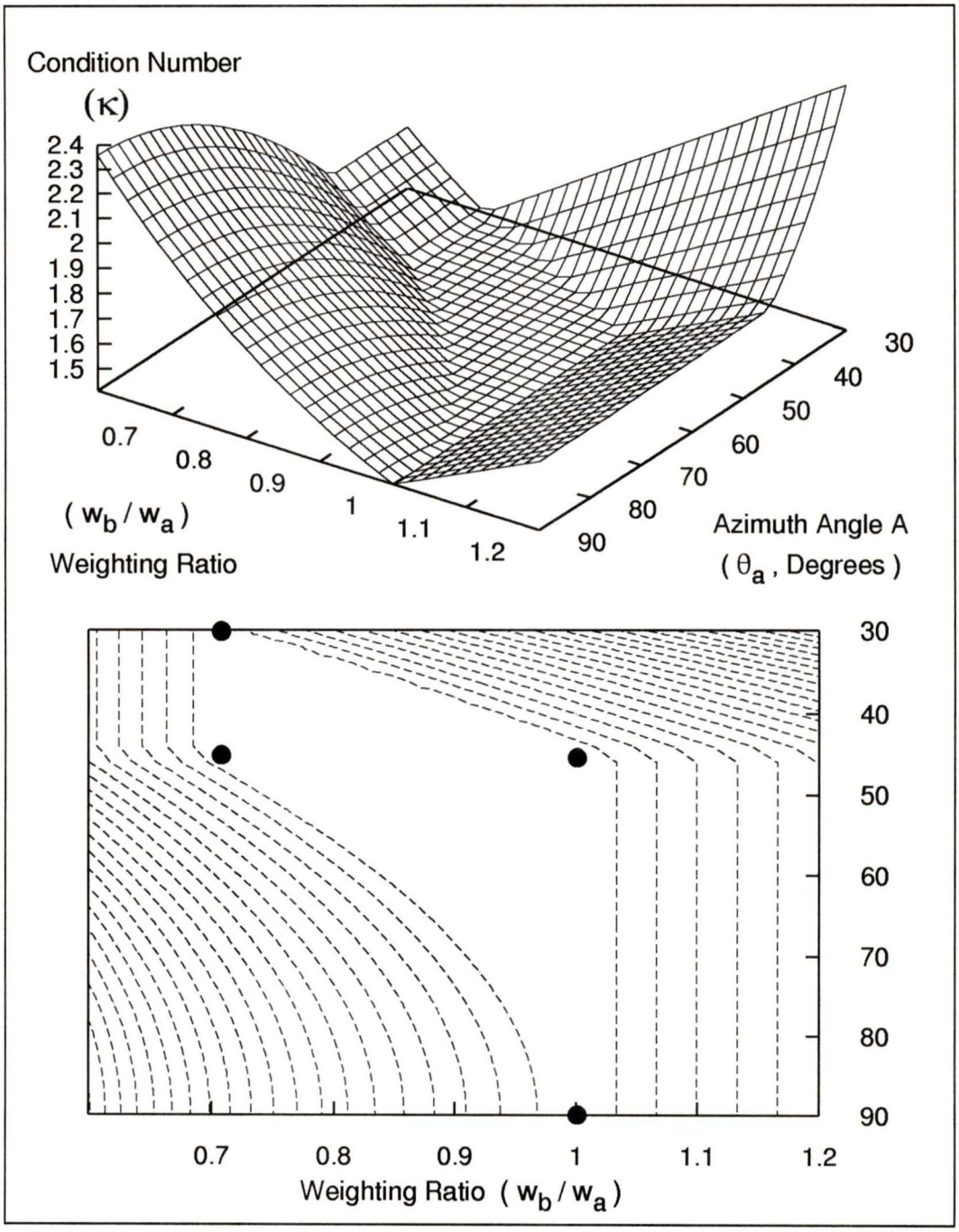

Figure 5.11: Surface and Contour Plot of Condition Number vs. Horizontal Reciprocal Screw Direction and Reciprocal Screw Weighting Ratio

5.4 Kinematically Simple Hybrid Manipulator Optimum Configurations

A unique reciprocal screw geometry for three-branch hybrid manipulators optimizing local dexterity was isolated in the previous section (Section 5.3). This optimum reciprocal screw geometry is composed of pairs of equally weighted reciprocal screws at each of the actuator attachment points on the platform. In each pair of reciprocal screws one reciprocal screw is normal to the plane of the platform (vertical) and the other is in the plane of the platform (horizontal) tangent to the platform circle. Optimum configurations of three-branch manipulators employing the kinematically simple branch structures found in Section 5.2 can now be determined using this optimum reciprocal screw geometry.

The three main-arm joint reciprocal screws for each of the five unique kinematically simple branch structures were found in Section 5.3.1 and illustrated in Figure 5.4. Only two of the three main-arm joints of the branches are actuated when non-redundant actuation is considered. Therefore, there are three possible actuated branch types for each unique kinematically simple branch structure and fifteen different actuated branch types in total. Each of these actuated branch types must be considered independently to determine branch configurations, and finally manipulator configurations, having the optimum reciprocal screw geometry.

The optimal reciprocal screw geometry requires that the pair of reciprocal screws associated with the actuated joints of each branch be perpendicular. The optimal reciprocal screw geometry also requires that all reciprocal screws have equal weightings as determined by the reciprocal products of the reciprocal screws and their associated joint screws. Recall that these reciprocal products are equivalent to the

"effective moment arms" (Section 2.2.2) of the reciprocal screws about the screw axis of the corresponding actuated joint. Using these two requirements on the geometry of the branches, branch configurations resulting in optimal manipulator configurations were found for each branch type and actuation. These branch configurations are illustrated in Figures 5.12 to 5.16 along with top views of the resulting optimum manipulator configurations. The actuated joint screws, associated reciprocal screws, and the "effective moment arm" distances (labelled with the dimension "d") are also shown on each branch configuration illustrated in these figures.

Finally, it is important to note that the branch and manipulator configurations illustrated in Figures 5.12 through 5.16 represent only one possible configuration for each branch type and joint actuation. Excluding scaling, there exists a one or two parameter family of branch configurations having perpendicular reciprocal screws and equal reciprocal products depending on branch type and actuation. Furthermore, the resulting branches can be mounted to the platform with either of the two reciprocal screws being perpendicular to the platform plane, yielding two optimum manipulator configurations for each branch configuration. Additional design considerations or further optimization utilizing performance measures other than kinematic dexterity can be used to isolate a unique manipulator configuration for each branch type and actuation. Performance measures and design considerations which could be utilized include dexterity gradients, workspace size, exploitation or avoidance of singular configurations, and factors and measures relating to dynamic performance.

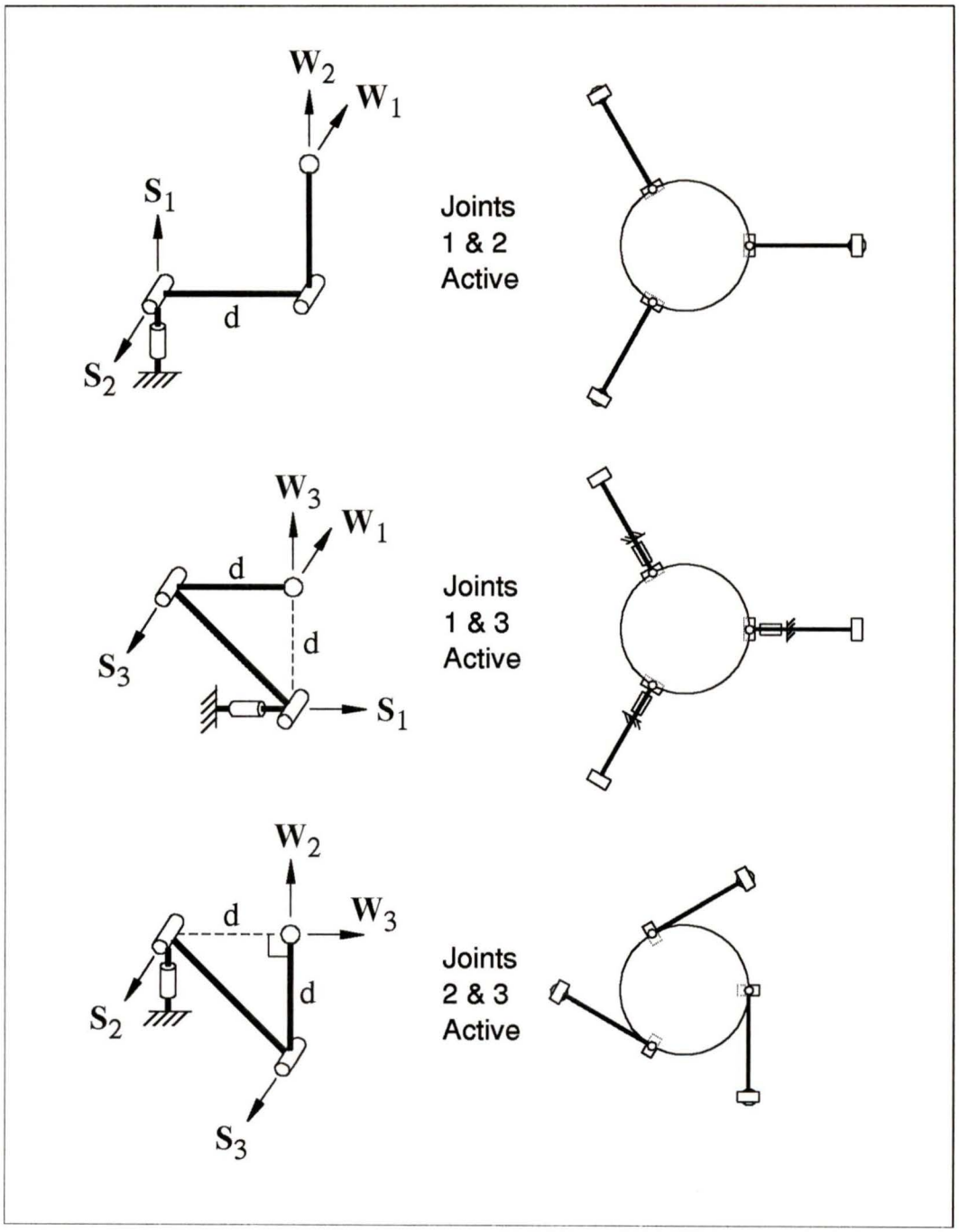

Figure 5.12: Optimum Branch and Manipulator Configurations for Hybrid Manipulators (Top Views) Based on the "CBE" Branch Type

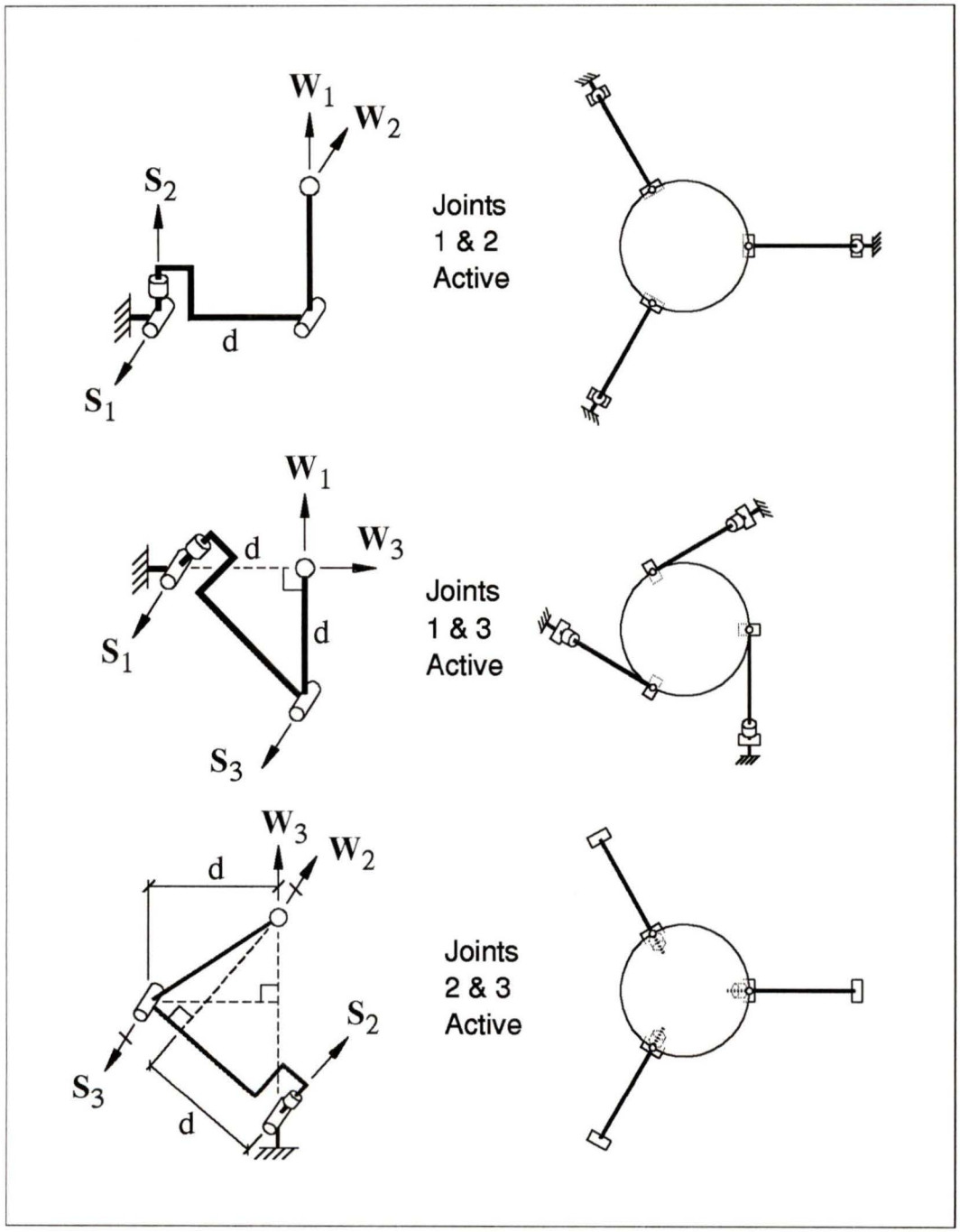

Figure 5.13: Optimum Branch and Manipulator Configurations for Hybrid Manipulators (Top Views) Based on the "CAE" Branch Type

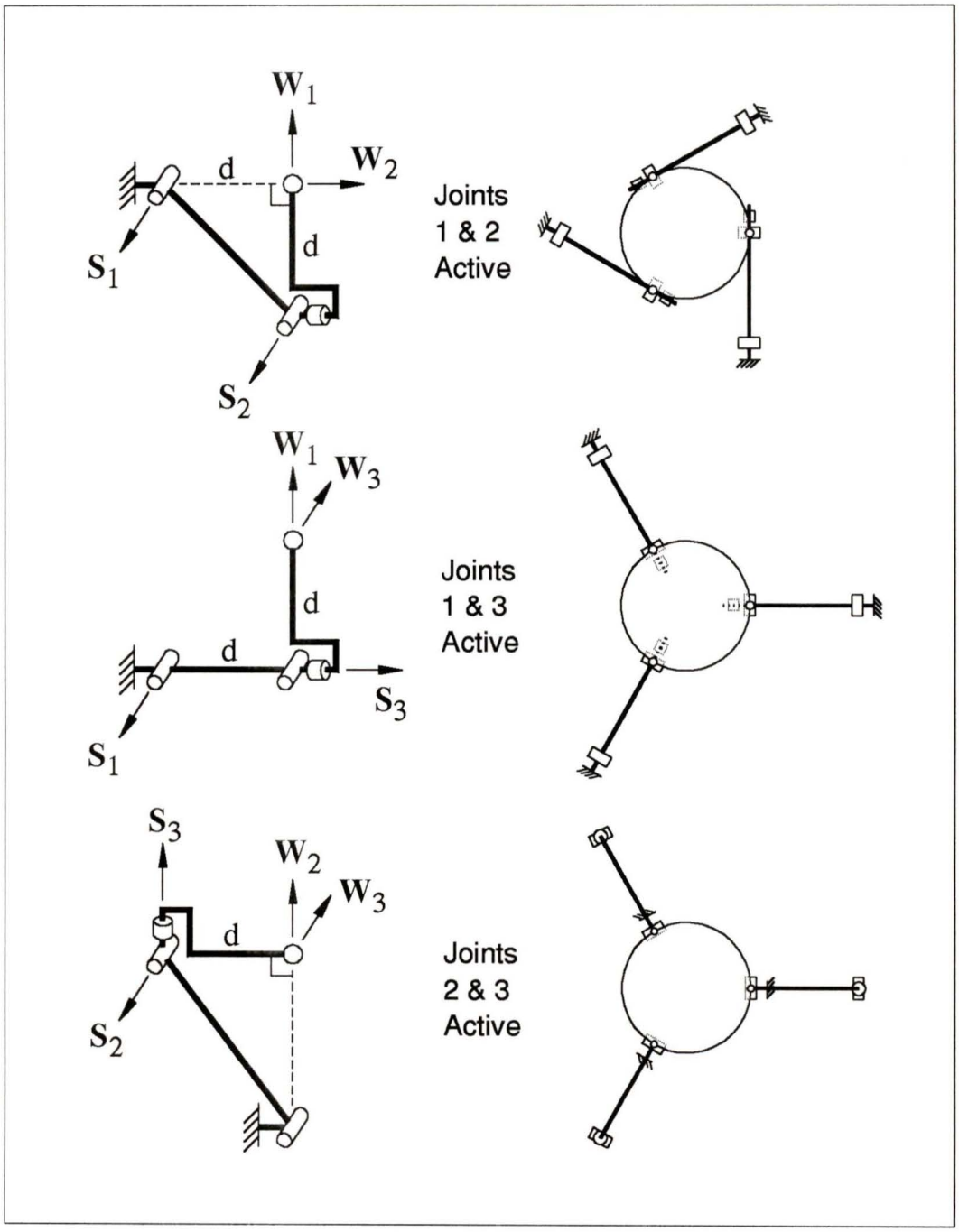

Figure 5.14: Optimum Branch and Manipulator Configurations for Hybrid Manipulators (Top Views) Based on the "BEF" Branch Type

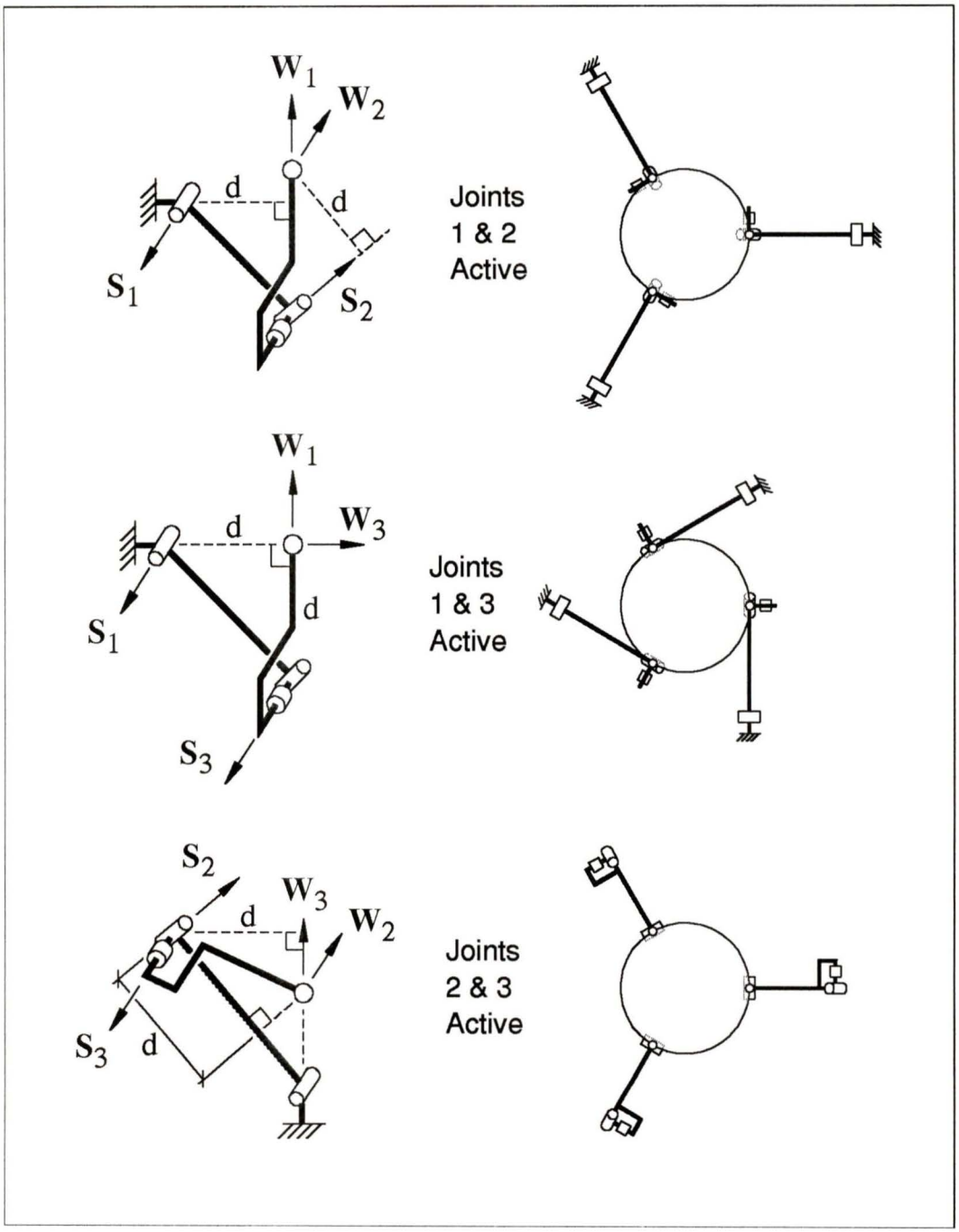

Figure 5.15: Optimum Branch and Manipulator Configurations for Hybrid Manipulators (Top Views) Based on the "AEF" Branch Type

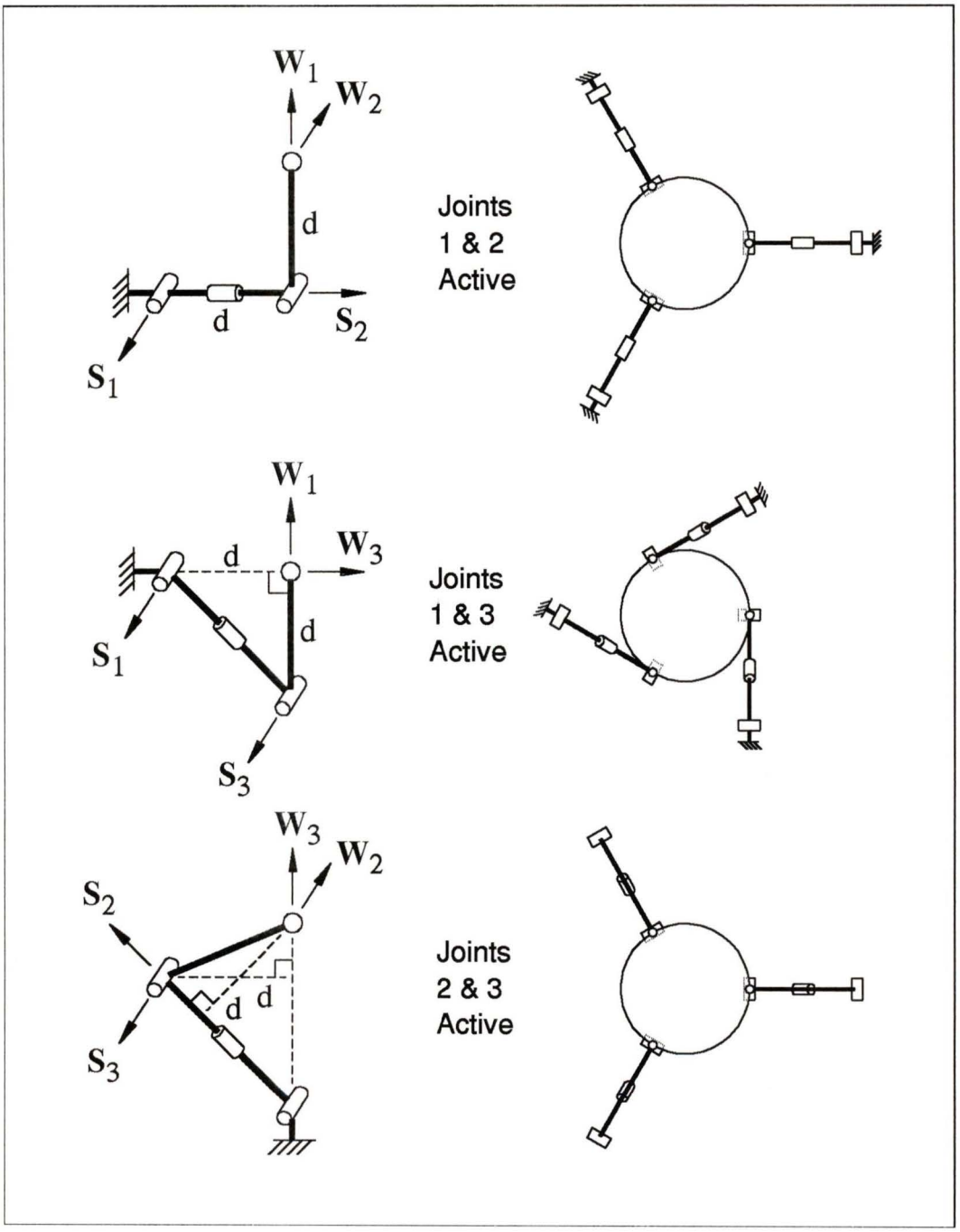

Figure 5.16: Optimum Branch and Manipulator Configurations for Hybrid Manipulators (Top Views) Based on the "BFE" Branch Type

Chapter 6

Conclusions and Recommendations

6.1 Conclusions of Presented Work

The design of six degree-of-freedom (DOF) fully-parallel and hybrid manipulators were examined for the objective of optimal dexterity. Both kinematic and geometric dexterity measures were examined for their suitability for use as objective functions in the optimum design of the closed-chain structures. It was concluded that present geometric dexterity measures were generally unsuitable as design objectives for closed-chain devices. Kinematic dexterity measures, which are based upon instantaneous kinematic characteristics of the manipulator, were found to be widely applicable to both open and closed-chain devices. The frame and unit variability of kinematic dexterity measures was demonstrated. The need to select a unit of length measure and a frame of reference location with physical significance were emphasized in order for the kinematic dexterity measures to have meaningful interpretations.

The fully-parallel Stewart platform was the first manipulator structure examined for design optimization using kinematic dexterity as a performance measure. Manipulator configurations (manipulator architectures and end effector positions and orientations) optimizing local kinematic dexterity were first determined. Using the radius of the platform as a characteristic length to weight angular and translational velocities equally, and a platform centred reference location, a two-parameter family containing an infinite number of optimal configurations was shown to exist. This result differs from that reported by Ma and Angeles [30] where only one optimum manipulator configuration was found. Three relations, (4.9), (4.10), and (4.11), defining the family of locally optimal configurations were derived for the given choices of length measure and reference location. The configuration optimization results were shown to be easily extended for reference locations vertically displaced from the centre of the platform. This involved the consideration of a *virtual platform.*

A Stewart Platform in an optimal configuration was found to require $\sqrt{2}$ times more joint effort (measured by $\|\dot{\mathbf{q}}\|$) to translate or rotate in the vertical direction than is required to translate or rotate in any direction in the horizontal plane. As a consequence of work-energy relations, $\sqrt{2}$ times as much joint effort (measured by $\|\boldsymbol{\tau}\|$) is required to produce a force or moment in the horizontal plane than is required to produce a force or moment in the vertical direction.

Global performance measures introduced in previous literature were found to be excessively computationally intensive when used as objectives in optimizing the design of six DOF manipulators. A new performance measure possessing global implications and having reduced computational expense was introduced to overcome these problems. This new measure utilizes spatial gradients of kinematic dexterity to form a first-order approximation to the characteristics of the manipulator at points displaced

from a local optimum configuration. The new measure was employed to isolate a unique optimum Stewart platform architecture from the family of those possessing optimum local characteristics. The resulting optimum manipulator architecture is one in which the dimensions of the base is twice that of the platform ($r_b = 2\,r_p$) and the linear actuator attachment points at the base and platform meet in alternating pairs ($\phi_b = \phi_p = 0$).

The optimum design of hybrid manipulators were then examined. In the context of this work, hybrid manipulators were defined as manipulators consisting of serial branches, each comprised of actuated and passive joints, acting in parallel on a common end effector. Potential non-redundant six DOF hybrid manipulator structures were enumerated. Based on considerations of desired kinematic and dynamic attributes, structures having three serial branches with two actuated joints per branch were concluded to have preferred characteristics. A class of kinematically simple branches suitable for hybrid manipulator structures was defined. Based upon mobility and branch equivalency considerations, it was concluded that only five unique branch structures employing revolute joints belong to the kinematically simple class.

A novel approach to manipulator configuration optimization for optimal local kinematic dexterity was introduced. This new approach involved finding reciprocal screw directions and reciprocal product weighting factors optimizing kinematic dexterity, and then finding actual manipulator configurations having these optimum reciprocal screw directions and reciprocal products. The method was applied to the configuration optimization of three-branch hybrid manipulators and a one-parameter family of optimum reciprocal screw directions and weightings was shown to exist. Each member of this family of optima have the same instantaneous kinematic characteristics as those of the optimum Stewart platform configurations given above. Based upon

considerations of changes in the reciprocal screw directions and weightings as the hybrid manipulator is moved from its optimum configuration, a unique set of reciprocal screw directions and reciprocal product weighting factors was concluded to be potentially advantageous. Optimal configurations of three-branch hybrid manipulators corresponding to the chosen reciprocal screw directions and reciprocal product weighting factors were illustrated. These optimal manipulator configurations utilized the previously identified kinematically simple branch structures.

6.2 Recommendations for Future Research

The three-branch hybrid manipulator optimal configurations illustrated at the end of this thesis utilized the kinematically simple branch structures previously identified in the work. However, many different configurations of these kinematically simple branch structures can result in the manipulator having an optimum configuration. To complete the optimal architectural design of three-branch hybrid manipulators utilizing these branch structures, a second set of optimizations should be carried out for manipulators with each branch type and set of actuated joints. Considerations of branch workspace size, singular positions, isotropic configurations, and other characteristics can be used initially to narrow the scope of branch types to be studied. However, other performance measures based on global characteristics of the assembled manipulator must be used to isolate a unique optimum manipulator architecture for each considered branch type. Dexterity gradients about the manipulator's optimal configuration are one such measure that could be employed. Comparison of manipulators utilizing each of the kinematically simple branch types considered will allow the selection of a single optimal three-branch hybrid manipulator architecture.

Finally, the work presented in this thesis constitutes only an initial investigation into the optimum design of six DOF parallel and hybrid manipulators. Merely one fully-parallel and a class of hybrid structures with three kinematically simple branches were studied. Much work needs to be done in order to fully investigate the design of these and other closed-chain manipulator structures. Other design considerations which should be examined as part of a complete design study include: workspace size and shape, dynamic performance, and the position of singularities within the workspace. The design of required passive joints such as the branch-end spherical joints should also be investigated. Other manipulator structures which could be considered are: three-branch hybrid manipulators with kinematically simple branches containing prismatic joints, fully-parallel manipulators utilizing six kinematically simple branches, and manipulators possessing joint and actuation redundancy. Properly designed manipulators with actuation redundancy can possess many performance benefits such as the elimination of uncertainty configurations, the possibility of actuator load sharing and optimization, as well as having closed form solutions to the forward displacement problem if all actuated joints are instrumented with displacement transducers. It is believed that these benefits of redundantly actuated closed-chain manipulators will prompt future research and development into their design and application.

References

[1] Angeles, J., "On the Numerical Solution of the Inverse Kinematic Problem," *The International Journal of Robotics Research*, Vol. 4, No. 2, 1985, pp. 21–37.

[2] Angeles, J., and López-Cajún, C.S., "The Dexterity Index of Serial-Type Robotic Manipulators," *Proceedings of the 20'th ASME Biennial Mechanisms Conference*, Kissimme, FL, 1988, pp. 79–84.

[3] Asada, H., "A Geometrical Representation of Manipulator Dynamics and Its Application to Arm Design," *ASME Journal of Dynamic Systems, Measurement, and Control*, Vol. 105, September 1983, pp. 131–135, p. 142.

[4] Asada, H., Cro Granito, J.A., "Kinematic and Static Characterisation of Wrist Joints and their Optimal Design," *Proceedings of the 1985 IEEE International Conference on Robotics and Automation*, St. Louis, MO, March 1985, pp. 244–250.

[5] Asada, H., Youcef-Toumi, K., *Direct Drive Robots: Theory and Practice*, MIT Press, 1987.

[6] Ball, R.S., *The Theory of Screws: A Study in the Dynamics of a Rigid Body*, Hodges, Foster, and Co., Dublin, 1876.

[7] Chiu, S.L., "Kinematic Characterization of Manipulators: An Approach to Defining Optimality," *Proceedings of the 1988 IEEE International Conference on Robotics and Automation*, Philadelphia, PA, April 1988, pp. 828–833.

[8] Cleary, K., Arai, T., "A Prototype Parallel Manipulator: Kinematics, Construction, Software, Workspace Results, and Singularity Analysis," *Proceedings of the 1991 IEEE International Conference on Robotics and Automation*, Sacramento, CA, April 1991, pp. 566–571.

[9] Craig, J.J., *Introduction to Robotics: Mechanics and Control*, Addison-Wesley, 1986.

[10] Fichter, E.F., "A Stewart Platform-Based Manipulator: General Theory and Practical Construction," *The International Journal of Robotics Research*, Vol. 5, No. 2, 1986, pp. 157–182.

[11] Forsythe, G.E., Moler, C.B., *Computer Solutions of Linear Algebraic Systems*, Prentice-Hall, Englewood Cliffs, N.J., 1967.

[12] Golub, G.H., Van Loan, C.F., *Matrix Computations*, Johns Hopkins University Press, Baltimore, 1983.

[13] Gosselin, C. and Angeles, J., "The Optimum Kinematic Design of a Planar Three-Degree-of-Freedom Parallel Manipulator," *ASME Journal of Mechanisms, Transmissions, and Automation in Design*, Vol. 110, No. 1, 1988, pp. 35–41.

[14] Gosselin, C. and Angeles, J., "The Optimum Kinematic Design of a Spherical Three-Degree-of-Freedom Parallel Manipulator," *ASME Journal of Mechanisms, Transmissions, and Automation in Design*, Vol. 111, No. 2, 1989, pp. 202–207.

[15] Gosselin, C., "Determination of the Workspace of 6-DOF Parallel Manipulators," *ASME Journal of Mechanical Design*, Vol. 112, September 1990, pp. 331–336.

[16] Gosselin, C. and Angeles, J., "Singularity Analysis of Closed-Loop Kinematic Chains," *IEEE Transactions on Robotics and Automation*, Vol. 6, No. 3, 1990, pp. 281–290.

[17] Gosselin, C. and Angeles, J., "A Global Performance Index for the Kinematic Optimization of Robotic Manipulators," *ASME Journal of Mechanical Design*, Vol 113, September 1991, pp. 220–226.

[18] Gough, V.E., Whitehall, S.G., "Universal Tyre Test Machine," *Proceedings of the 9'th International Automobile Technical Congress*, FISITA, Institute of Mechanical Engineering (London), May 1962, pp. 117-137.

[19] Griffis, M., Duffy, J., "A Forward Displacement Analysis of a Class of Stewart Platforms," *Journal of Robotic Systems*, Vol. 6, No. 6, 1989, pp. 703–720.

[20] Hunt, K.H., *Kinematic Geometry of Mechanisms*, Claridon Press, Oxford, 1978.

[21] Hunt, K.H., "Structural Kinematics of In-Parallel-Actuated Robot-Arms," *ASME Journal of Mechanisms, Transmissions, and Automation in Design*, Vol. 105, December 1983, pp. 705–712.

[22] Innocenti, C., Parenti-Castelli, V., "Direct Position Analysis of the Stewart Platform Mechanism," *Mechanism and Machine Theory*, Vol. 25, No. 6, 1990, pp. 611–621.

[23] Inoue, H., Tsusaka, Y., and Fukuizumi, T., "Parallel Manipulator," *Proceedings of the 3'rd International Symposium on Robotics Research*, Gouvieux, France, 1985, pp. 321-327.

[24] Klein, C.A, Huang, C-H., "Review of Psuedoinverse Control for use with Kinematically Redundant Manipulators," *IEEE Transactions on Systems, Man, and Cybernetics*, Vol. SMC-13, No. 3, 1983, pp. 245–250.

[25] Klein, C.A., and Blaho, B.E., "Dexterity Measures for the Design and Control of Kinematically Redundant Manipulators," *The International Journal of Robotics Research*, Vol. 6, No. 2, 1987, pp. 72–83.

[26] Kokkinis, T., and Stoughton, R., "Optimal Parallel Actuation Linkage for 3 DOF Elbow Manipulators," *Proceedings of the 20'th ASME Biennial Mechanisms Conference*, Kissimme, FL, 1988, pp. 465–472.

[27] Kumar, A., Waldron, K.J., "The Workspaces of a Mechanical Manipulator," *ASME Journal of Mechanical Design*, Vol. 103, No. 3, 1981, pp. 665–672.

[28] Kumar, V., "Instantaneous Kinematics of Parallel-Chain Robotic Mechanisms," *Proceedings of the 21'st ASME Biennial Mechanisms Conference*, Vol. DE-25, Chicago, IL, Sept. 1990, pp. 279–287.

[29] Liègeois, A., "Automatic Supervisory Control of the Configuration and Behaviour of Multibody Mechanisms," *IEEE Transactions on Systems, Man, and Cybernetics*, Vol. SMC-7, No. 12, 1977, pp. 868–871.

[30] Ma, O., and Angeles, J., "Optimum Architecture Design of Platform-Type Parallel Manipulators," *Technical Report of McGill Research Centre for Intelligent Machines (McRCIM) and the Department of Mechanical Engineering*, McGill University, Montreal, 1990.

[31] McCallion, H., Truong, P.D., "The Analysis of a Six-Degree-of-Freedom Work Station for Mechanised Assembly," *Proceedings of the 5'th World Congress on Theory of Machines and Mechanisms*, 1979, pp. 611-616.

[32] Merlet, J-P., "Parallel Manipulators, Part I: Theory, Design, Kinematics, Dynamics and Control," INRIA research report No. 646, France, March 1987.

[33] Merlet, J-P., "Manipulateurs Paralleles, 4eme Partie: Mode D'Assemblage et Cinematique Directe sous Forme Polynomiale," INRIA research report No. 1135, France, December 1989.

[34] Merlet, J-P., Gosselin, C., "Nouvelle Architecture Pour un Manipulateur Parallelle a Six Degres de Liberte," *Mechanism and Machine Theory*, Vol. 26, No. 1, 1991, pp. 77–90.

[35] Mohamed, M.G., Duffy, J., "A Direct Determination of the Instantaneous Kinematics of Fully Parallel Robot Manipulators," *ASME Journal of Mechanisms, Transmissions, and Automation in Design*, Vol. 107, June 1985, pp. 226–229.

[36] Nanua, P., Waldron, K.J., Murthy, V., "Direct Kinematic Solution of a Stewart Platform," *IEEE Transactions on Robotics and Automation*, Vol. 6, No. 4, 1990, pp. 438–444.

[37] Nelder, J.A., Mead, R., "A Simplex Method for Function Minimization," *The Computer Journal*, Vol. 7, 1965, pp. 308–313.

[38] Paden, B., Sastry, S., "Optimal Kinematic Design of 6R Manipulators," *The International Journal of Robotics Research*, Vol. 7, No. 2, 1988, pp. 43–61.

[39] Paul, R.P., *Robot Manipulators: Mathematics, Programming, and Control*, MIT Press, 1981.

[40] Paul, R.P., Stevenson, C.N., "Kinematics of Robot Wrists," *The International Journal of Robotics Research*, Vol. 2, No. 1, 1983, pp. 31–38.

[41] Pieper, D., "The Kinematics of Manipulators Under Computer Control," Ph.D. Thesis, Stanford University, 1968.

[42] Pierrot, F., Dauchez, P., Fournier, A., "Fast Parallel Robots," *Journal of Robotic Systems*, Vol. 8, No. 6, 1991, pp. 829–840.

[43] Pittens, K.P., and Podhorodeski, R.P., "Considerations of Kinematic Equivalency in Stewart Platform Configuration Optimization," *Proceedings of the 2'nd National Applied Mechanisms and Robotics Conference*, Cincinnati, OH, Nov. 1991, paper No. IXC.3.

[44] Pittens, K.P. and Podhorodeski, R.P., "A Family of Stewart Platforms with Optimal Dexterity," to appear in *Journal of Robotic Systems*, Vol. 10, No. 6, 1993.

[45] Podhorodeski, R.P., and Pittens, K.P., "A Class of Hybrid-Chain Manipulators Based on Kinematically Simple Branches," *Proceedings of the 22'nd ASME Biennial Mechanisms Conference*, Vol. DE-27, Phoenix, AZ, Sept. 1992, pp. 59-64.

[46] Podhorodeski, R.P., "A Screw Theory Based Forward Displacement Solution for Hybrid Manipulators," *Proceedings of the 2'nd National Applied Mechanisms and Robotics Conference*, Cincinnati, OH, Nov. 1991, paper No. IIIC.2.

[47] Raghavan, M., Roth, B., "Inverse Kinematics of the General 6R Manipulator and Related Linkages," *Proceedings of the 21'st ASME Biennial Mechanisms Conference*, Vol. DE-25, Chicago, IL, Sept. 1990, pp. 59–65.

[48] Salisbury, K., and Craig, J., "Articulated Hands: Force Control and Kinematic Issues," *The International Journal of Robotics Research*, Vol. 1, No. 1, 1982, pp. 4–17.

[49] Shahinpoor, M., "Kinematics of a Parallel-Serial (Hybrid) Manipulator," *Journal of Robotic Systems*, Vol. 9, No. 1, 1992, pp. 17–36.

[50] Singh, J.R., Rastegar, J., "Optimal Synthesis of Robot Manipulators Based on Global Kinematic Parameters," *Proceedings of the 21'st ASME Biennial Mechanisms Conference*, Vol. DE-26, Chicago, IL, Sept. 1990, pp. 207–213.

[51] Stewart, D., "A Platform with Six Degrees of Freedom," *Proceedings of the Institute of Mechanical Engineering (London)*, Vol. 180, Pt. 1, No. 15, 1965, pp. 371–386.

[52] Sugimoto, K., "Kinematic and Dynamic Analysis of Parallel Manipulators by Means of Motor Algebra," *ASME Journal of Mechanisms, Transmissions, and Automation in Design*, Vol. 109, March 1987, pp. 3–7.

[53] Vijaykumar, R., Waldron, K.J., Tsai, M.J., "Geometric Optimization of Serial Chain Manipulator Structures for Working Volume and Dexterity," *The International Journal of Robotics Research*, Vol. 5, No. 2, 1986, pp.91–103.

[54] Vinogradov, I.B., Kobrinski, A.E., Stepanenko, Y.E., Tives, L.T., "Details of Kinematics of Manipulators with the Method of Volumes," (in Russian), *Mekhanika Mashin*, No. 27–28, 1971, pp. 5–16.

[55] Waldron, K.J., Hunt, K.H., "Series-Parallel Dualities in Actively Coordinated Mechanisms," *The International Journal of Robotics Research*, Vol. 10, No. 5, 1991, pp. 473–480.

[56] Wampler, C., Morgan, A., "Solving the 6R Inverse Position Problem Using a Generic-Case Solution Methodology," *Mechanism and Machine Theory*, Vol. 26, No. 1, 1991, pp. 91–106.

[57] Woo, L., Freudenstein, F., "Application of Line Geometry to Theoretical Kinematics and the Kinematic Analysis of Mechanisms," *ASME Journal of Mechanisms*, Vol. 5, 1970, pp. 417-460.

[58] Yang, D.C.H., Lee T.W., "Feasibility Study of a Platform Type of Robotic Manipulators from a Kinematic Viewpoint," *ASME Journal of Mechanisms, Transmissions, and Automation in Design*, Vol. 106, June 1984, pp. 191-198.

[59] Yang, D.C.H., Lai, Z.C., "On the Dexterity of Robotic Manipulators—Service Angle," *ASME Journal of Mechanisms, Transmissions, and Automation in Design*, Vol. 107, June 1985, pp. 262–270.

[60] Yoshikawa, T., "Analysis and Control of Robot Manipulators with Redundancy," *Proceedings of the First International Symposium of Robotics Research*, Bretton Woods, N.H., Aug. 28-Sept. 2, 1983.

[61] Yoshikawa, T., "Dynamic Manipulability of Robot Manipulators," *Journal of Robotic Systems*, Vol. 2, No. 1, 1985, pp. 113–124.

[62] Yoshikawa, T., *Foundations of Robotics: Analysis and Control*, MIT Press, 1990.

Appendix A

Screws, Screw Quantities and Screw Algebra

A.1 Screws and Screw Coordinates

A *screw* is geometric entity consisting of a line in space with an associated linear *pitch* [6]. A screw can be represented by its unit *screw coordinates* as defined by Woo and Freudenstein [57],

$$\$ = \left\{ \begin{array}{c} \$ \\ \$_o \end{array} \right\} = \left\{ \begin{array}{c} \mathbf{l} \\ \mathbf{l}_o + p_L \mathbf{l} \end{array} \right\} \quad ; \quad \|\mathbf{l}\| = 1 \,, \quad \mathbf{l} \cdot \mathbf{l}_o = 0 \tag{A.1}$$

where $\mathbf{l}$ and $\mathbf{l}_o$ are the direction of the screw axis and its moment about the origin of a frame of reference, respectively; p_L is the pitch of the screw. $\$$ is the primary vector and $\$_o$ the secondary vector of the screw coordinates. The screw coordinates $\mathbf{L} = \{\mathbf{l}\,;\,\mathbf{l}_o\}^T$ are referred to as the *Plücker coordinates* of the line associated with the screw axis. These quantities and their relationships are illustrated in Figure A.1.

Associating an *amplitude* with a screw allows a *screw quantity* to be defined. For example, a screw quantity $\mathbf{S}$ of amplitude α can be described by the following screw coordinates:

$$\mathbf{S} = \left\{ \begin{array}{c} \mathbf{s} \\ \mathbf{s}_o \end{array} \right\} = \alpha \left\{ \begin{array}{c} \$ \\ \$_o \end{array} \right\} = \alpha \$ \tag{A.2}$$

Screw quantities are natural entities for describing instantaneous spatial motions (velocities) and for describing forces and moments acting on a body. That is, any instantaneous spatial velocity $\mathbf{V}$ of a rigid body can be described as a *twist* of amplitude ω about a unique instantaneous screw axis $\$$,

$$\mathbf{V} = \omega \$ = \omega \left\{ \begin{array}{c} \$ \\ \$_o \end{array} \right\} = \left\{ \begin{array}{c} \boldsymbol{\omega} \\ \mathbf{v} \end{array} \right\} \tag{A.3}$$

where $\boldsymbol{\omega}$ is the angular velocity vector of the body and $\mathbf{v}$ is the translational velocity of a point on the rigid body (extended to be) instantaneously coincident with the origin of the frame of reference.

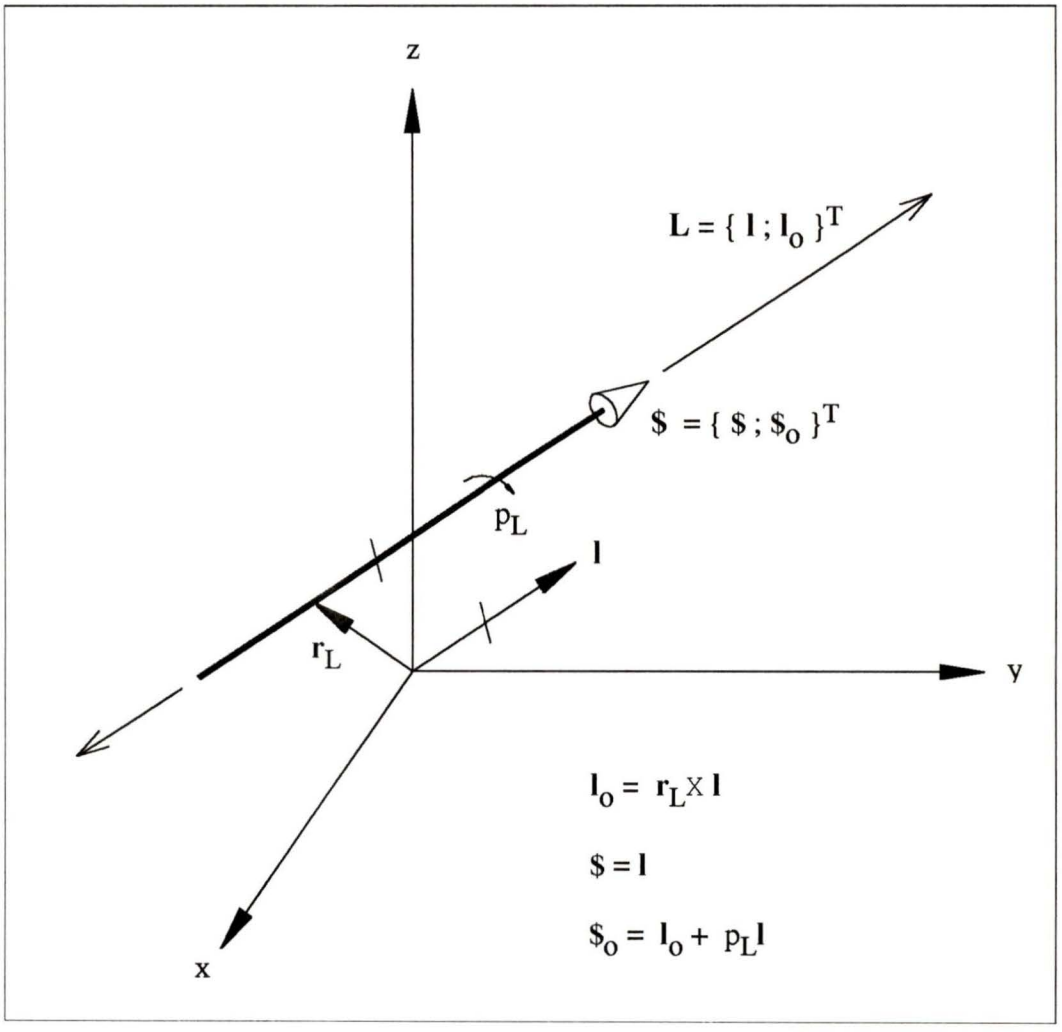

Figure A.1: A screw and its line screw coordinates

A pure rotation or angular velocity about an instantaneous axis are described as twists about a screw of zero pitch. Since p_L is zero, the unit screw coordinates as given by equation (A.1) become identical to the Plücker coordinates of the line which the rotation is occurring about. The revolute joints of a manipulator or other mechanism can be represented by zero pitch screws since these kinematic pairs only allow a single pure relative rotational freedom. A pure translation or translational velocity along a line are described as an infinitesimal twist about a screw of infinite pitch. Normalizing the screw coordinates for a screw of infinite pitch results in the screw coordinates becoming $\$ = \{ \mathbf{0} ; \mathbf{l} \}^T$, where $\mathbf{l}$ is a unit vector in the direction of the translational motion. The prismatic joints of a manipulator can be modelled as infinite pitch screws since the joint allows only a single translatory freedom.

Any system of forces and moments acting on a body can be represented as a *wrench* $\mathbf{F}$ of *intensity* f acting on a screw,

$$\mathbf{F} = f\$ = f \left\{ \begin{array}{c} \$ \\ \$_o \end{array} \right\} = \left\{ \begin{array}{c} \mathbf{f} \\ \mathbf{m} \end{array} \right\} \tag{A.4}$$

where

$$\mathbf{f} = \sum \mathbf{f}_i \quad ; \quad \mathbf{m} = \sum \mathbf{m}_i + \mathbf{r}_i \times \mathbf{f}_i$$

In the above relation $\mathbf{f}_i$ are forces and $\mathbf{m}_i$ are moments acting on the body, and $\mathbf{r}_i$ are position vectors from the origin of the frame of reference to any point along the line of action of force $\mathbf{f}_i$. $\mathbf{f}$ is the resultant force acting on the body and $\mathbf{m}$ is the resultant moment as seen from the origin of the frame of reference.

A pure force acting on a body is described as a wrench acting on a screw of zero pitch, the intensity of the wrench being equal to the magnitude of the force. As for the case of twists acting on a screw of zero pitch, the screw coordinates for a wrench of zero pitch are identical to the Plücker coordinates of the line of action of the force.

A pure moment or couple acting on a body is a wrench of infinitesimal intensity acting on a screw of infinite pitch. In this case the unit screw coordinates become $\$ = \{ 0 ; \mathbf{l} \}^T$, indicating that no force is created when the screw is acted on by a wrench of any intensity.

Examining equation (A.4), it is important to note that the wrench is not merely the resultant of a system of forces and moments acting on a body, but more generally can be considered to be the resultant of a system of wrenches acting on it. This resultant wrench is the sum of all wrenches acting on the body demonstrating that wrenches act in parallel with one another. This is in contrast to twists about instantaneous screw axes which act in series with one another, summing to produce a resultant motion of a body. This inherent difference between wrenches and twists is due to the *reciprocity*, or *duality*, which exists between statics and instantaneous kinematics [20]. Both forces in statics and rotational velocities in instantaneous kinematics are line vectors, both obeying the same laws of vector algebra. Similarly, moments in statics and translational velocities in instantaneous kinematics are both free vectors where only directions are important, the vectors not being confined to any specific line of action. This allows both statics (wrenches acting on screws) and instantaneous kinematics (twists acting on screws) to be treated in a homogeneous manner algebraically, further demonstrating the duality between the two systems.

A.2 Reciprocal Products and Reciprocal Screws

The *reciprocal product* of two screw quantities, $\mathbf{S}_1$ and $\mathbf{S}_2$, is defined as the inner product

$$\mathbf{S}_1 \chi \mathbf{S}_2 = \left\{ \begin{array}{c} \mathbf{s}_1 \\ \mathbf{s}_{o_1} \end{array} \right\} \chi \left\{ \begin{array}{c} \mathbf{s}_2 \\ \mathbf{s}_{o_2} \end{array} \right\} = \mathbf{s}_1 \cdot \mathbf{s}_{o_2} + \mathbf{s}_{o_1} \cdot \mathbf{s}_2 \tag{A.5}$$

where χ is the reciprocal product operator. The reciprocal product of a wrench and a twist quantifies a rate of work. Two screws are *reciprocal* when their reciprocal product is zero. For example, a body having a motion described by the twist $\mathbf{V}$ subjected to a force system described by a wrench $\mathbf{F}$ reciprocal to $\mathbf{V}$ performs no work since $\mathbf{V} \chi \mathbf{F} = 0$. It is important to note that the property of reciprocity is invariant of a change in frame of reference since work is a scalar quantity which is inherently frame invariant.

The reciprocal product of two screw quantities can be expressed in standard vector algebraic notation by the introduction of a *complement operator*. This operator exchanges the two elements of a screw quantity when expressed in screw coordinate form,

$$\mathbf{S}^* = \left\{ \begin{array}{c} \mathbf{s} \\ \mathbf{s}_o \end{array} \right\}^* = \left\{ \begin{array}{c} \mathbf{s}_o \\ \mathbf{s} \end{array} \right\} \tag{A.6}$$

where $(\cdot)^*$ is the complement operator. This operator can also be described as a pre-multiplication by a transformation matrix which transforms the screw into its complement,

$$\mathbf{S}^* = \left\{ \begin{array}{c} \mathbf{s} \\ \mathbf{s}_o \end{array} \right\}^* = \left[\begin{array}{cc} [\mathbf{0}]_{3\times3} & [\mathbf{I}]_{3\times3} \\ [\mathbf{I}]_{3\times3} & [\mathbf{0}]_{3\times3} \end{array} \right] \left\{ \begin{array}{c} \mathbf{s} \\ \mathbf{s}_o \end{array} \right\} \tag{A.7}$$

where $[\mathbf{I}]_{3\times3}$ is a three by three identity matrix and $[\mathbf{0}]_{3\times3}$ is a three by three matrix with all zero entries. Using the complement operator, the reciprocal product of screws

as defined by equation (A.5) can be rewritten as

$$\mathbf{S}_1 \chi \mathbf{S}_2 = \mathbf{S}_1^T \mathbf{S}_2^* = \mathbf{S}_1^{*T} \mathbf{S}_2 \tag{A.8}$$

A.3 Screw Transformation

A screw quantity ${}^j\mathbf{S} = \{ {}^j\mathbf{s} \, ; \, {}^j\mathbf{s}_o \}^T$ which is known with respect to a frame of reference j can be transformed and expressed with respect to a frame of reference i by

$${}^i\mathbf{S} = \left\{ \begin{array}{c} {}^i[\mathbf{R}]_j \, {}^j\mathbf{s} \\ {}^i\mathbf{r}_{ij} \times {}^i[\mathbf{R}]_j \, {}^j\mathbf{s} + {}^i[\mathbf{R}]_j \, {}^j\mathbf{s}_o \end{array} \right\} = {}^i[\mathbf{T}]_j \, {}^j\mathbf{S} \tag{A.9}$$

where

$${}^i[\mathbf{T}]_j = \left[\begin{array}{cc} {}^i[\mathbf{R}]_j & [\mathbf{0}]_{3\times 3} \\ [{}^i\tilde{\mathbf{r}}_{ij}] \, {}^i[\mathbf{R}]_j & {}^i[\mathbf{R}]_j \end{array} \right]$$

In the above equation ${}^i[\mathbf{R}]_j$ is a 3×3 rotation matrix describing the orientation of frame j with respect to frame i, and $[{}^i\tilde{\mathbf{r}}_{ij}]$ is a 3×3 skew symmetric of the location of the origin of frame j with respect to frame i, ${}^i\mathbf{r}_{ij}$. The 6×6 transformation matrix $[\mathbf{T}]$ is referred to as a *screw transformation.* Note that the general screw transformation is not an orthogonal transformation.

A.4 Screw Systems

The screws $\$_i$, $i = 1, \ldots, n$ are linearly independent if there exists no set of c_i, $i = 1, \ldots, n$ such that

$$c_1\$_1 + c_2\$_2 + \cdots + c_n\$_n = \mathbf{0} \tag{A.10}$$

other than the trivial solution $c_i = 0$, $i = 1, \ldots, n$. If a non-trivial solution to equation (A.10) exists, the screws are linearly dependent. This concept of linear dependence of screws also extends directly to screw quantities.

A set of r linearly independent screws forms a basis for an r-system of screws. That is, an r-system of screws is comprised of all screw quantities resulting from any linear combination of r linearly independent screws. A zero-system contains no screws, and a six-system represents all possible screws in space. Reciprocal to an r-system of screws is a $(6-r)$-system of screws. Any screw belonging to a screw system will be reciprocal to all screws belonging to its reciprocal screw system[1]

A.5 Application to the Instantaneous Kinematics of Manipulators

If a rigid body is acted upon by twists of amplitudes ω_i, $i = 1, \ldots, n$ on a chain of screws $\$_i$, $i = 1, \ldots, n$ the resulting velocity of the body is

$$\mathbf{V} = \omega_1 \$_1 + \omega_2 \$_2 + \cdots + \omega_n \$_n \tag{A.11}$$

In application to the modelling of the instantaneous kinematics of manipulators, the joint axes are the screws $\$_i$, and the joint rates, $\dot{\mathbf{q}}$, $i = 1, \ldots, n$ are the twist amplitudes. The twist $\mathbf{V}$ is the velocity of the end the serial chain (the end effector velocity of an open chain manipulator or branch end velocity of a closed chain manipulator). The joint screws define a screw system Ψ_{jt} of order equal to the number of linearly independent $\$_i$. In the inverse velocity problem we are concerned with finding $\dot{\mathbf{q}}$ (ω_i) such as to provide a required $\mathbf{V}$. To be feasible, $\mathbf{V}$ must belong to Ψ_{jt}. In other words, if Γ_{jt} represents the screw system reciprocal to Ψ_{jt}, then $\mathbf{V}$ must be reciprocal to all screws in this reciprocal screw system for the motion to be feasible.

[1] For a further discussion of screw systems and reciprocal screw systems the reader is referred to Hunt [20].

The force equilibrium condition for a member of a closed chain manipulator can be stated in a similar manner to equation (A.11). Let f_i, $i = 1, \ldots, n$ be wrench intensities acting on unit screws $\$_i$, $i = 1, \ldots, n$ equilibrating an applied wrench $\mathbf{F}$. This force balance can be expressed as

$$\mathbf{F} = f_1\$_1 + f_2\$_2 + \cdots + f_n\$_n \tag{A.12}$$

For a closed chain manipulator, f_i represent the magnitudes of the wrenches generated by actuated joints in branches connected to the member under study (usually the output member, or end effector of the manipulator). The unit screws $\$_i$ represent restraint directions available from the actuation of each active joint in a branch. The wrench $\mathbf{F}$ is the wrench to be generated or resisted by the member of the manipulator. In the inverse static force problem of a closed chain manipulator we are concerned with finding the required f_i in order for the manipulator to sustain a known load $\mathbf{F}$ applied to the end effector. The torque or force output required of each actuator can be found from the calculated wrench intensities f_i and by considering the configuration of the manipulator. If Ψ_r represents the screw system defined by the restraint screws $\$_i$, then for the manipulator to be capable of sustaining the load, $\mathbf{F}$ must belong to Ψ_r. If $\mathbf{F}$ does not belong to Ψ_r then the manipulator is incapable of sustaining the load and uncontrollable end effector instantaneous motion will occur. This instantaneous end effector motion will belong to the system Γ_r reciprocal to Ψ_r.

Appendix B

The Singular Value Decomposition

B.1 The Singular Value Decomposition

The *singular value decomposition*[1], or *SVD*, is a fundamental theorm of linear algebra. The theorm states that any $m \times n$ matrix $[\mathbf{A}]$ can be factored into

$$[\mathbf{A}] = [\mathbf{U}]\,[\mathbf{\Sigma}]\,[\mathbf{V}]^T \tag{B.1}$$

where

$$[\mathbf{\Sigma}] = \text{diag}\,(\sigma_1, \sigma_2, \ldots, \sigma_p) \quad ; \quad p = \min\{m, n\}$$

$$\sigma_1 \geq \sigma_2 \geq \cdots \geq \sigma_p \geq 0$$

The matrix $[\mathbf{U}]$ is an $m \times m$ orthogonal matrix whose columns are the eigenvectors of $[\mathbf{A}]\,[\mathbf{A}]^T$, and the matrix $[\mathbf{V}]$ is an $n \times n$ orthogonal matrix whose columns are the eigenvectors of $[\mathbf{A}]^T\,[\mathbf{A}]$. The p entries on the diagonal of $[\mathbf{\Sigma}]$ are called the *singular values* of $[\mathbf{A}]$ which are equivalent to the square roots of the eigenvalues of both $[\mathbf{A}]\,[\mathbf{A}]^T$ and $[\mathbf{A}]^T\,[\mathbf{A}]$. The number of nonzero singular values, r, is equal to the rank of $[\mathbf{A}]$.

The columns of $[\mathbf{U}]$ and $[\mathbf{V}]$ give orthonormal bases for the four fundamental subspaces of $[\mathbf{A}]$. The first r columns of $[\mathbf{U}]$ form an orthonormal basis for the column space of $[\mathbf{A}]$ and the last $m - r$ columns form an orthonormal basis for the left nullspace of $[\mathbf{A}]$ (the nullspace of $[\mathbf{A}]^T$). Similarly, the first r columns of $[\mathbf{V}]$ form an orthonormal basis for the row space of $[\mathbf{A}]$ (the column space of $[\mathbf{A}]^T$), and the last $n - r$ columns of $[\mathbf{V}]$ form an orthonormal basis for the nullspace of $[\mathbf{A}]$.

[1] For further information on the singular value decomposition the reader is reffered to Golub and Van Loan [12] or Forsythe and Moler [11].

The singular values of a matrix are lengths of the semi-axes of the hyperellipsoid $\mathcal{E}$ defined by

$$\mathcal{E} = \{\mathbf{y} \mid \mathbf{y} = [\mathbf{A}]\,\mathbf{x},\ \|\mathbf{x}\| = 1\} \tag{B.2}$$

The directions of the semi-axes are given by the unit vectors u_i of the corresponding columns of $[\mathbf{U}]$. If a singular value σ_j becomes zero the hyperellipsoid collapses to zero dimension in the direction given by u_j, demonstrating a reduction in the span of the column space of $[\mathbf{A}]$ and the exsitence of a nullspace with basis vector v_j (the j'th column of $[\mathbf{V}]$).

B.1.1 Example A

The 2×2 matrix

$$[\mathbf{A}] = \begin{bmatrix} 0.96 & 1.72 \\ 2.28 & 0.96 \end{bmatrix}$$

has the following singular value decomposition:

$$[\mathbf{A}] = [\mathbf{U}]\,[\mathbf{\Sigma}]\,[\mathbf{V}]^T = \begin{bmatrix} 0.6 & -0.8 \\ 0.8 & 0.6 \end{bmatrix} \begin{bmatrix} 3 & 0 \\ 0 & 1 \end{bmatrix} \begin{bmatrix} 0.8 & 0.6 \\ 0.6 & -0.8 \end{bmatrix}^T$$

The matrix $[\mathbf{A}]$ having all nonzero singular values demonstrates that the matrix is of full rank (rank = 2). The ellipsoid associated with $[\mathbf{A}]$ and the linear system $\mathbf{y} = [\mathbf{A}]\,\mathbf{x}$ is shown in Figure B.1A. The unit vectors $\mathbf{u}_1$ and $\mathbf{u}_2$ are the columns of $[\mathbf{U}]$ which represent an orthonormal basis for the column space, or range, of $[\mathbf{A}]$.

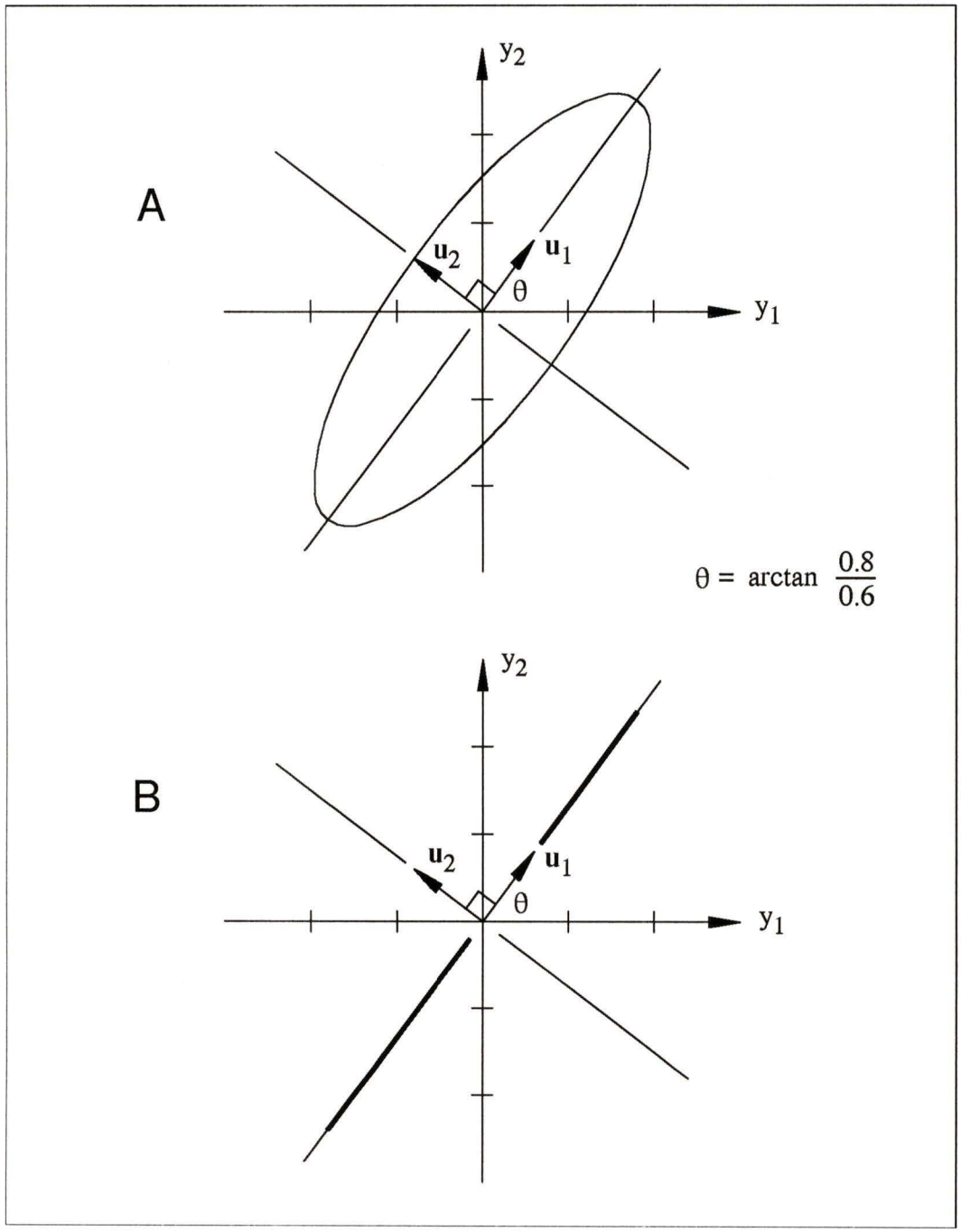

Figure B.1: Ellipsoids associated with singular values of examples

B.1.2 Example B

As an example of a rank deficient square matrix, the matrix

$$[\mathbf{B}] = \begin{bmatrix} 1.44 & 1.08 \\ 1.92 & 1.44 \end{bmatrix}$$

has a singular value decomposition

$$[\mathbf{B}] = [\mathbf{U}][\mathbf{\Sigma}][\mathbf{V}]^T = \begin{bmatrix} 0.6 & -0.8 \\ 0.8 & 0.6 \end{bmatrix} \begin{bmatrix} 3 & 0 \\ 0 & 0 \end{bmatrix} \begin{bmatrix} 0.8 & 0.6 \\ 0.6 & -0.8 \end{bmatrix}^T$$

The second singular value of [**B**] being equal to zero, $\sigma_2 = 0$, indicates that the rank of the matrix is one instead of two as was the case for example A. This fact can also be seen by noting that the second column of [**B**] is equal to the first column multiplied by 0.75. Note that the matrices [**U**] and [**V**] are the same in both example A and example B. This indicates that the set of basis vectors describing the fundamental subspaces are identical in both cases but some of the vectors belong to different subspaces. In the first example both $\mathbf{u}_1$ and $\mathbf{u}_2$ formed a basis for the column space of [**A**]. In the second example $\mathbf{u}_1$ is the only basis vector for the column space of [**B**] indicating the range of [**B**] is a line in two dimensions instead of the entire plane. The ellipsoid associated with [**B**] is shown in Figure B.1B. The fact that the ellipsoid collapses to a line in this case clearly demonstrates the reduction in the range space of [**B**]. In the second example the vector $\mathbf{u}_2$ is a basis vector for the left nullspace of [**B**] which did not exist in the first example. The vector $\mathbf{u}_2$ can be easily verified to be in the left nullspace of [**B**] by noting that

$$\mathbf{u}_2^T[\mathbf{B}] = \begin{bmatrix} -0.8 & 0.6 \end{bmatrix} \begin{bmatrix} 1.44 & 1.08 \\ 1.92 & 1.44 \end{bmatrix} = \begin{bmatrix} 0 \\ 0 \end{bmatrix}$$

In the first example both $\mathbf{v}_1$ and $\mathbf{v}_2$ formed a basis for the row space of [**A**]. In the second example the only basis vector for the row space of [**B**] is $\mathbf{v}_1$. The vector $\mathbf{v}_2$

is the basis for the nullspace of [**B**] which did not exist for example A. This can be verified by confirming that the vector maps to the zero vector when operated on by the matrix [**B**],

$$[\mathbf{B}]\,\mathbf{v}_2 = \begin{bmatrix} 1.44 & 1.08 \\ 1.92 & 1.44 \end{bmatrix} \begin{bmatrix} 0.6 \\ -0.8 \end{bmatrix} = \begin{bmatrix} 0 \\ 0 \end{bmatrix}$$

Vita

Surname: Pittens *Given Names:* Kenneth Henrichus

Place of Birth: Oakville, Ontario Canada *Date of Birth:* May 11, 1965

Educational Institutions Attended

University of Victoria	1990 to 1992
University of Waterloo	1984 to 1989

Degrees Awarded

B.A.Sc. (First Class Honours)	University of Waterloo	1989

Honours and Awards

Charles S. Humphrey Graduate Award	University of Victoria	1991-92
President's Research Scholarship	University of Victoria	1991-92
NSERC Postgraduate Scholarship, Year 2	University of Victoria	1991-92
President's Research Scholarship	University of Victoria	1990-91
NSERC Postgraduate Scholarship, Year 1	University of Victoria	1990-91
Engineering Upper Year Scholarship	University of Waterloo	Jan. 1989
Engineering Upper Year Scholarship	University of Waterloo	Sep. 1988
Engineering Upper Year Scholarship	University of Waterloo	Jan. 1988
Engineering Upper Year Scholarship	University of Waterloo	May 1987
Undergraduate Research Assistantship	University of Waterloo	Sep. 1986
Engineering Upper Year Scholarship	University of Waterloo	Sep. 1986
Undergraduate Research Assistantship	University of Waterloo	Jan. 1986
Engineering Upper Year Scholarship	University of Waterloo	Jan. 1986

Other Awards at Graduation

CSME Gold Medal for Academic Achiev.	University of Waterloo	1989
Sir Sandford Fleming Foundation Award	University of Waterloo	1989

Work Experience

May 1989 - August 1990	New Automation Inc.	Full Time Employment
Jan - April 1987	Istec Incorporated	Work Term Employment
September - December 1987		Work Term Employment
May - August 1988.		Work Term Employment
September - December 1985	Prochem Limited	Work Term Employment
May - August 1986		Work Term Employment

Publications

1. Pittens, K.P., and Podhorodeski, R.P., "Considerations of Kinematic Equivalency in Stewart Platform Configuration Optimization," *Proceedings of the 2'nd National Applied Mechanisms and Robotics Conference*, Cincinnati, OH, Nov. 1991, paper No. IXC.3. Submitted to the *Journal of Applied Mechanisms and Robotics* (invited submission).

2. Podhorodeski, R.P., and Pittens, K.P., "Kinematic Design and Analysis of Hybrid-Chain Manipulators," *Proceedings of the IASTED International Conference on Control and Robotics*, Vancouver, BC, Aug. 1992, pp. 211–214.

3. Podhorodeski, R.P., and Pittens, K.P., "A Class of Hybrid-Chain Manipulators Based on Kinematically Simple Branches," *Proceedings of the 22'nd ASME Biennial Mechanisms Conference*, Vol. DE-27, Phoenix, AZ, Sept. 1992, pp. 59–64. Submitted to the *Journal of Mechanical Design.*

4. Podhorodeski, R.P., and Pittens, K.P., "Three Branch Hybrid-Chain Manipulators: Design Considerations," to be presented at the *Fourth International Symposium on Robotics and Manufacturing*, Santa Fe, NM, Nov. 1992.

5. Pittens, K.P. and Podhorodeski, R.P., "A Family of Stewart Platforms with Optimal Dexterity," to appear in *Journal of Robotic Systems*, Vol. 10, No. 6, 1993.

Partial Copyright License

I hereby grant the right to lend my thesis to users of the University of Victoria Library, and to make single copies only for such users or in response to a request from the Library of any other university, or similar institution, on its behalf or for one of its users. I further agree that permission for extensive copying of this thesis for scholarly purposes may be granted by me or a member of the University designated by me. It is understood that copying or publication of this thesis for financial gain shall not be allowed without my written permission.

Title of Thesis: OPTIMAL ARCHITECTURAL DESIGN OF PARALLEL AND HYBRID MANIPULATORS

Author: [redacted]
(Signature)

KENNETH H. PITTENS
(Name)

NOVEMBER 25, 1992
(Date)